Economic Geology
Monograph 5, 1983, pp. 439–487

An Analysis of the Hydrothermal System Responsible for Massive Sulfide Deposition in the Hokuroku Basin of Japan

L. M. CATHLES

Chevron Oil Field Research Company, P.O. Box 446, La Habra, California 90631

Abstract

The hydrothermal system responsible for Miocene massive sulfide mineralization in the Hokuroku basin of northern Japan is analyzed by combining simple heuristic calculations with critical field data, and by incorporating redistribution of anhydrite, silica, and $\delta^{18}O_r$ into a finite difference model of the hydrothermal system and comparing model chemical predictions to field observations. Kinetic constraints are taken into account. The exercise suggests that the Kuroko massive sulfide deposits were formed as the result of multiple small (1 × 3 km in cross section) intrusive pulses that cooled by convection and formed individual sulfide and sulfate lenses in less than 5,000 years and probably ~100 years. The general formation permeability was at least a few millidarcies and probably a few hundred millidarcies. Sulfate and silica deposition preceded sulfide deposition, performing the necessary function of isolating hot deeply circulating solutions from cool shallowly circulating solutions so they could vent uncooled into the sea. Surface discharge was controlled by major fractures. Calculated $\delta^{18}O_r$ anomalies are in excellent agreement with those observed near the Fukazawa massive sulfide deposit. The model deduced for the Kuroko hydrothermal system is compatible with and supported by observations that have been made on ophiolite suites, and on hot and warm springs at mid-ocean ridges. The correspondence between $\delta^{18}O_r$ profiles calculated here and those measured in the complete composite section through the Semail Ophiolite, Oman, is particularly striking. Insights are gained into the nature of deep (greater than 2 km) equilibrium oxygen isotope alteration. Exploration implications are indicated and a confirmatory test suggested.

Contents

Introduction 439
Analysis of hydrothermal systems responsible for massive sulfide deposition 441
Heuristic calculations 441
District metal resources: A constraint on the size of the heat source required for the mineralization 442
Paleoheat flow: A constraint on permeability at the time of mineralization 443
Convection in the sulfide blanket 446
Slumping of the sulfide blanket 447
Constraints on bottom current velocities during mineralization 447
Physical-chemical models of the massive sulfide hydrothermal system 448
Physical models of convective cooling 449
Dike injection at a ridge 449
Convective cooling of a small magma chamber 450
Chemical consequences of convective cooling 454
Chemical alteration that does not depend on rock composition 454
Chemical alteration that depends on rock composition 458
Discussion of physical-chemical models in light of field evidence 461
Brief summary of field evidence from the Hokuroku district 461
Discussion of calculated models from the Hokuroku district 465
Evidence from ophiolite suites 470
Evidence from warm and hot springs at mid-ocean ridges 472
Summary and conclusions 474
Acknowledgments 476
Glossary of appendix notation 479
Appendix I. Modeling techniques 480
Physical model 480
Chemical model 481
Appendix II. Kinetics of silica solution-precipitation and oxygen isotope exchange 482
Oxygen isotope exchange 483
Kinetics of silica solution and deposition 485
Reactive surface area per unit volume of rock 485
ϕa if fluid-rock chemical interaction is restricted to the edges of flow fractures 485
ϕa if fluid-rock interaction occurs uniformly throughout the rock formation 486
Thickness of the reaction zone near a fracture and its effect on the rate of chemical alteration 486

Introduction

THE hydrothermal system responsible for Kuroko-type massive sulfide mineralization in Japan lived and died 5 to 14 million years ago. The objective of this paper is to build a numerical model of this hydrothermal system and demonstrate that it is geologically and geochemically reasonable. The attempt to build and test a rigorous model forces consideration of the proper questions regarding ore genesis, leads to useful insights,

0361-0128/83/253/439-50$2.50

and identifies critical questions to be tested in the field. Ideally, any scientific investigation would proceed by iteratively building models or hypotheses, testing, and improving them. Processes of ore deposition are so complex that we are only now, utilizing computer techniques, in a position to construct appropriately quantitative models (hypotheses).

The most reliable data for testing any model of the Kuroko hydrothermal system are chemical in nature. It is the chemical consequences of the hydrothermal system that operated in the Hokuroko basin in Miocene Japan that remain today for us to study. Physical measurements such as permeability are unlikely to be reliable if for no other reason than that the deposits have been uplifted ~4 km and quite possibly significantly faulted after they were formed. The chemical consequences of the hydrothermal system are reflected in the ore deposits themselves, in rock silicification, in anhydrite deposition, in oxygen isotope alteration, and in many other ways (see other papers in this volume). Our objective is to put enough chemistry into a physical model of the hydrothermal system that chemical predictions can be made and the model tested by comparing the chemical predictions to field observations. It is useful to develop as many simple chemical models as possible, so that independent tests of the physical model can be made. In this paper, we report models of silica, anhydrite, and $\delta^{18}O_r$ redistribution. The three kinds of alteration are considered to be chemically independent.

The range of possible physical parameters (permeability and its spatial, temporal, and thermal variations, intrusive size, dimension, depth, etc.), let alone chemical parameters, is enormous. To narrow the reasonable range of physical parameters, a number of heuristic calculations are made to draw conclusions from particularly critical pieces of geologic data. The range of physical parameters can be quite considerably restricted using this approach.

To restrict the range of possible models further we choose to be deliberately conservative whenever a choice presents itself. For example, we initially opt for a small intrusion. Later we find this was probably a reasonable choice for other reasons, but our initial decision was based on conservatism—to make it harder for the intrusion to form the deposits. If a small intrusion can do it, a bigger one should do it more easily. Similarly, we choose to consider dissolution and precipitation of amorphous silica rather than quartz. Observed silica deposition in siliceous ore zones requires shallow as well as deep circulation. Less shallow circulation is required to deposit a fixed amount of silica with the greater solubility of amorphous silica.

Finally, to increase the amount of geologic data available to constrain the models, all systems analogous to the Hokuroku basin in Miocene Japan (a rift environment, Cathles et al., 1983) are considered. Data, or constraints, are taken from the Noranda Archean massive sulfide camp in Canada, from presently active hydrothermal systems including those at mid-ocean ridges, and from ophiolite suites. This approach is vulnerable to the criticism that apples and oranges are being mixed, and many may disagree with it. This volume reports studies of volcanogenic massive sulfide deposits in Canada and Japan and ocean-ridge hydrothermal systems because it is believed that comparison of these systems can contribute to overall understanding. They are geologically certainly close relatives. The real justification, however, for our using data, when useful, from all systems is that quantitative modeling of the kind of hydrothermal system operative in all these cases is at an early stage of development and we need all the data we can get to constrain even crude models.

The methodologies used in the heuristic calculations are certainly not new. To my knowledge this is the first time many of these heuristic techniques have been explicitly applied to ore deposits, however. The techniques may prove useful in other ore deposit applications, and for this reason, are discussed in some detail.

The basis of the physical modeling is given in Appendixes I and II. The physical model is based on the simultaneous conservation of fluid mass, momentum, and energy. The modeling techniques have been discussed by many authors and applied to a diversity of geologic situations (see review by Cathles, 1981, and references cited therein). In the application closest to the topic of this paper, Parmentier and Spooner (1978) analyzed the kind of convection that might be expected very near an ocean ridge and discussed their results specifically in terms of the ophiolitic massive sulfide deposits of Cyprus. Convection in their numerical model is driven by high (50 heat flow units) basal heat flow. They pointed out, as we do, that only a small volume of rock is required to provide the metal found in the massive sulfide deposits. Their physical model differs from ours in that (1) it involves shallower (2 km rather than 5 km) circulation and (2) it is driven by basal heat rather than the cooling of a small intrusion. Oxygen isotopes have recently provided direct evidence that deep (7 km) circulation has taken place in ophiolite suites (Gregory and Taylor, 1981). We make arguments that small intrusive magma chambers were involved in Kuroko mineralization in Japan.

The chemical calculations require a global chemical model and a local alteration kinetic model. The global chemical model is simply an expression of mass balance for any chemical component—an "actuarial" accounting of losses or gains of a chemical species from the fluid as it travels from the sea into and through the rock formation. The rate of chemical alteration can be controlled by spatial temperature variations and the

rate of fluid circulation (if chemical kinetics are fast compared to the rate at which this fluid flow alteration will take place) or by the rate at which the rock can chemically alter (chemical kinetics). The chemical kinetic model is important only if the kinetics are slow enough to be rate controlling. Chemical kinetic models for the oxygen isotope alteration of basalt and for the dissolution and precipitation of silica have recently become available (Rimstidt and Barnes, 1980; Cole, 1980). We use these kinetic models in our calculations.

No one to my knowledge has previously attempted the simultaneous modeling of silica, anhydrite, and $\delta^{18}O_r$ redistribution. Several have modeled $\delta^{18}O_r$ alteration as we do, however. Spooner et al. (1977a) considered the isotopic consequences of up-temperature circulation with fluid in isotopic equilibrium with rock and suggested deep negative $\delta^{18}O_r$ isotope anomalies could exist of the kind we compute, and the kind recently observed by Gregory and Taylor (1981). They did not include kinetics in their model and doubted their equilibrium calculations would apply to real cases, however. Our calculations, which include realistic kinetics, show the equilibrium model will apply to reasonable geologic situations if the temperature is greater than ~100°C. Indeed, the observation of deep negative anomalies by Gregory and Taylor (1981), essentially identical to those predicted by an equilibrium isotopic model, potentially provides significant constraints on the nature of ocean ridge hydrothermal circulation and the kinetics of rock isotope alteration.

Norton and Taylor (1979) have recently modeled the $\delta^{18}O_r$ alteration of the Skaergaard Intrusion using techniques similar to those we use. Their model differs most fundamentally from ours in allowing flow through rock at temperatures up to 1,000°C. Most (75%) of the hydrothermal solution circulates through their Skaergaard gabbro intrusion when it is hotter than 400°C. We argue, to the contrary, that intrusions will be quite impermeable and very little or no flow will occur through them until their temperature is reduced below 400°C. There are other differences. Norton and Taylor maintain a constant rock and fluid $\delta^{18}O$ at boundaries, whereas we allow fluid to vent at the isotopic composition determined by kinetics, temperature, and $\delta^{18}O_r$. Our inflow solutions have $\delta^{18}O_f = 0$ per mil (seawater), whereas Norton and Taylor effectively consider the inflow of light (~ meteoric) water. This is appropriate for the Skaergaard but not for the Hokuroku basin. We calculate a positive anomaly associated with the upward migration of the thermal front of the intrusion. Norton and Taylor show no such anomaly. Its absence is probably related to differences in the chemical alteration kinetics. We have been unable to compare our kinetics to theirs confidently because of the cryptic description given kinetics in their paper. Differences are to be anticipated since we use a model based on alteration of volcanic glass and Norton and Taylor use a model based on the alteration of plagioclase. But at temperatures $\lesssim$200°C the differences should not be as large as they apparently are.

Parmentier (1981) has also modeled the oxygen isotope alteration expected from the cooling of an intrusion. He does not take into account the temperature dependence of isotopic fractionation between rock and water. Plagioclase is isotopically altered by solid state diffusion into mineral grains 0.1 to 1 mm in diameter. These kinetics are quite slow compared to ours and presumably Norton and Taylor's. Despite this, Parmentier finds, as we do, that isotopic alteration occurs over quite a narrow front at the side of the intrusion. Fluid downstream from this front in the hot part of the system is in isotopic equilibrium with the rock and causes no further exchange. Exchange is produced downstream where temperature changes occur, in our case because the temperature dependence of water-rock isotope fractionation is included in our calculations.

Analysis of Hydrothermal Systems Responsible for Sulfide Deposition

Heuristic calculations

Simple calculations and geologic data can be used to estimate the intrusive mass required to produce the Kuroko deposits of the Hokuroku district, the permeability of the host rock at the time of mineralization, and the time duration of the mineralizing event and to provide other useful insights. In particular, the total metal tonnage and the tonnage of silica precipitated near the paleosurface indicates the minimum intrusive mass necessary to sustain the mineralizing hydrothermal system. Geologic evidence of the near-surface temperature distribution at the time of mineralization indicates the rate of vertical flow and suggests the average or bulk-rock permeability. The formation permeability in turn suggests bounds on the duration of the mineralizing event. Criteria for convection within an accumulating sulfide blanket can be stated and the thermal consequences of such convection defined. Since the mineralogical consequences on intrasulfide blanket convection are not observed, constraints are placed on the blanket's permeability and on possible models for chemical alteration within the blanket. The conditions under which fluid flow through the sulfide blanket will cause slumping also constrain the in situ, unslumped sulfide blanket permeability. Finally, the dimensions of the sulfide ore lenses and the size of the sulfide crystal agglomerates, which presently are forming as a result of thermal quenching in the black smoky plumes at 21° N on the East Pacific Rise, suggest that quiescent bottom conditions are required for the formation of Kuroko massive sulfide blankets. In this sec-

tion we consider the simple heuristic calculations that allow such conclusions to be made and which identify an appropriate range of parameter values for the more sophisticated physical-chemical models that will be presented in the next section.

District metal resources: A constraint on the size of the heat source required for mineralization: A simple relationship exists between the size of an intrusion and the total mass of hydrothermal fluid above a given temperature that an intrusion can cause to circulate (Cathles, 1981, eq. A7):

$$M_w = M_I \frac{c_m}{c_f} \ln \frac{\Delta T_0}{\Delta T}. \quad (1)$$

In the above expression M_w is the total mass of hydrothermal fluid circulated through the intrusion; M_I, the mass of the intrusion, c_m, the heat capacity of the intrusion in cal/g/°C; c_f, the heat capacity of water in cal/g/°C; ΔT_0, the initial contrast in temperature between the intrusion and its environment; and ΔT, the temperature contrast after some cooling. For example, if a 700°C pluton intrudes at a ~4 km depth—where the temperature is ~100°C, circulates hydrothermal fluids, and cools to 300°C, the mass of fluid circulated is 22 percent of the mass of the intrusion. In other words, in such circumstances a 700°C intrusion can circulate a mass of hydrothermal fluid above 300°C equal to about 22 percent its own mass. If the intrusion entered at 1,300°C, it would circulate a mass of hydrothermal solution hotter than 300°C equal to about 36 percent of its own mass.

Table 1 estimates the metal resources of the Hokuroku district in Japan and the Noranda district in Canada. Table 2 shows how the relationships given in equation (1) may be used to calculate the size of intrusion required to circulate enough hydrothermal fluid to precipitate the resources of the Noranda or Hokuroku districts. It is assume that precipitation occurs as the hydrothermal fluid crosses the sea-sediment interface into cold seawater, and that all the hydrothermal fluid that circulated through the intrusion also circulated into the sea. The case where the hydrothermal solution is of magmatic origin, i.e., where water exsolves from the magma during cooling, is given for comparison. It is assumed that 1,000 ppm total Cu + Zn + Pb precipitated from magmatic fluid upon entering the sea, but only 100 ppm from heated and circulated formation or seawater.

Several conclusions can be drawn from Table 2. First of all, the size of intrusion required for Hokuroku or Noranda district mineralization is ~70 km^3. The size is similar whether mineralization precipitates from magmatic or formation fluids. The constraints on intrusion size imposed by the amount of hydrothermal fluid the intrusion can circulate are more severe than the requirement that the intrusion provide enough metal for mineralization. This can be seen from Table 2 but is best shown by Table 3, which compares the ppm of Cu, Zn, and Pb that must be extracted from a 1.5×10^{11} metric ton intrusion to account for the Hokuroku district metal resources. Except for perhaps Pb, the amount of metals that would have to be extracted is substantially less than the amount found in igneous rocks in the area. Thus, the intrusion could be substantially smaller than 1.5×10^{11} metric tons, and still provide the metal resources of the district—metal balance is a less severe constraint on intrusion size than the mass of hydrothermal solution the intrusion can circulate.

TABLE 1. Estimated Metal Resources for the Hokuroku Massive Sulfide District in Japan and the Noranda Massive Sulfide District in Canada

	(Millions of metric tons)	
	Noranda	Hokuroku district
Copper	3.1	1.2
Zinc	1.6	2.5
Lead	—	0.8
Total	4.7	4.5

The Hokuroku resources are somewhat arbitrarily taken to be 40 percent bigger than the reserves estimated by Lambert and Sato (1974); the Noranda resource estimates are 20 percent larger than reserve figures provided by Dave Watkins, Falconbridge Copper Company; the 20 percent increase was suggested by Watkins

Near-surface silica deposition can also be used to estimate the size of the intrusion. For example, most massive sulfide deposits at Noranda occur stratigraphically just above the upper Amulet Rhyolite. The upper 20 m of the Amulet Rhyolite is heavily silicified and in fact is considered by Falconbridge geologists to be a basalt to which about 20 weight percent silica has been added by hydrothermal activity. The volcanostratigraphic sequence dips 35° to 80° to the east, so the deposits are exposed nearly in cross section at the surface. The silicified cap of the Amulet Rhyolite can be traced for at least 10 miles (16 km) across the Noranda camp (Gibson et al., 1981; D. Watkins, Falconbridge Copper, pers. commun.).

Addition of 20 weight percent silica to a 20-m layer of basalt represents an addition of 1.2 kg SiO_2 per square centimeter surface area of the layer. If the silicification occurred originally over an area of 12 × 12 miles (3.7×10^{12} cm^2), then 4.5×10^{12} kg silica would have been deposited near the paleosurface. The solubility of silica in 300°C hydrothermal solution is less than 2,000 ppm (see Appendix II and Fig. 14). Thus, at least 2.3×10^{15} kg of hydrothermal solution

TABLE 2. Calculation of Intrusive Mass Required by 4.7 Million Metric Tons of Total Cu, Zu, Pb

	Magmatic	Convected pore water
Metal mass		
$M_e =$	$[H_2O]_{magma}[Me]_{H_2O}M_I$	$[Me]_{H_2O}\left(\frac{M_w}{M_M}\right)M_I$
Intrusive mass		
$M_I =$	$\frac{M_{Me}}{[H_2O]_{magma}[Me]_{magmatic\ H_2O}}$	$\frac{M_{Me}}{[Me]_{hydro\ H_2O}}\left(\frac{M_w}{M_I}\right)$
	1.2×10^{11} metric tons (44 km^3)	2.1×10^{11} metric tons (78 km^3)
Parameter values used	$[H_2O]_{magma} = 0.04$	$\frac{M_w}{M_I} = 0.22$
	$[Me]_{Magmatic\ H_2O} = 10^{-3}$	$[Me]_{hydro\ H_2O} = 10^{-4}$
	$M_{Me} = 4.7 \times 10^6$ metric tons	

Assume the mineralizing solutions are hydrothermal solutions of magmatic origin or are heated and circulated pore fluids initially present in the country rock, meteoric water, or seawater. M_{Me} is the total mass of Cu, Zn, and Pb in the district, $[H_2O]_{magma}$ is the mass fraction of water in the magma, $[Me]_{H_2O}$ the mass fraction of Cu, Zn, and Pb precipitated from the hydrothermal fluid that is thermally quenched as it crosses the sea-sediment interface, M_I is the mass of the intrusion, and M_W is the mass of hydrothermal solution above 300°C circulated through the intrusion. Parameter values used in the calculation are given above. It is unlikely the intrusion will contain more than 4 wt percent water, even if it is quite silica rich (Burnham, 1979, and pers. commun.). Magmatic water is assumed to be more metal rich than scavaging formation fluids; 1,000 ppm is a reasonable total Cu, Zn, Pb concentration (Crerar and Barnes, 1976). Heated formulation waters or seawaters are likely to be less metal rich, but how much less (i.e., 100 ppm) is uncertain

above 300°C would be required for the near-surface silicification, and, using equation (1) and assuming a 700°C intrusion, this would require a 10^{13} metric ton intrusive mass. Such an intrusion is about 50 times bigger than that required by the metal resources at Noranda estimated in Table 2 but is similar in size to the Flavrian "granite" that is exposed stratigraphically beneath the ore deposits and which is considered by many to have been the heat source for the mineralizing hydrothermal system. The exposed part of the Flavrian granite measures 9 × 12 miles. If the exposed portion reflects the size of the intrusion, the full intrusion might measure ~9 × 12 × 10 miles and have a mass of ~1.2 × 10^{13} metric tons. The Flavrian granite is a composite intrusion.

We can conclude that an intrusive mass of at least 1.5 × 10^{11} metric tons and probably ~10^{13} metric tons was responsible for massive sulfide mineralization in major districts like Noranda and Hokuroku. There were likely many episodes of intrusion (composite intrusion), but the intrusions need not necessarily have coalesced into a composite body as they have at Noranda.

Paleoheat flow: A constraint on the permeability at the time of mineralization: Surface heat flow is strongly affected by vertical fluid flow. If the fluid flow is purely vertical (into or out of the sediment-seawater interface), the equations that describe the steady-state relationship between the fluid flow and the subsurface temperature can be easily solved (Bredehoft and Papadopulos, 1965). If q_z is the vertical mass flux toward the surface in $g_{H_2O}/cm^2/sec$, the temperature at the surface is 0°C, the temperature at depth L is T_L, and the temperature profile as a function of depth T(z) is:

$$T(z) = T_L \frac{1 - e^{-z/\delta}}{1 - e^{-L/\delta}}. \quad (2)$$

TABLE 3. Comparison of Metal Extraction Required from a 1.5- × 10^{11}-Metric Ton Intrusive Mass to Account for Hokuroku Metal Resources, and the Metal Content Observed in Igneous Rocks in the District and Surrounding Areas

	Required	Metal content			
Metal	Extraction from 1.5 × 10^{11} metric ton intrusion	Hokuroku district rhyolite of mineralization age	Dacite	Takadate andesite	Basalt
Cu	8 ppm	3–83	4–14	63–161	67–134
Zn	16.7 ppm	18–71	76–103	81–115	80–95
Pb	5.3 ppm	1–16	10–11	8–11	9–12

Generally the required metal extraction is substantially less than the typical metal abundance. An intrusion smaller than 1.5 × 10^{11} metric tons could provide the metal for the Hokuroku resources; metal balance is a less severe constraint on intrusion size than the mass of circulated hydrothermal fluid. Metal content data are from Isihara (1974, table 1, p. 244)

Depth, z, is measured positively downward in this equation, and the thermal skin depth, δ, is defined as:

$$\delta = K_m/q_z c_f. \quad (3)$$

K_m is the thermal conductivity of the water-saturated rock formation in cal/cm/°C, and c_f is the heat capacity of the fluid in cal/g/°C.

Figure 1 plots equation (2) for several values of L/δ. This ratio really reflects variations in q_z, since L is fixed for a given situation, and c_f and K_m vary over a restricted range of geologically reasonable values. Figure 1 shows that the thermal gradient is linear (i.e., is a normal conductive gradient) at zero or low vertical flow rates (small values of L/δ) but becomes isothermal at depth and steeper near the surface as the vertical flow rate increases. If L is greater than about 3δ, T_L closely approximates the hottest temperature at any depth, and the value of L does not affect the temperature profile. In these circumstances the profile is characterized entirely by δ; δ is the depth at which the temperature is $\left(1 - \frac{1}{e}\right) T_L$ or $0.63\ T_L$. Thus, δ characterizes the thickness of the low temperature, near surface skin—hence the name skin depth. The heat flow can be found by differentiating equation (2) with respect to z and multiplying by the thermal conductivity K_m. When $L > 3\delta$, the heat flow is

$$J[\text{cal/cm}^2/\text{sec}] \cong \frac{K_m T_L}{\delta}. \quad (4)$$

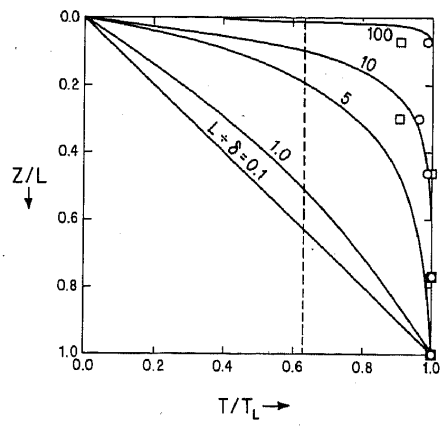

FIG. 1. Temperature as a function of depth for various rates of vertical fluid flow. Vertical flow rate increases as δ decreases. Depth (Z) is normalized to L and temperature to T_0. The curves are generated from equation (2) in the text. The boxes represent the mean filling temperatures in quartz from black silicious ore (□) and yellow silicious ore (O) in various mining levels of the Uwamuki 4 Kuroko deposit (see Fig. 2), plotted with L = 65 m. The fluid inclusion filling temperatures indicate L/δ is between 10 and 100. As discussed in the text, this information can be used to deduce the rate of vertical fluid flow and the heat flow at the time of mineralization, and to estimate the formation permeability.

Later detailed calculations show that the rates of near-surface fluid flow and the near-surface temperature change little from the time the thermal front arrives till the time the temperature has dropped everywhere below 300°C. The steady state assumption made above is thus justified during the most active phase of fluid venting. The importance of equations (1 to 4) and Figure 1 is that they allow an estimate to be made of the minimum vertical flow rate from available geologic data. From this estimate the permeability of the rock formation, the paleoheat flow, and the duration of the mineralizing event can be estimated. The vertical fluid flow rate is reflected by any geologic evidence that records the thermal skin depth at the time of mineralization.

The thermal skin depth at the time of mineralization is indicated, for example, by fluid inclusion filling temperatures from the siliceous zone beneath the Uwamuki 4 deposit. The fluid inclusion data from quartz associated with black and yellow siliceous ore of Marutani and Takenouchi (1978, fig. 10) are shown in Figure 2. Figure 2 shows quite isothermal conditions prevailed in the silicified feeder zone and in the massive Kuroko lens itself, whose top represented the surface at the time of mineralization. Taking L equal to 65 m, the range of working levels sampled by Marutani and Takanouchi, the average fluid inclusion filling temperature for each level can be plotted in Figure 1 and seen to indicate that L/δ is between 10 and >100, or that δ is between 6.5 and <0.65 m. Taking $c_f = 1$ cal/g/δC, and $K_m = 6 \times 10^{-3}$ cal/cm/sec/°C, δ values in this range indicate a vertical mass flow rate from 290 to >2,900 g/cm^2/yr. There is some suggestion that venting may have been more vigorous during yellow ore deposition than during black ore deposition.

The Uwamuki 4 deposit contains about 230,000 tons of Zn + Cu + Pb in a pod 350 × 100 × 17 m (Urabe and Sato, 1978, p. 165) or 660 g Zn + Cu + Pb per cm^2 surface area of the deposit. If discharge occurred uniformly over the area now occupied by the deposit at the rate indicated by the fluid inclusion temperature gradient, and 100 ppm Zn + Pb + Cu precipitated from the hydrothermal solution as it passed into cold seawater, 22,000 to <2,200 years would be required to form a deposit. Furthermore, from equation (4), the heat flow at the time of mineralization was 2,770 to >27,000 HFU.[1]

Similar estimates can be derived from other kinds of geologic evidence. Eldridge et al. (1983), for example, show that sphalerite is replaced by chalcopyrite within the massive sulfide blanket. This requires a temperature of ~300°C within ~10 m of the surface.

[1] HFU = heat flow unit = 10^{-6} cal/cm^2/sec; normal heat flow is about 1.5 HFU.

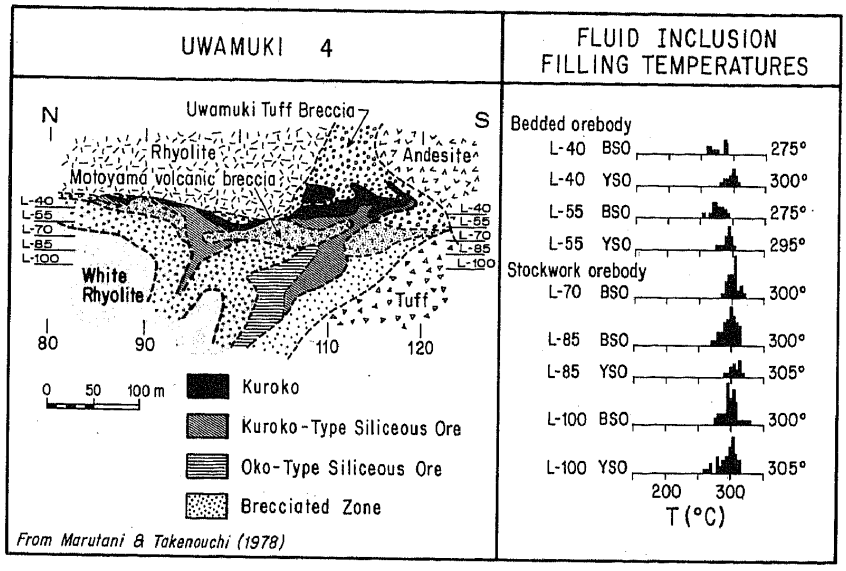

FIG. 2. Cross section of the Uwamuki 4 Kuroko massive sulfide deposit and fluid inclusion filling temperatures in quartz from various working levels of the mine. BSO = black silicious ore, YSO = yellow silicious ore. The figure is modified from several in Marutani and Takenouchi (1978). Notice that isothermal ~300°C conditions were maintained very close to the paleosurface at the time of mineralization (i.e., the top of the black ore lense). The mean filling temperatures are plotted in Figure 1 and are used in the text to estimate the formation permeability, the rate of vertical fluid flow, and the heat flow at the time of mineral deposition.

The vertical flow rate required to maintain 300°C inside the sulfide blanket can be estimated: the thermal conductivity of sphalerite is 63×10^{-3} and pyrite 90×10^{-3} cal/cm/sec/°C (Clark, 1966, p. 465). Assuming 50 percent water saturation of the blanket, taking a conservative thermal conductivity of 30×10^{-3} cal/cm/sec/°C, and taking $\delta \sim 5$ m, equation (3) requires a vertical upflow through the sulfide blanket of ~1,900 g/cm^2/yr and indicates a local heat flow of 18,000 HFU. At 1,900 g/cm^2/yr, 3,300 years would be required to form the Uwamuki 4 deposit if 100 ppm Pb + Zn + Cu precipitated from the hydrothermal solution.

At the Noranda camp in Canada, the observation that the upper 20 m of the upper Amulet Rhyolite is heavily silicified provides an estimate of the rate of circulation and paleoheat flow. Presumably, silica was precipitated as the result of a near-surface drop in temperature of upward-venting solution. Taking δ = 20 m and $K_m = 6 \times 10^{-3}$ cal/cm^2/sec/°C, equations (1) and (4) give a general upflow of 94 g/cm^2/yr and a general heat flow of 900 HFU.

The Noranda estimate differs from the fluid inclusion and the sulfide blanket estimates of vertical flow in being an estimate of a more general, less-focused upflow. Massive sulfide deposits and their feeder pipes clearly represent local discharge at fractures or particularly permeable locations. Silicification of the upper Amulet Formation of Noranda is widespread and fairly uniform. In fact, Gibson et al. (1981) suggest that silicification and plugging the surface were a required preparation for the fracture-focused discharge that produced the massive sulfide deposits. Certainly a general upflow of 94 g/cm^2/yr is not sufficient to vent 300°C solution into the sea and form a massive sulfide blanket. A sufficient flow rate, and a flow rate similar to that deduced by the other methods discussed in this section, would result if the discharge was concentrated for a factor of 20 or so by the siliceous cap.

A formation permeability can, however, be inferred from the general vertical flow of 94 g/cm^2/yr. The maximum general vertical flow rate is related to the thermal anomaly that drives the fluid circulation, the formation permeability, and the fluid viscosity (Cathles, 1981, eq. A1):

$$q_z = k\rho_0 \frac{\Delta T \alpha g}{\nu} . \qquad (5)$$

Taking the fluid viscosity, $\nu = 0.002$ stokes, the coefficient of thermal expansion $\alpha = 10^{-3}$, gravitational acceleration $g = 10^3$ cm/sec^2, $\Delta T = 250$°C, $\rho_0 = 1$ g/cm^3, and $q_z = 94$ g/cm^2/yr, equation (5) indicates a formation permeability of 2.4 mD (2.4×10^{-11} cm^2). A 2.4-mD formation permeability will cause a 1.5-$\times 10^{11}$-metric ton intrusion 3.25 km high, 1 km wide, and 17 km long to cool below 300°C in about ~2,500 years, provided the pluton has the same permeability as the country rock (Cathles, 1981, eq. A4).

The above estimates are crude and tend to be minimum estimates. We have shown how fluid inclusion

and mineralogical data can be used to infer that the fluid discharge through the siliceous stockwork and massive ore blankets was at least ~2,000 g/cm^2/yr. This discharge rate could be accommodated by a general subsurface formation permeability of 2.5 mD, provided the surface discharge was focused by a factor of ~20—that is, provided venting occurred through only about 1/20 of the total surface area above an intrusive mass. Focusing of at least this degree is reasonable. Kuroko massive sulfide deposits cover only a very small fraction of the total surface area of the Hokuroku basin.

A general formation permeability of 2.5 mD, although perhaps adequate, seems small when compared to the known permeabilities of likely rock types and of known geological analogs such as the geothermal systems in the Taupo graben in New Zealand. The permeability of the Waraikei geothermal field has been estimated at 10s to 100s of millidarcies (Elder, 1966; Mercer et al., 1975; Spooner, 1977). Basalts can be very permeable and commonly have permeabilities of ~100 mD to 100 D (Brace, 1980). Anderson and Zoback (1981) have recently measured the bulk permeability of 6.2-m.y.-old ocean crust on the Costa Rica rift. They found the permeability of the upper ~200 m to be ~40 mD. The permeability of the lower 3 to 15 m was 2 to 4 mD. We conclude that the formation hosting massive sulfide deposits had a general permeability of at least a few millidarcies, but the permeability could have been hundreds of millidarcies. Deposits almost certainly are formed in less than a few thousand years but could have formed in a few hundred years or less.

Convection in the sulfide blanket: It is more difficult to obtain an upper bound on permeability. If the permeability of a sulfide blanket is high enough, convection in the blanket is possible even though there is a net vertical flow of fluid up through the blanket. For any given permeability, vertical through-flow greater than a certain magnitude will shut off intrablanket convection, however. The apparent lack of convection in the sulfide blankets of massive sulfide deposits may thus allow an upper bound of 250 to 600 mD to be placed on sulfide ore, vent, and formation permeabilities.

As discussed in the previous section, a vertical flow of at least ~2,000 g/cm^2/yr is required to maintain temperatures of ~300°C within the sulfide blanket and allow chalcopyrite to replace sphalerite. The conditions that allow convection in a porous layer with net vertical solution through-flow have been elucidated by Wooding (1960), Sutton (1970), and Homsy and Sherwood (1976). The criterion for convection is essentially the same as for the case of no net vertical through-flow: that a critical Rayleigh number be exceeded. The layer thickness is defined by the skin depth (eq. 3), and the critical Rayleigh number is changed from 27 (free flow out the top, no flow-through base) to between 5.8 and 14.3 (Homsy and Sherwood, 1976, eq. 23). The criterion for the onset of convection is therefore:

$$\frac{g\alpha K \Delta T}{\nu W} > 5.8 \text{ to } 14.3, \qquad (6)$$

where W is the net vertical Darcy velocity in cm^3/cm^2/sec, and the other variables are as previously defined and as given in the appendix glossary. Taking $\Delta T = 300°C$, $W = 2{,}000$ cm^3/cm^2/yr, $\nu = 0.002$ stokes, and $g\alpha = 1$, equation (6) states that sulfide blanket convection will occur provided the permeability of the blanket is greater than 246 to 605 mD. These permeabilities are high but by no means unreasonable. Convection in the sulfide blanket is therefore a possibility.

The consequences of intrasulfide blanket convection for the temperature distribution within the blanket are dramatic, however. The previous section showed substantial vertical flow is needed to maintain 300°C temperatures within the blanket. Convection will not only eliminate but actually reverse this upward vertical flow. Areas where the flow is downward into the blanket from the overlying sea will have a very low temperature relative to neighboring zones of about twice average upflow. Inflow zones will be separated from outflow zones by a distance about equal to the thickness of the sulfide blanket.

If the boundary between black ore and yellow ore is a thermal boundary, as Eldridge et al. (1983) suggest, the black ore-yellow ore boundary should reflect convection by showing large variations in elevation within the blanket. The expected variations seem both large and local enough to have been noticed. Sulfide zoning is generally considered stratiform. I have not observed, nor seen referenced, the kind of inversely correlated variations in black ore and yellow ore thickness that would be expected from a combination of sulfide blanket convection and mineralogical zoning by replacement of sphalerite by chalcopyrite at temperatures >300°C.

A stratiform contact between black and yellow ore indicates either that the permeability of the sulfide blanket is low enough (e.g., less than ~250 mD) that convection in a blanket cannot occur, or that the black ore-yellow ore contact is not a thermal boundary. If the former is the case, the upper bound on the sulfide blanket permeability roughly applies also to the feeder zone and country rock. The feeder zone must have a higher permeability than the sulfide blanket if discharge through the blanket is to be uniform and a flat topography of the black ore-yellow ore contact produced. The permeability of the sulfide blanket cannot be much less than the feeder zone, however, or it

would choke off discharge or slump (see discussion in next section). Similarly, the host rock cannot be more permeable than the vent (or the sulfide blanket) or the discharge would not be focused through the vent. Thus, if sulfide blanket convection must be avoided, 250 mD may be a rough upper bound on the permeability of the sulfide blanket, vent, and host rock.

Alternatively, the black ore-yellow ore boundary might not be a thermal boundary but instead represents a change in the mix of metal sulfide originally deposited in the blanket. The observed replacement of sphalerite by chalcopyrite would, in this view, be a minor mineralogical phenomenon that alters, but does not completely convert, sphalerite to chalcopyrite. In this case, only a detailed petrologic study of an unslumped sulfide blanket could determine if there are the kinds of spatial variation in the replacement of sphalerite by chalcopyrite that might reflect convection or the lack of it in a sulfide blanket. Such a study has not yet been carried out.

Slumping of the sulfide blanket: There is another constraint on sulfide blanket permeability that helps account for the fact that sulfide blankets are very frequently accumulations of slumped sulfides—graded piles of sulfide sediment and breccia. A permeable fracture system 5 km deep filled with 300°C fluid will be about 0.2 g/cc lighter than surrounding fluids at normal temperatures for their depth. The hot column has a buoyancy of ~100 bars and thus could generate an upward pressure at the sea-sediment interface sufficient to lift a 4-g/cc sulfide blanket 250 m thick. Since most sulfide blankets are at most ~50 m thick, the hydrothermal system would have little difficulty removing a sulfide blanket that had become too restrictive to fluid through-flow.

The permeability below which the sulfide blanket becomes sufficiently restrictive to be levitated and slumped by the venting fluids can be estimated (Cathles, 1978). Slumping will occur when the resistance to fluid flow equals or exceeds the lithostatic pressure gradient in the sulfide blanket:

$$\frac{\nu q}{k} > \rho_s g.$$

Taking ρ_s = density of the sulfide blanket $\cong$ 4 g/cc, $\nu \sim$ =0.002 stokes, q = 2,000 g/cm^2/yr, and g = 980 cm/sec^2, we can solve the above expression and find the critical blanket permeability is ~3.2 mD. If the sulfide blanket becomes plugged during mineral deposition so the average permeability is less than about 3 mD, a through-flow of 2,000 g/cm^2/yr (needed to maintain the temperatures in the blanket indicated by chalcopyrite replacement of sphalerite) will lift the blanket off the feeder pipe and reduce the frictional resistance to the point where even a very slight slope will cause slumping. In-place (i.e., unslumped) sulfide blanket permeability will therefore be greater than ~3 mD and perhaps less than ~250 mD. We might note that the blanket will slump whether or not it is indurated. If it is not indurated, the sulfide mud will fluidize at flow off the vent, provided the vent is elevated relative to its immediate surroundings. If the blanket is indurated but does not have great cohesive strength, it may fragment and slump. If the blanket has sufficient cohesive strength, it may fracture and promote focused black smoker discharge (see next section).

Constraints on bottom current velocities during mineralization: On the sea floor hydrothermal discharge has been observed to occur at localized vents. When the ~350° fluid enters, mixes with, and is thermally quenched by seawater, a black smoker plume results. The black smoke consists of precipitated sulfide minerals (mainly pyrrhotite). Very little or none of the black smoke is settling and accumulating around the observed vents, although sulfides are precipitating in chimneys that grow over the vents (see, e.g., Rise, 1980). It is possible that, at a more mature stage, flow through a blanket consisting of fallen chimneys would be diffuse enough, and allow sufficient temperature drop, that substantial sulfide precipitation would occur within the blanket and a situation similar to that discussed in the previous section would be realized. Eldridge et al. (1983) provide convincing evidence for thermal reworking of Kuroko mineralization.

It is also possible that under certain circumstances smoke from black smoker plumes could settle and accumulate around the plume. Thin tuff layers interstratified in Kuroko massive sulfide blankets, suggesting massive sulfide blankets, may in part accumulate by sedimentation of sulfide particles raining down from above the sea-sulfide blanket interface. For this model to work, bottom currents must not blow the sulfide smoke away before it has a chance to settle. Stokes law can be used to calculate the settling velocity of sulfide agglomerates; the requirement that sulfide particles settle within ~500 m of the vent (massive sulfide ore lenses are rarely larger than 500 m in their largest plan dimension) can then be used to constrain bottom current velocities.

Stokes law states that a sphere of radius, a, and density contrast with a surrounding fluid, $\Delta\rho$, will settle at a velocity, V, through a fluid of viscosity, μ:

$$V[\mathrm{cm/sec}] = \frac{2\Delta\rho g a^2}{9\mu}.$$

Taking μ = 0.01 poise, $\Delta\rho$ = 4 g/cc, g = 980 cm^2/sec, and a = 5 μm, we find a settling for velocity, for example, of 0.022 cm/sec. The smoke particles are agglomerates of smaller sulfide crystals and typically

less than 20 μm in diameter (e.g., Rise, 1980, fig. 6). The black smoke plume height at 21° N is, unfortunately, unknown, but if it were 50 m high and if the ocean bottom currents were equal to the sulfide settling velocity (0.022 cm/sec), the smoke particles would settle within 50 m of the plume. Figure 3 depicts the relationships between sulfide agglomerate diameter, the ratio of sulfide blanket diameter to plume height, and bottom current velocity. The shaded region indicates conditions required for effective sulfide sedimentation. The right boundary of the shaded region roughly corresponds to a plume height of 50 m and reflects the constraint that settling must occur within 250 m. The upper boundary indicates the smoke particles will have diameters less than 20 μm as at 21° N.

Figure 3 shows that very quiescent bottom conditions (< ~0.5 cm/sec) are probably required for sulfide accumulation. Currents in the vicinity of black smokers are sufficient to cause navigational problems for submersibles, and are probably typically ~0.5 knots (~25 cm/sec) (R. D. Ballard, pers. commun., 1982). The vertical velocity of the black smoker plume is 1 to 5 m/sec (Macdonald et al., 1980), so the plume rises nearly vertically and is not significantly disturbed by these bottom currents. Plume height is a critical observation that remains to be made. The important point is that if sulfide setting is an important process, economic massive sulfide deposits may only form in restricted seas or basins where bottom currents are unusually low.

Physical-Chemical Models of the Massive Sulfide Hydrothermal System

Simple heuristic calculations and available selected geologic evidence suggest that the intrusive heat source

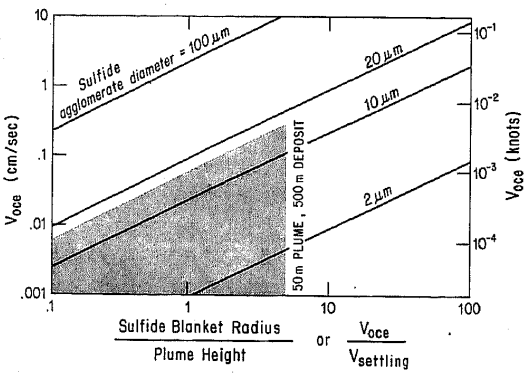

FIG. 3. Shaded area shows ocean current conditions which will allow agglomerated sulfide particles in the "smoke" of black smoker plumes to settle within 250 m of the vent chimney. Lines are for sulfide agglomerates of different diameter. Smoke particles in plumes on the East Pacific Rise at 21° N are agglomerates less than 20 μm in diameter. The right boundary of the shaded region assumes a 50-m plume height. The figure shows bottom currents must be very weak if sulfide smoke is to accumulate in a massive sulfide lense and not be blown away. V_{oce} = ocean current velocity.

responsible for Kuroku mineralization is at least 1.5 × 10^{11} metric tons and perhaps ~10^{13} metric tons. A vertical fluid flow rate in the vent area of ≲2,000 g/cm^2/yr is needed and this requires, with a 20-fold focusing of surface discharge into fractures, a bulk background permeability of at least 2.5 mD. The permeability of the sulfide blanket and fracture feeder system was at least 3 mD (to avoid slumping) and perhaps less than 250 mD (to avoid convection in the blanket). Unusually quiescent bottom conditions may have been required to allow accumulation of a sulfide blanket by settling of sulfide smoke. These conclusions fit well with the rifted-arc, restricted sea setting we envision for Kuroko mineralization (Cathles et al., 1983) and provide reasonable minimum starting values for regional permeability in our models.

The ultimate source of heat for the mineralizing hydrothermal system in the Hokuroku district in Japan was probably mafic magma that invaded the island-arc crust in response to the rifting and extension that occurred ~5 to 14 m.y. ago (Cathles et al., 1983). A composite intrusive mass of the requisite size can easily be produced by such an event.[2]

Heat could have immediately been scavaged by convecting pore fluids from injected dikes as spreading took place. Alternatively, a mafic magma chamber could have formed as the result of a pulse of spreading. Silicic magma bodies might have been produced by the mafic magma through differentiation or crustal melting. Either kind of magma chamber could have sustained local mineralizing hydrothermal systems. Caldera collapse of near-surface magma chambers could have prepared the ground for mineralization by fracturing the area intimately and increasing permeability and fluid/rock contact (Ohmoto, 1978).

In this section, we first examine physical models of convective cooling and impose the requirement that venting hydrothermal solutions be no hotter than 350° to 400°C. Almost all geothermal systems observed worldwide to date are less than 400°C; most are less than 300°C (McNitt, 1970; White, 1970). The black smokers at 21° N are at 350°C, yet vent rapidly enough to reflect (except for cooling by adiabatic expansion) the maximum temperature encountered by moving fluids at depth. Venting temperatures this cool require the permeability of an intruded mass to drop off sharply as temperature increases above ~300°C. The physical models also indicate the permeability conditions under which mafic magma chambers will form at spreading centers and provide an additional constraint on the combination of permeability and spreading rate. Be-

[2] An average spreading rate of even 1 cm/yr over 4 m.y. will cause an extension of 40 km, about the separation of the parallel Oū and Dewa Hills volcanic chains in the Hokuroku area. The Hokuroku basin is 40 km long. A composite mass 40 × 16 × 5 km has a mass ~10^{13} metric tons.

cause geologic evidence suggests ridge magma chamber formation is common, and calculations suggest magma chamber formation in rifted island arcs should be more likely than at ocean ridges, we select a reasonable physical model of the convective cooling of a small magma chamber. The chemical consequences of the convective cooling of this magma chamber are then investigated.

Physical models of convective cooling

Dike injection at a ridge: First consider the convective cooling of dikes that might be injected by crustal spreading. Accumulating evidence indicates spreading is episodic even at fast-spreading mid-ocean ridges such as in the East Pacific Rise (Ballard and van Andel, 1977; Hall and Robinson, 1979; van Andel and Ballard, 1979). Consequently, the model we consider (Fig. 4) is calculated for 200 m of total crustal extension, but that extension may occur at 2 cm/hr over 5,000 years, at 20 cm/yr for 500 years followed by no spreading for 4,500 years, or at 100 cm/yr for 100 years followed by no spreading for 4,900 years. The details of modeling are discussed in the first part of Appendix I. The flow pattern after 500 years for 20 cm/yr spreading in a domain of uniform 500 mD permeability is shown in Figure 5. The upflow is concentrated very near the ridge axis; the maximum temperature attained at the ridge axis (and the temperature of solution venting into the sea) is 332°C. As discussed in Appendix I,

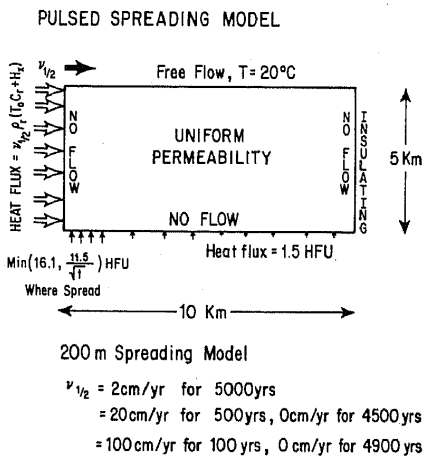

FIG. 4. The model parameters and boundary conditions chosen to model hydrothermal circulation near a spreading ridge and elucidate the conditions under which an axial magma chamber will form. Heat is introduced along the spreading axis at the left-hand side by dike injection as the crustal plate moves to the right with velocity $v_{1/2}$. Models assume spreading at rates between 2 and 100 cm/yr for periods of 5,000 to 100 years. In all cases the total amount of spreading (formation of new crust) is 200 m. In areas where new crust has been formed (either by the current or previous spreading pulses) basal heat flow is assumed to be the smaller of 16.1 or $11.5/\sqrt{t}$ HFU, where t is measured in millions of years. Elsewhere the basal heat flux is a normal 1.5 HFU. The results of calculations are shown in Figures 5 through 7. Spacing of the finite difference grid is very small near the ridge axis.

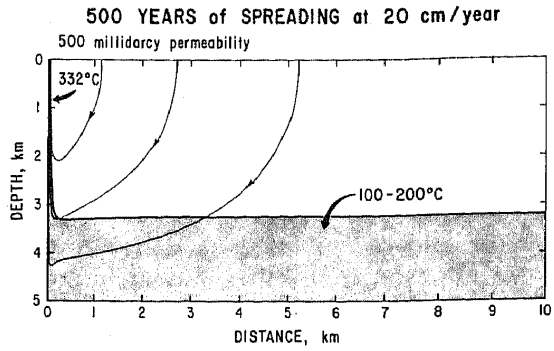

FIG. 5. Streamlines showing fluid circulation and isotherms for a 500-mD plate spreading at $v_{1/2}$ = 20 cm/yr. The flow and temperature pattern is shown after 500 years of spreading, but the pattern is little changed after the first 50 years. Notice fluid flow and high temperatures are concentrated very close to the spreading ridge axis. Model parameters and boundary conditions are given in Figure 4. The maximum fluid temperature is 332°C; this is also the temperature at which the fluids vent into the sea.

fluids are allowed to vent without temperature drop at the surface (i.e., the sediment or rock-water interface) if the convective transport of heat in the model calculation just below the surface is more than 25 percent of the conductive heat transport at the surface with the surface held at fixed, ambient temperature. This simulates rapid venting through a fracture or hot spring where there is generally little or no temperature drop as the fluid crosses the rock interface into the sea. Steady-state temperatures are attained after about 50 years of spreading.

Figure 6 shows the steady state venting temperature for the three spreading rates as a function of perme-

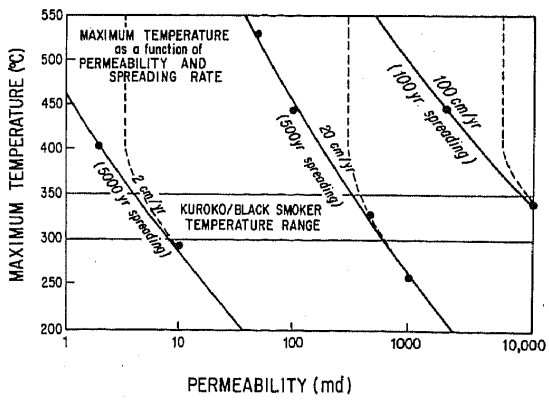

FIG. 6. The maximum temperature in calculations like that shown in Figure 5 as a function of spreading rate and plate permeability. Higher plate permeability is required to remove heat introduced at greater spreading rates and maintain equivalent temperatures. The range of temperatures observed in fluids venting into the sea in black smoker plumes at locations like 21° N on the East Pacific Rise, and inferred from fluid inclusion to vent during Kuroko mineralization, is shown. If rock permeability is reduced at temperatures above ~300°C, near-ridge temperatures will increase sharply as soon as fluid circulation becomes too weak to carry off heat as it is introduced. Under these circumstances magma axial chambers will form. This is shown by the dashed lines.

ability. In these models the permeability is the same throughout the computation domain—from the axis of dike injection out to 10 km from that axis. Figure 6 shows that at faster spreading rates, larger permeabilities are required to keep the venting temperature within the 300° to 350°C range observed for presently active hydrothermal systems. Fluid circulation must be faster (as allowed by higher rock permeability) if the heat that is introduced by dike injection and spreading is increased and fluid venting temperature is to be kept constant.

Spreading rate, particularly an episodic spreading rate, is likely to be quite variable. It is unlikely that country-rock permeability will always be such that solutions vent at ≲350°C. It is likely, therefore—and this conclusion will be reinforced in the next section—that permeability decreases quite strongly as rock temperature increases above ~300°C. A decrease in permeability above ~300°C is reasonable from a physical point of view. Flow in igneous rocks is fracture controlled. Fractures are propped open by mineral grains and topographic mismatches. At higher temperatures these grains and topographic bumps dissolve in pore solutions and redeposit in areas of lower rock pressures (Morrow et al., 1981). The critical temperature at which the rate of grain dissolution becomes significant in closing fractures might be calculated; ~300°C is not an unreasonable starting temperature for these processes (see, e.g., Morrow et al., 1981).

If the removal of heat from injected dikes is inhibited at temperatures above ~300°C, the curves in Figure 6 are valid only below ~300°C. If the rock becomes impermeable at ~400°C, maximum temperature curves might look something like the dashed high-temperature spurs shown in Figure 4. If continued, the spurs would extend upward to the dike injection temperature, 1,300°C, and indicate that if the country-rock permeability is too low to allow convection to carry off heat advected from the ridge axis, axial magma chambers will form. For example, if the country rock permeability is less than ~350 mD a magma chamber will be formed by a 20 cm/yr (half velocity) spreading pulse. Figure 7 summarizes the conditions for magma chamber formation.

Diverse geologic, topographic, and geochemical studies of mid-ocean ridges (see summary of Sleep and Rosendahl, 1979) indicate magma chambers are present at both slow (Atlantic) and fast (East Pacific Rise) spreading ridges. The magma chambers and zones of cumulated mush associated with fast spreading ridges may be larger (20 km wide and ~5 km thick) than the magma chambers associated with slow spreading ridges (~1 km wide and 2 km thick) as Sleep and Rosendahl (1979) suggest.

If spreading at the mid-Atlantic ridge occurs at 20 cm/yr for 500 years followed by 4,500 years of no spreading, Figure 7 shows that the existence of an axial

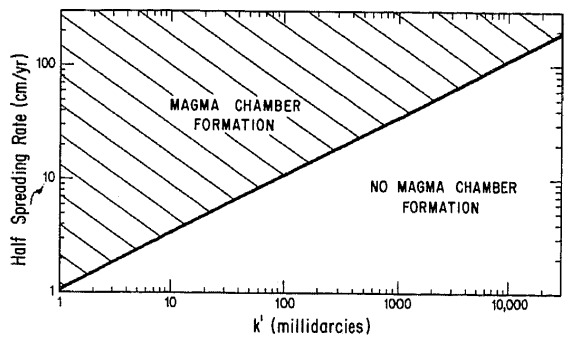

FIG. 7. The conditions (plate permeability and spreading rate) under which an axial magma chamber will form, summarized from Figure 6.

magma chamber requires the permeability of the middle portion of the oceanic crust be less than ~350 mD. The existence of a 1½ to 2-km-thick sheeted dike complex above the gabbro (solidified magma chamber) layer in ophiolite suites (e.g., Hopson et al., 1981) indicates that the near-surface permeability is high enough to prevent magma chamber formation even though the deeper permeability is low enough to allow a magma chamber to form. In the case of the mid-Atlantic ridge, the existence of a sheeted dike complex would indicate near-surface permeabilities greater than ~350 mD, if the episodic spreading rate were 20 cm/yr.

Because of vesicles, fracturing, and pillow formation, basalts are generally the most permeable type of crystalline rock (Brace, 1980). Hence both because magma chambers seem to form at all ocean ridges, and because low permeability favors magma chamber formation and the host rock permeability in an island arc is anticipated to be less than at an ocean ridge, spreading pulses will probably produce magma chambers in rifted island arcs. For this reason, our models from here on consider the convective cooling of small magma chambers.

Convective cooling of a small magma chamber: Figure 8 shows the cooling history of a 2.3-km-wide, 3.3-km-high intrusion where, from the start, the permeability of the intrusion and its surroundings is 1 mD. Figure 8 shows the effluent solutions at 5,000 years are hotter than 500°C. Figure 9 shows they are in fact 562°C at 5,000 years, having fallen from about 600°C at 4,000 years. Both figures unequivocally show that if a formation with permeability of 1 mD is intruded, and the intrusion is as permeable as the formation, the temperature of vented solution will be close to the initial temperature of the intrusion (700°C). Intrusion at depths greater than 1.7 km shown in Figure 6 would not significantly change the maximum temperature. The only effective way to decrease the temperature at which hydrothermal solutions vent is to make the intrusion less permeable or impermeable at higher temperatures. Stated another way we conclude

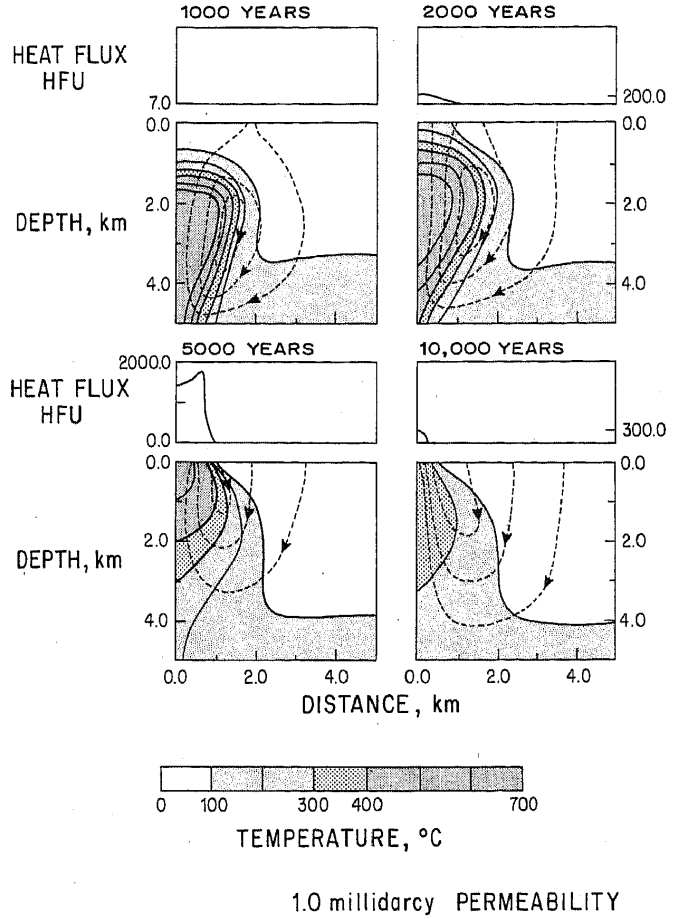

FIG. 8. Cross section showing the convective cooling of a 2.3-km-wide, 3.3-km-high intrusion if the permeability of both the rock intruded and the intrusion is a uniform 1.0 mD. Temperature ranges are shaded and demarcated by isotherms. Streamlines show the patterns of fluid circulation. The surface heat flow in HFU is plotted above each cross section. The intrusion cools in about 10,000 years. Fluids close to 600°C are vented at ~5,000 years after intrusion.

that intrusions hotter than ~350°C must be quite impermeable—otherwise surface venting of solutions 400° to 500° or even 600°C or hotter would be commonplace.

Figure 9 shows how decreasing rock permeability at temperatures >300°C affects the maximum temperature of effluent (i.e., surface crossing) solution. If the rock permeability decreases an order of magnitude for each 100°C above 300°C, the temperature of solutions vented through the rock surface do not exceed the maximum observed range.

The size of magma chambers at mid-ocean ridges is generally thought to depend on spreading rate. At fast rates, the magma chambers formed by multiple magma injections may be funnel-shaped—a kilometer or so wide at the base, ~20 km wide at the top, and ~8 km thick. For slow-spreading ridges the magma bodies are perhaps 2 km thick and 1 km wide (Hopson et al., 1981; Sleep and Rosendahl, 1979). Ocean-ridge magma chambers lie above a peridotite layer that deforms plastically. Isotopic studies indicate that little fluid flow takes place in the peridotite layer (Gregory and Taylor, 1981). The boundary between the gabbro layer, which represents the cooled magma bodies, and the peridotite layer is the oceanic moho.

In our modeling we choose to be conservative. We calculate the chemical consequences of convective cooling of a small magma body 3.25 km thick and 1.0 km wide intruded to 1.75 km depth (Fig. 10). Rock is considered impermeable below a depth of 5 km. The model is patterned after a magma chamber that might exist at a slow-spreading ocean ridge. The magma bodies at the Hokuroku district could have had a greater depth extent and could have been much wider—more like possible magma chambers at fast-spreading ocean ridges or like the Flavrian granite at Noranda. Fluids may well have circulated deeper than 5 km in the thicker island-arc crust of Japan. If, however, a single pulse of spreading and a small magma chamber can be shown to be able to produce the ore deposit of the Hokuroku district, multiple spreading pulses (~50, Cathles et al., 1983) or larger magma chambers can do so more easily. We will conclude later that a small magma chamber is appropriate for the Hokuroku area for other reasons.

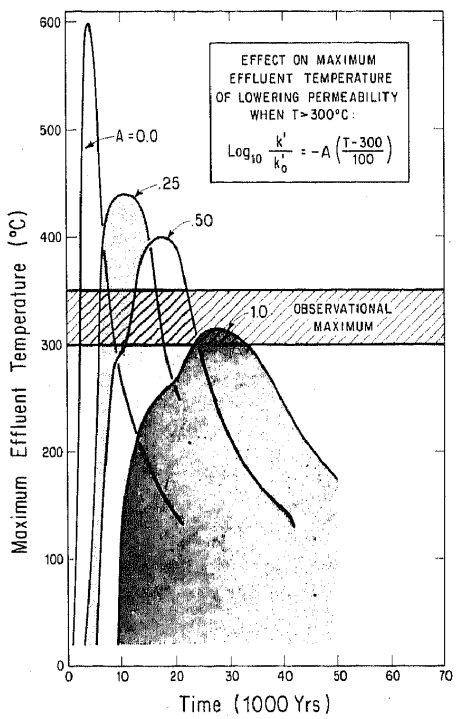

FIG. 9. The calculated maximum temperature of vented solutions drops rapidly if the permeability of rock is decreased exponentially from its base level, k_0, at temperatures above 300°C. Such a temperature dependence on permeability is reasonable because the rate of rock dissolution reactions increases rapidly at T > 300°C, allowing removal of the topographic irregularities that prop fractures open and make them permeable (see discussion in previous section of text). If A in the formula shown is given a value of ~1.0, the calculated temperatures of venting fluids are within the range geologically observed.

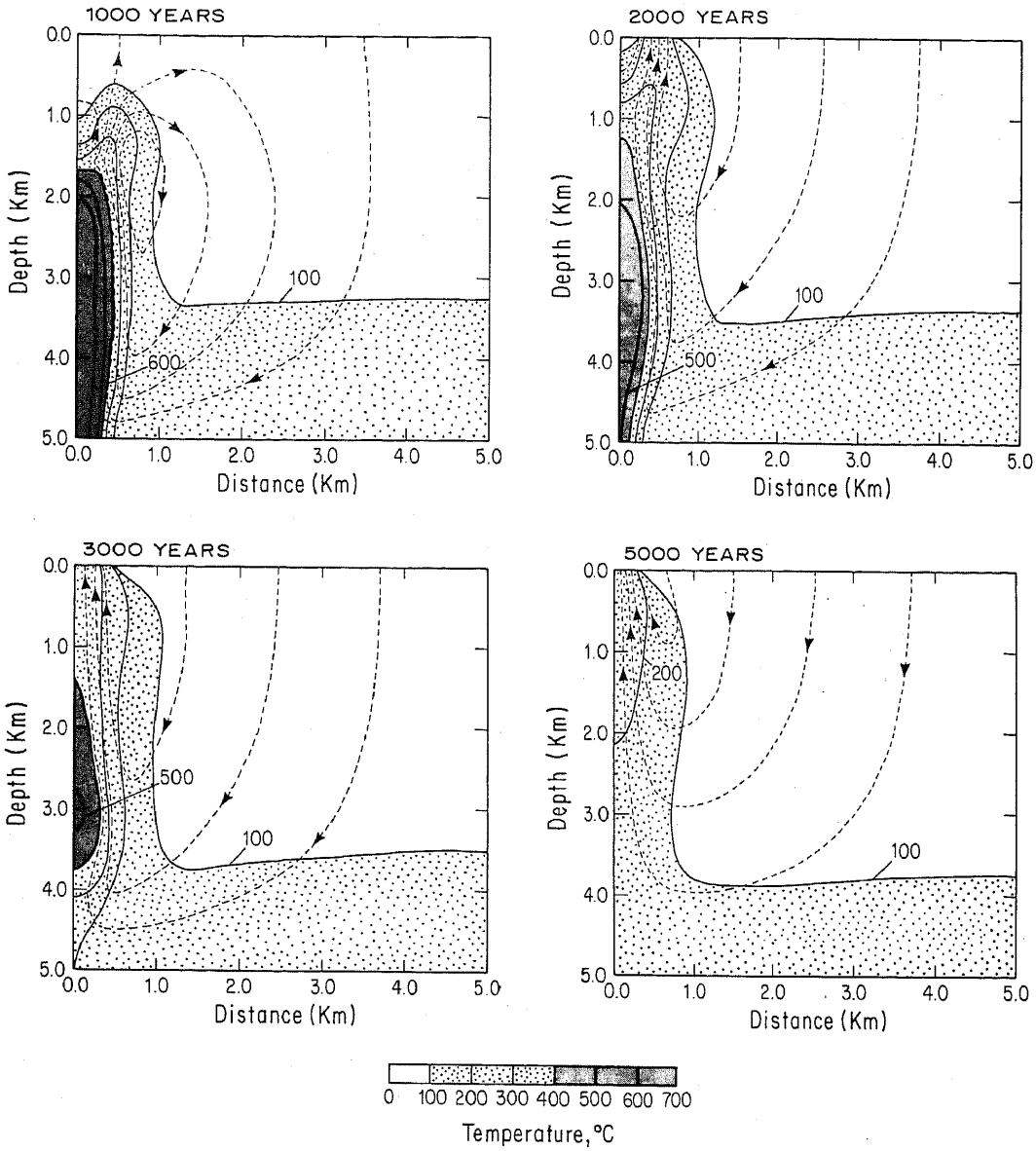

FIG. 10. Cross section showing the convective cooling of the base case magma chamber used in subsequent chemical calculations. The magma chamber is 1.0 km wide and 3.25 km high. Permeability is 5.0 mD but is decreased by a factor of 5 for each 100°C above 300°C in rock hotter than 300°C. Flow lines and isotherms are shown at 1, 2, 3, and 5 thousand years after intrusion. Notice the fluid avoids (circulates around) the pluton when it is hot and relatively impermeable. Fluid gains access to the intrusion only after it has cooled to ~350°C.

Figure 10 shows how the basic magma chamber we consider henceforth is cooled by ground-water convection. The regional permeability is 5 mD but is decreased by a factor of 5 for each 100°C above 300°C. The calculations are carried out on a finite difference grid 39 points wide and 29 points high. Point spacings are much smaller at the intrusion side and top of the computation domain. The grid points are 35 m apart at the left side but 520 m apart at the right side, 20 m apart at the top surface but 260 m apart at the base. This grid is fine enough to allow calculation of the convective cooling of a 5-mD domain. A finer grid would be required to compute the cooling histories of higher permeability domains. Since computation time increases on the square of the number of grid points on a side, and a large number of calculations are required to understand the chemical consequences of the convective flow, we limit our investigation to permeabilities of 5 mD or less.

Figure 10 shows that flow lines avoid the magma chamber until it is quite cool, as required by the temperature-dependent permeability. By 5,000 years after intrusion, the temperature is everywhere less than 300°C. The thermal history of solutions that vent

through the rock surface is shown in Figure 11. In this calculation solutions 300°C or hotter vent for about 3,000 years—from roughly 2,000 years after the sudden formation of the magma chamber to ~5,000 years. The maximum temperature attained by venting solution is 362°C, but the temperature of the most rapidly venting solution is always close to 300°C (Fig. 11)—a consequence of the temperature dependence of permeability in the model.

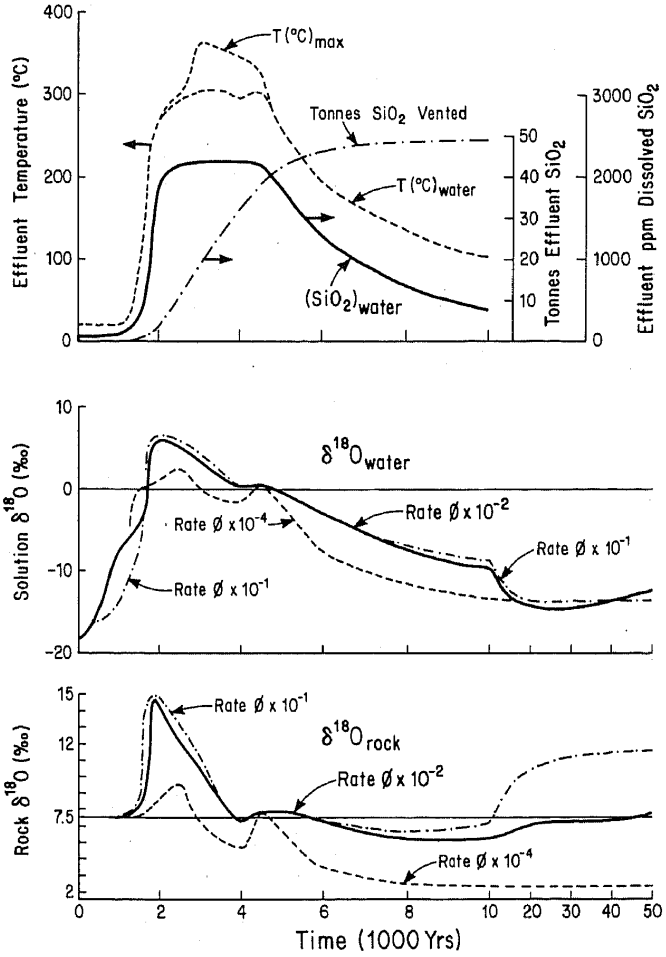

FIG. 11. Properties of the hydrothermal fluids that most rapidly vent the surface in the model shown in Figure 10. The temperature of the fluid most rapidly discharging into the sea increases sharply at the time of arrival of the thermal front (at ~1,500 years) and remains at about 300°C. The maximum temperature of vented solution is 362°C. Also shown is the concentration of amorphous dissolved silica, the total cumulative amount of silica discharged into the sea, and the $\delta^{18}O$ of the discharging fluid and rock at the seawater-rock interface for various kinetic rates of oxygen exchange. The dissolved silica and $\delta^{18}O_f$ are given for solutions that are at the rock-water interface and that are moving most rapidly across that interface (i.e., for the most rapidly venting solutions whose temperature is plotted in the top diagram). As discussed in the text the amount of silica vented could account for the paleosurface silicification observed at Noranda. The history of $\delta^{18}O_w$ venting matches very well the history of the Fukazawa Kuroko deposit in Japan. The final $\delta^{18}O_r$ alteration is compatible with that observed in Kuroko deposits in Japan and elsewhere.

In cooling, the intrusion shown in Figure 10 circulates 8,160 metric tons of hydrothermal solution hotter than 300°C through the top (rock) surface. This water mass is 18.6 percent of the mass of the intrusion, in good agreement with our heuristic estimate of 22 percent. If the intrusive dike system extended the full 40 km length of Hokuroku basin, the total mass of water vented above 300°C would be 3.3×10^{10} metric tons. If this fluid precipitated 100 ppm Zn + Cu + Pb upon being thoroughly quenched by seawater, 3.3 million tons of metal would be precipitated. This is nearly the 4.5 million metric tons of estimated metal resources of the Hokuroku basin (Table 1). Thus a single spreading pulse such as shown in Figure 10 (say 100 cm/yr half-spreading rate lasting for 500 years) could almost account for the total metal resource of the Hokuroku district of Japan. As we shall see later, there were almost certainly many such spreading pulses and massive sulfide mineralization is associated with at least several of the pulses.

Before turning to calculation of chemical alteration it is useful to gain a feeling for how fast fluid circulates through the system shown in Figure 10—how quickly a nonreactive tracer component would permeate the rock environment. Figure 12 answers this question. The total rock porosity is assumed to be 2 percent and the inert tracer (say salinity) is assumed to have enough time to diffuse into and saturate the impermeable matrix blocks between flow fractures as the fluid moves through the rock formation. This is true everywhere provided the flow fractures are less than about a meter apart. If the flow fractures are farther apart than this, the tracer front in the flow fractures will move through the rock formation faster than shown in Figure 12, with tracer-unsaturated regions left behind between flow fractures. Such a fracture tracer front could move through the formation in an order of magnitude or more faster than shown in Figure 10.[3]

Figure 12 shows the tracer will break through and vent into the sea after about 1,700 years, having saturated a rock pathway from intake to discharge. Thus, in this particular calculation, by the time the thermal front reaches the surface at about 2,000 years (see Figs. 10 and 11), the intake fluid will control the chemistry of the fluid discharged for those solution components that do not react quickly with the rock, or which are carried at much greater concentration in the circulating fluid than they can be stored in altered rock. The relative time of arrival of the thermal and trace fronts is sensitive to the formation porosity and depth to the top of the intrusion.

[3] This would require flow fractures to be about 10 m apart in the region of rapid (~200 g/cm²/yr) upflow along the left side, and about 30 m apart in the slow (~10 g/cm²/yr) zones of inwelling. See Cathles (1981) for methods of calculation.

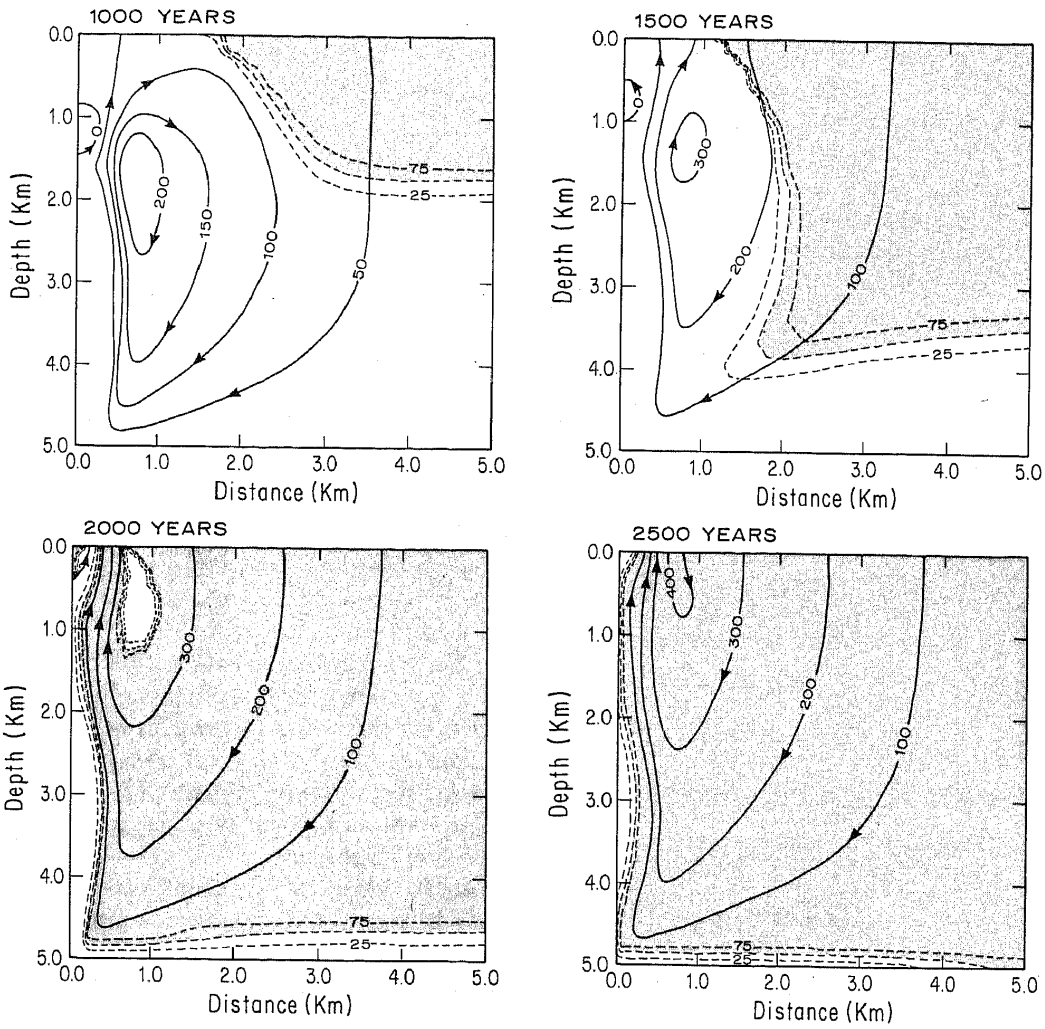

FIG. 12. The movement of a nonreactive tracer, initially confined to the sea, through the rock formation assuming a 2 percent total accessible (by flow or diffusion) formation porosity. Breakthrough of tracer (i.e., the first tracer in venting fluid) occurs about 1,700 years after intrusion and the start of circulation. Notice the point-tracking method gives excellent resolution of the tracer front (25% and 75% contours are shown), especially where the grid spacing is small along the vertical edge of the hot intrusion. Streamlines (lines with arrows) are also shown.

Figure 13 shows the integrated fluid mass flux in kg/cm^2 that has passed points in the calculation domain at various times after intrusion. This figure is useful for estimating bulk water-rock ratios. The figure shows, for example, that the integrated mass flux at 5,000 years is 50 to 60 kg/cm^2 in the areas of fluid intake on the right-hand side of the diagram. The mass of the rock column is 270 kg/km, so the bulk mass water-rock ratio at 1 km depth is about 0.2 g water per g rock at 5,000 years. At 5 km depth, it is about 0.04, and at 100 m depth about 2.0. After 50,000 years, the water-rock ratio in the intake areas is ~0.5 at 1 km depth. Note that substantial fluid circulation is sustained by the 1.5 HFU basal heat flux. Note also that mass fluxes are an order of magnitude greater in the upflow (discharge) zone at the left.

Chemical consequences of convective cooling

Chemical alteration that does not depend on rock composition: Two kinds of chemical alterations that do not depend strongly on rock composition are silica and anhydrite dissolution and precipitation. Both are important to the Kuroku environment. Silicified stockworks underlie many massive sulfide deposits. Massive anhydrite (gypsum) is associated with massive ore; anhydrite veins are present in feeder networks and in the massive ore lenses.

Bischoff and Seyfried (1978) have shown that SO_4^{-2} in seawater is precipitated first as anhydrite and then as magnesium hydroxy sulfate minerals if the seawater is heated above 150°C. If Ca^{+2} is present from alteration of formation minerals (we assume it

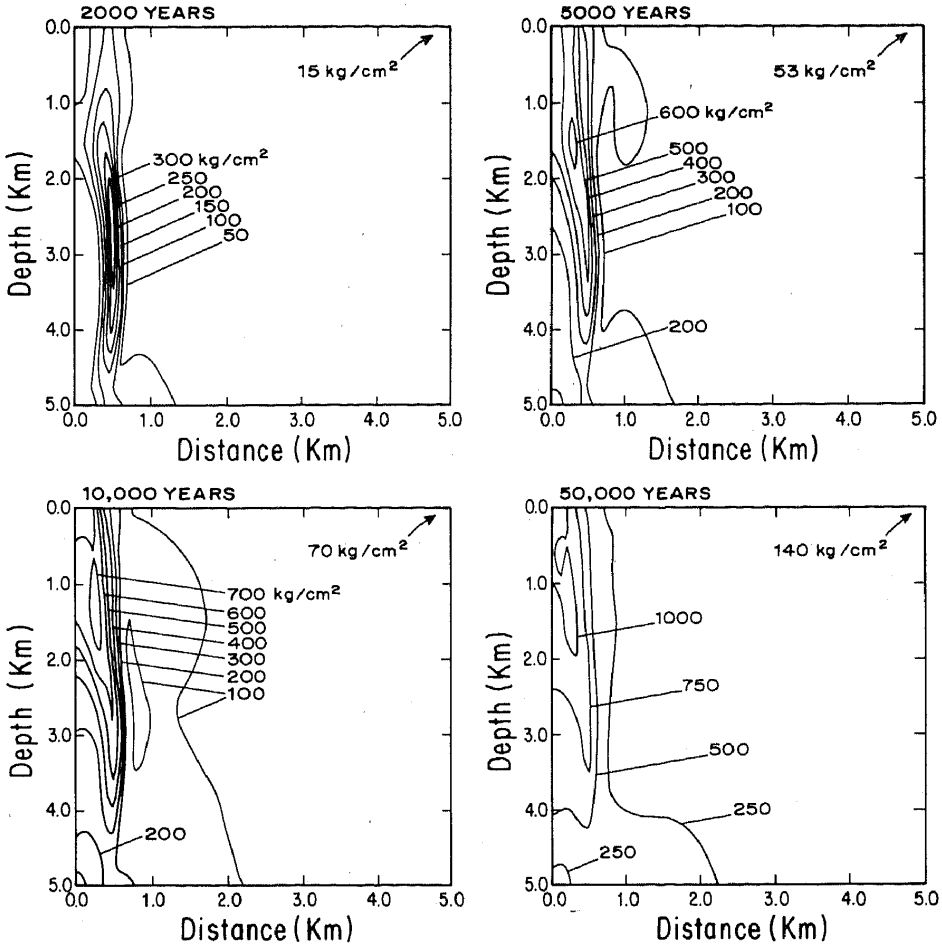

FIG. 13. Integrated mass flux of hydrothermal fluid through a unit area perpendicular to flow (in kg fluid/cm²) is contoured for different times after intrusion. The intake mass flux in the upper right of the computation domain is also shown (e.g., 15 kg/cm² at 2,000 yrs.). With a 5-mD permeability, significant convective circulation persists after the intrusion has cooled, driven by the normal basal heat flow of 1.5 HFU. As discussed in the text, the integrated mass flux may be used to estimate fluid/rock mass ratios.

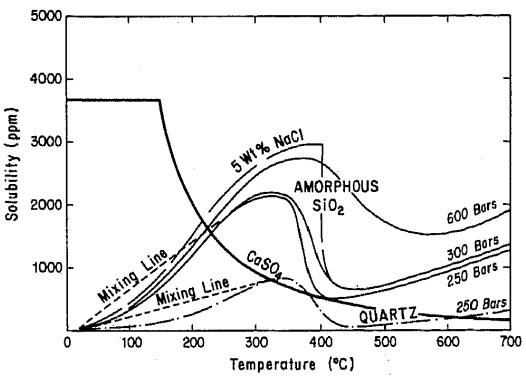

is), the 2.7×10^{-2} moles of SO_4^{-2} in seawater will all be precipitated as anhydrite. Each gram of seawater thus can precipitate ~3.7 mg of anhydrite. The solubility of silica depends on both temperature and fluid density (Fournier and Rowe, 1977). The expression we use for amorphous silica solubility is given and discussed in the second section of Appendix II. Figure 14 gives, as a function of temperature, the pressure-dependent solubility of silica and the solubility of anhydrite that we use in modeling.

FIG. 14. The equilibrium solubility of anhydrite as a function of temperature and of silica as a function of temperature and pressure. The concentration of anhydrite in grams $CaSO_4$ per gram of solution is assumed to equal 3.68×10^{-3} times the minimum of [1.0, $(150/T)^2$]. This matches well the curves shown in Bischoff and Seyfried (1978). The amorphous silica solubility curves are from a formula deduced from figures in Fournier and Rowe (1977) as discussed in Appendix II. One curve is for solutions containing 5 wt percent NaCl at 300 bars. This curve crosses the two phase boundary from liquid to vapor at 409°C. All the other curves are supercritical. The bottom curve shows the solubility of quartz silica and is calculated using a regression formula provided by R. O. Fournier (written commun.). Lines showing the consequences of mixing with cold seawater containing no dissolved silica are shown for the two 250-bar curves. Mixing will lead to solutions saturated in silica for solutions cooler than ~300°C. For solutions hotter than 300°C, the shape of the silica solubility curve is important. Silica precipitation will not easily occur between ~300° and 400°C.

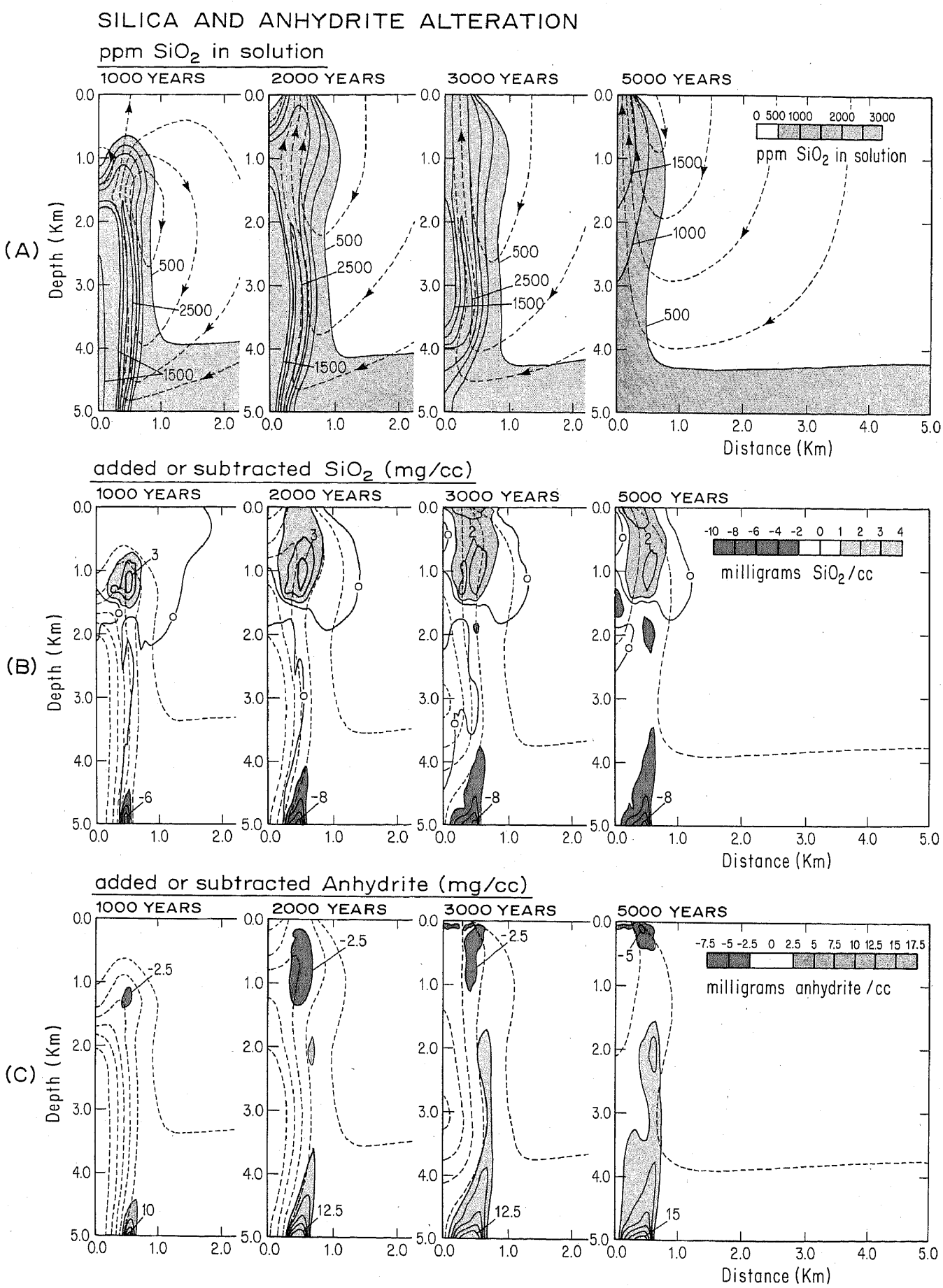
SILICA AND ANHYDRITE ALTERATION
ppm SiO2 in solution
1000 YEARS
2000 YEARS
3000 YEARS
5000 YEARS
0 500 1000 2000 3000
ppm SiO2 in solution
(A)
Depth (Km)
Distance (Km)
added or subtracted SiO2 (mg/cc)
-10 -8 -6 -4 -2 0 1 2 3 4
milligrams SiO2/cc
(B)
added or subtracted Anhydrite (mg/cc)
-7.5 -5 -2.5 0 2.5 5 7.5 10 12.5 15 17.5
milligrams anhydrite /cc
(C)

Figure 15 shows how silica and anhydrite are redistributed by the hydrothermal system of Figure 10. The model assumes realistic chemical kinetics for silica dissolution and precipitation. The surface supporting the heterogeneous dissolution or precipitation is assumed to be restricted to flow fracture surfaces. Twenty percent of the fracture surface is assumed to be amorphous silica or its kinetic equivalent. The fracture surface area per unit volume is calculated from permeability, as discussed in Appendix II. Anhydrite is assumed always to be in equilibrium with the fluid. That is, we assume the kinetics of anhydrite precipitation or dissolution are effectively infinitely fast. The calculations show that solution silica concentration is out of equilibrium (e.g., different from the saturation value) only very near the surface at inflow zones or in the cool area above the thermal anomaly before the thermal anomaly reaches the sea-rock interface. The kinetics of silica dissolution and precipitation thus do not significantly control the pattern of silica alteration except near areas of surface inflow. In other areas, alteration is dominantly controlled by temperature and fluid flow, as in the case of anhydrite.

Consider Figure 15 from this equilibrium viewpoint. Solution silica concentration accurately reflects temperature (compare Fig. 15A to Fig. 10). The maximum silica concentration is ~2,800 mg SiO_2/kg solution in an anulus around the hot intrusion at temperatures of ~350° to 400°C. At higher temperatures, the silica concentration at first drops (due to the density decrease of the fluid) and then increases again. Anhydrite solubility (not shown) would also mirror the temperature distribution, with the solubility dropping quickly toward zero inside the 150°C contour.

Flow lines indicating the pattern of fluid circulation are shown in Figure 15A. Initially, fluid circulates up the temperature gradient as it approaches and enters the intrusion and down the temperature gradient as it travels above the thermal anomaly of the pluton. Later, after the intrusion's thermal anomaly has reached the surface, fluid circulates up the temperature gradient as it approaches and enters the intrusive heat anomaly, and then moves nearly isothermally to the surface. As the fluid approaches the intrusion (and temperature increases), silica is removed from the rock (Fig. 15B). This is a mass balance requirement—silica concentration increases in solution and this silica is taken from the rock. Where the fluid circulates above the intrusion's thermal anomaly, the silica concentration decreases in the cooling fluids and silica is precipitated as fast as is kinetically allowed. A positive silica anomaly (e.g., zone where silica is added to the rock) thus moves upward with the pluton's thermal anomaly. A fringe of silica depletion records areas of solution inflow. Actually a ring of depletion roughly surrounds the original intrusion. The upper part or cap of this ring results from the density dependence of silica solubility. Hot but low density fluid has a lower silica concentration than cooler, more dense fluids above (see Fig. 15B) and upward circulation therefore adds silica to solution and removes it from the rock formation.

Exactly the same principles apply to anhydrite. Here the model always assumes complete equilibrium. Anhydrite is precipitated around the edges of the intrusion (where silica is dissolved), because in these regions seawater has circulated up the temperature gradient and anhydrite has a retrograde solubility. Anhyrite is dissolved above the top of the intrusion where fluid moves down the temperature gradient. Of course, this is realistic only if anhydrite is present in the rock, perhaps from the operation of previous hydrothermal systems.

The magnitude of silica and anhydrite addition or subtraction is small. For silica about 2 mg/cc (0.07 wt %) silica is removed or added. For anhydrite about 5 mg/cc (0.2 wt %) is added and 2.5 mg/cc (0.1 wt %) removed. The added anhydrite would correspond to roughly a 1-cm vein of anhydrite every 6 m or a 1-mm vein every 60 cm. The added silica would correspond to a 1-cm vein every 10 m or a 1-mm vein every meter.

The amount of silica and anhydrite dissolved or precipitated can be estimated. The heat capacity of rock is ~0.54 cal/cm^3/°C whereas that of water is about 1 cal/g/°C. Therefore, a thermal front will migrate at about twice the darcy velocity and the water-rock ratio during passage of the front will be about 0.5 g fluid/cm^3 rock. The chemical anomaly left behind should therefore be about half the concentration drop across the thermal front or about ±1.2 mg SiO_2/cc and ±1.8 mg anhydrite/cc. Generally, the anomalies shown in Figure 15 are of this magnitude. Higher values result where conductive heat transfer slows the migration of the thermal front. The anomalies at the base of the intrusion are also greater because the heat capacity of the intrusion has been increased to take into account crystallization effects. The most important point here is that the amount of silica and anhydrite precipitated or dissolved at any point in the subsurface is not very large.

FIG. 15. Silica and anhydrite dissolved and precipitated by the hydrothermal circulation shown in Figure 10. Anhydrite is assumed always to be at equilibrium concentration in the fluid (see Fig. 14), but the kinetics of silica dissolution or precipitation are taken into account in silica redistribution. Silica is dissolved by fluids circulating up the temperature gradient into the intrusion and is deposited by solutions that circulate down the temperature gradient above the intrusion. The concentration of silica in solution at various times is shown. Anhydrite is precipitated as solutions warm, and dissolved (assuming it is present) as solutions cool.

On the other hand, the amount of silica vented into the sea is quite large. Figure 11 shows that about 50 tons of SiO_2 is dumped into the sea—mostly in the first 6,000 years of cooling. This occurs across a strip ~0.5 km wide (Fig. 15A). By convention the calculations apply to a 1-cm-thick cross sectional slice of rock. Thus, 50 metric tons of silica vent through the rock surface area of $\sim 5 \times 10^4$ cm^2. If precipitated within 20 m of the surface (the computational grid is too coarse to model this kind of very near surface precipitation), the silica content of the rock would be increased 18.5 weight percent. The paleosurface silicification observed at Noranda and discussed in the first part of this paper, therefore, could be produced by a system similar to the one in our model. To account fully for the silicification at Noranda about 20 of our model dikelike intrusions each 20 km long would be required.

Chemical alteration that depends on rock composition: Oxygen isotope alteration differs from that of silica and anhydrite because the equilibrium isotopic composition of the fluid depends on the isotopic composition of the rock. The composition of the rock thus in part determines the course of alteration. Chemical kinetics are probably of greater importance in the isotopic exchange reactions than in the silica reactions discussed in the last section. As discussed in Appendix II, we envision that at any time active oxygen isotope exchange occurs in a fraction of the total rock mass. Active exchange occurs at the far edge of the alteration halos that surround flow fractures. Spooner et al. (1977a) have noted oxygen isotope alteration is related to the proximity of fractures. Given an estimate of the rock surface area exposed to pore fluids in the matrix blocks, a laboratory-determined kinetic model (Cole, 1980) predicts how fast the rock mass alters if 100 percent of the matrix is contacted. This rate is referred to as rate ϕ in Figures 17 to 20. This maximum rate of alteration is reduced by various estimates (10–0.01%) of how much of the rock will be altering at any given time. From estimates of the width of the oxygen isotope exchange halo and a reasonable guess at the distance between fractures transmitting fluid at any given time (Appendix II, last section), the most reasonable estimate of the fraction of rock undergoing alteration at any time is about 1 percent. Another uncertainty in the kinetic alteration-isotopic exchange model is its temperature dependence. We assume an activation energy of 15 kcal/mole. This is larger than indicated by experimental results. Thus, we may underestimate the rate of alteration at temperatures below ~100°C.

An important aspect of the model is the fractionation factor that gives, as a function of temperature, the difference beween the isotopic composition of rock and the water in equilibrium with it. We use the glass and small crystal smectite-water curve determined by Cole (1980) for basalt. This fractionation curve is used because (1) it is consistent with the kinetic model which is also adopted from Cole, and (2) it predicts that 0 per mil water will be in equilibrium with ~7.5 per mil rock at 300°C, which is observed to be the case in and near the Kuroko massive sulfide deposits in Japan (Green et al., 1983). Other commonly used smectite-water or rock-water fractionation curves would predict considerably different results (Fig. 16). For example, the general rock-water fractionation curve recommended by Taylor (1974) gives $\Delta_{rwe} = 4.6$ per mil at 300°C; O'Neil and Taylor's (1969) muscovite water curve gives $\Delta_{rwe} = 3.0$ per mil at 300°C (see Fig. 16). We assume the isotopic composition of the water is controlled by the smectites and chlorites that are readily formed by hydrothermal alteration of the glass components of basalt.

Figure 17 shows the evolution of the isotopic composition of water in the hydrothermal system of Figure 10. The rock is assumed to have an initial $\delta^{18}O_r$ of 7.5 per mil everywhere (see Green et al., 1983). The oxygen isotope equilibrium fractionation between rock and water used in our model is considerably greater than 7.5 per mil at temperatures below 300°C. Consequently, the water in most of the calculated domain is considerably lighter than 0 per mil. This general picture is modified by two phenomena. First, seawater

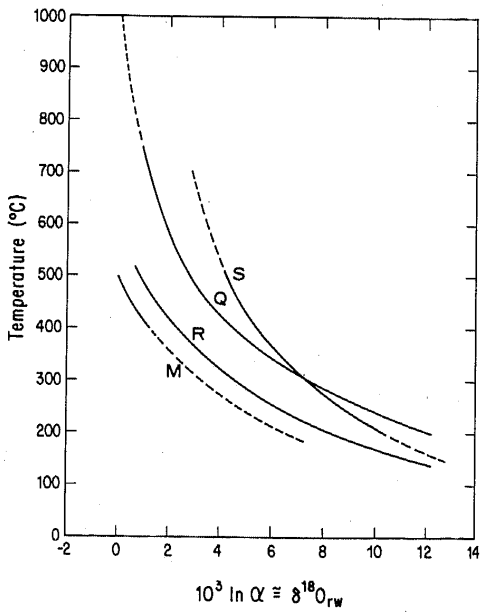

FIG. 16. The $\delta^{18}O_{rw}$ fractionation curves for various minerals. S is the smectite-water curve determined by Cole (1980) for basalt discussed in Appendix II and used in this study. Q is the quartz water curve of Clayton et al. (1972), R is the general rock-water curve recommended by Taylor (1974), and M is the muscovite water curve measured by O'Neil and Taylor (1969). The figure is largely after those in Friedman and O'Neil (1977). Note that these fractionation curves are quite different. The results of our calculations depend significantly on our choice of curve S.

with $\delta^{18}O = 0$ per mil flows into the rock domain over most of the top surface. The exchange kinetics are slow enough that the 0 per mil seawater penetrates a substantial distance into the crust before equilibrium is reached (see Fig. 18). Thus on the left-hand side of Figure 17, $\delta^{18}O$ water decreases from the seawater value of 0 per mil downward. If kinetics are fast (rate $\phi \times 10^{-1}$ or rate $\phi \times 10^{-2}$), the water comes into equilibrium with the rock at depths of two to three kilometers. The $\delta^{18}O$ then increases again, due to the normal increase in temperature with depth (Figs. 10 and 17).

Second, the thermal anomaly associated with the hot intrusion reduces the fractionation factor between rock and water. The water in the hot areas has a positive $\delta^{18}O_w$ as a result. This positive anomaly continues above the thermal anomaly of the intrusion because the exchange kinetics are not fast enough to erase it as soon as the anomalous fluid circulates upward into cooler rock (see Fig. 18).

Figure 18 shows where the water is out of equilibrium with the rock. In areas where the $\delta^{18}O$ of water differs from the value it would have if it were in equilibrium with the rock, chemical kinetics controls the rate of isotopic alteration. In areas where $\delta^{18}O_w - \delta^{18}O_{we} \sim 0$, alteration can still take place, but the rate of alteration is controlled by fluid flow and temperature not by chemical kinetics. Fluid flow and temperature control the rates of alteration at temperatures above ~100°C except for the rate $\phi \times 10^{-4}$ case, where the kinetic cutoff temperature is ~200°C.

Oxygen iosotope rock alteration is shown in Figure 19. In the equilibrium zones of the rate $\phi \times 10^{-1}$ and rate $\phi \times 10^{-2}$ cases ($T \gtrsim 100°C$), negative oxygen isotope anomalies are produced where cool fluids circulate into the hot intrusion; positive oxygen isotope anomalies are produced where hot fluids circulate into cooler regions above the intrusion. The reason for the anomalies is the same as for the silica and anhydrite anomalies. The fractionation factor between water and rock is greater at low temperatures than at high. Thus if a fluid circulates (in equilibrium) up a temperature gradient through 7.5 per mil rock, the water will become heavier (decreasing fractionation factor). The ^{18}O required to make the water heavier will be provided by the rock, which consequently will become lighter. Conversely, when water circulates from a hot region to a cool one, the fractionation factor becomes bigger—the water becomes lighter and the rock heavier.

As in the case of silica and anhydrite we can roughly estimate the magnitude of rock oxygen isotope anomalies associated with moving temperature anomalies. Fluid circulating into the intrusion goes from regions of ~100° to ~350°C. Fluid circulating through the top of the thermal anomaly goes from ~350° to ~100°C. At 350°C $\Delta_{rwe} = 6.17$ per mil and at 100°C $\Delta_{rwe} = 16.1$ per mil. Above 100°C fluid and rock are always close to equilibrium. Thus, the fluid experiences a change in isotopic composition of ~ ±10 per mil in moving through a thermal front. Since water contains ~0.055 moles O/g, rock contains ~0.37 moles O/g, and ~0.2 g_{H_2O} is required to move a thermal anomaly through one gram of rock, we would expect pluton-associated isotope anomalies of ~ ±3 per mil.[4] This is about what is initially observed (Fig. 17). The isotope fronts have a tendency to increase in magnitude as they migrate because changes in the isotopic signature of the rock increase the drop in fluid isotopic signature across the thermal front.

The heavy oxygen isotope anomaly can be seen to follow the intrusive heat anomaly upward till it impinges and breaks through the surface. Continued circulation punches a hole through the positive anomaly. Thus $\delta^{18}O_r$ in the vent area first increases to ~ ±15 per mil (rate $\phi \times 10^{-1}$ and rate $\phi \times 10^{-2}$) as the thermal front arrives, and then decreases to ~7.5 per mil or a little less as the positive anomaly is punched through (see Fig. 11 also). The water in the most active vent area increases from large negative signatures to ~7 per mil at the arrival of the thermal and positive oxygen isotope rock anomaly, and then decreases to ~0 per mil in the subsequent stages of 300°C venting. When the system cools, the $\delta^{18}O_w$ in the vent area decreases in equilibrium with the ~7.5 per mil rock as required by the increasing fractionation factor (Fig. 11).

Figure 20 shows the rock alteration for two much less permeable systems (rate $\phi \times 10^{-2}$ kinetics). The same general features are observed. The extent of alteration for the 0.2 mD case is dramatically reduced, emphasizing the importance of fluid flow in producing alteration.

Finally, Figure 21 shows the alteration for all models after 50,000 years. The three 5-mD cases show the pattern of alteration is strongly kinetics dependent. Faster kinetics produces a large positive isotope anomaly at inflow zones. This anomaly is underlain by a weaker but still substantial negative anomaly at depth. For slower kinetics (rate $\phi \times 10^{-4}$ case) there is no near-surface positive anomaly and no underlying negative anomaly. The near-surface positive anomaly is weakened and moved to depth.

The figures for 1-mD and 0.2-mD base permeabilities, when compared to the 5-mD rate $\phi \times 10^{-2}$ case, show that the depth extent of the positive inflow anomaly is controlled by the fluid flow rate as well as kinetics. The very near surface oxygen isotope alteration is controlled by kinetics alone and is the same for the three different permeabilities. Permeability (the total amount

[4] 3 per mil = (10‰) (0.2 g_{H_2O}/g) (0.055 mole O/g rock)/(0.037 mole O/g rock).

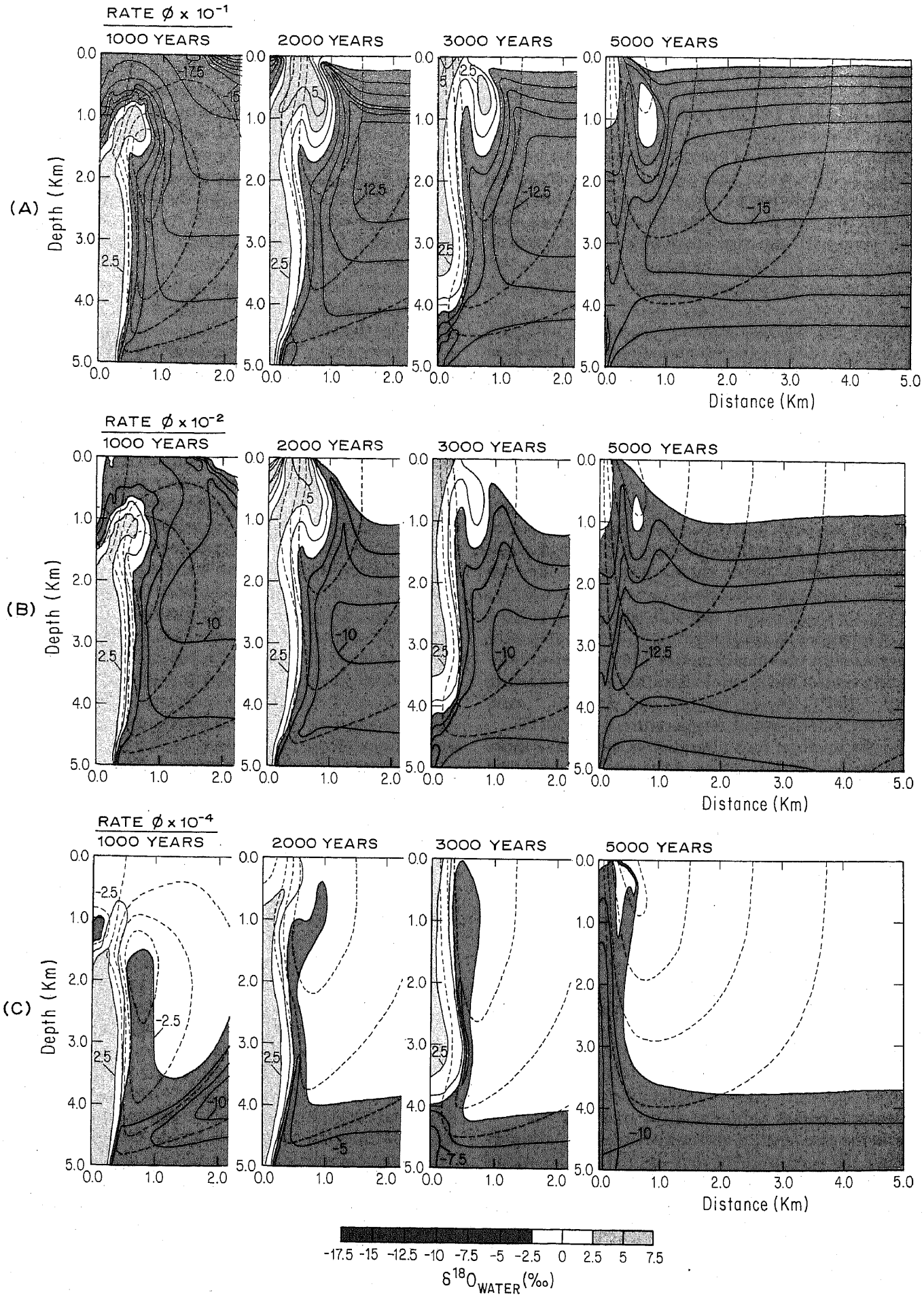
RATE Ø x 10⁻¹
1000 YEARS
2000 YEARS
3000 YEARS
5000 YEARS
(A)
Depth (Km)
Distance (Km)
RATE Ø x 10⁻²
(B)
RATE Ø x 10⁻⁴
(C)
-17.5 -15 -12.5 -10 -7.5 -5 -2.5 0 2.5 5 7.5
δ18O WATER (‰)

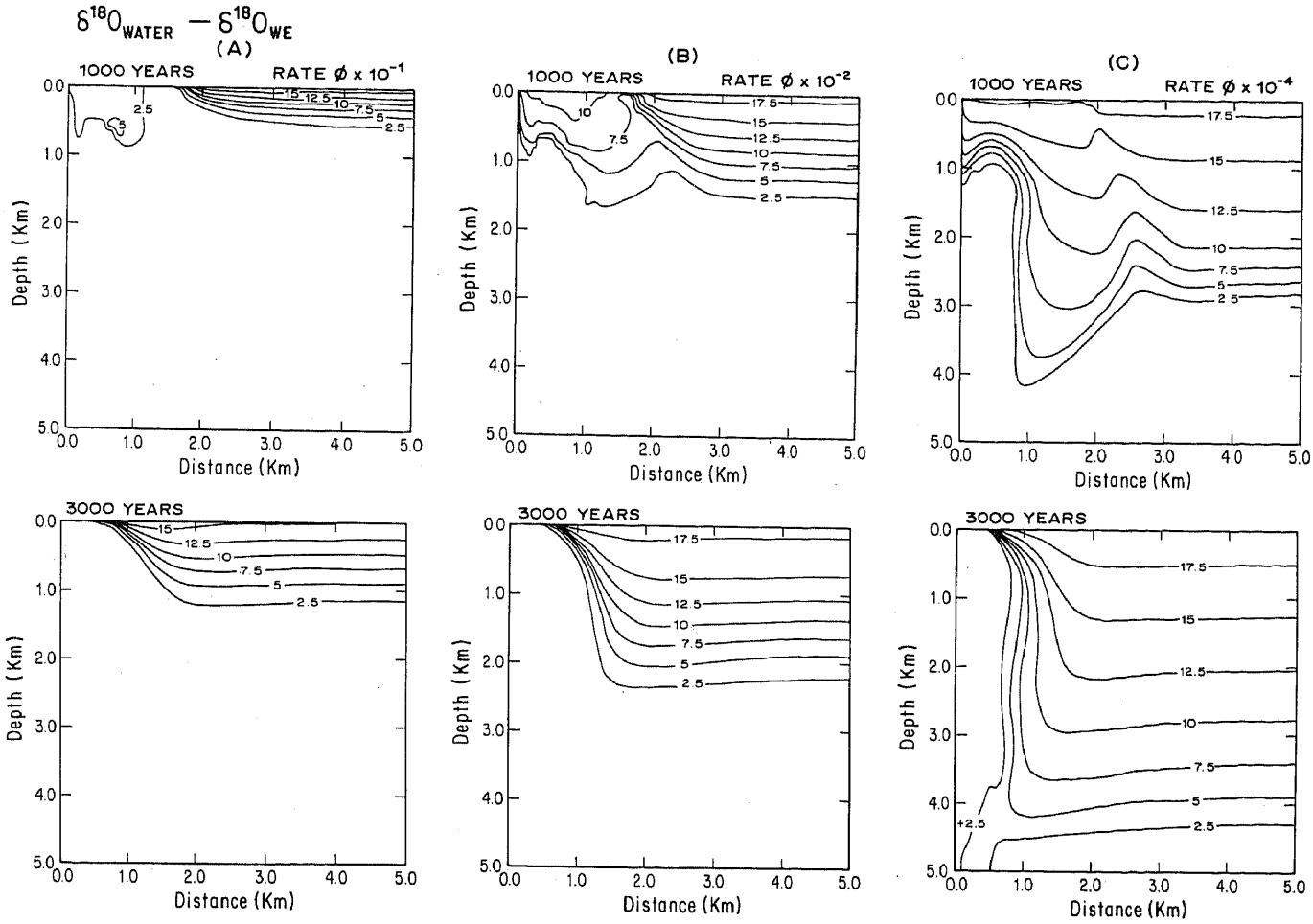

FIG. 18. The degree of fluid oxygen isotope disequilibrium with the rock is contoured for the three kinetic cases considered at 1,000 and 3,000 years. Comparison with Figure 10 shows that significant isotopic fluid-rock disequilibrium occurs where temperatures are $\lesssim$50°C for the rate $\phi \times 10^{-1}$ case, $\lesssim$75°C for the rate $\phi \times 10^{-2}$ case, and $\lesssim$175°C for the rate $\phi \times 10^{-4}$ case. Where significant disequilibrium exists (i.e., at fairly low temperature), the rate of isotopic rock alteration is controlled by chemical kinetics. In areas close to isotopic equilibrium (hotter areas), the rate of isotopic rock alteration is controlled by the rate of local fluid flow and the local temperature gradient parallel to that flow. $\delta^{18}O_{WE}$ is the isotopic composition of water that would be in equilibrium with the rock at the temperature and isotopic composition of the rock at that locality.

of fluid circulation) affects the intensity of the interior (equilibrium) isotope alteration but not the intensity of near-surface alteration.

Discussion of physical-chemical models in light of field evidence

Brief summary of field evidence from the Hokuroku district: The U. S.-Japan-Canada cooperative project reported in this issue focused study most intensively on the Fukazawa deposit in the central part of the Hokuroku basin. For this reason the model presented in the previous section will be discussed mainly in terms of the Fukazawa deposit, with references to other deposits when they differ in important respects.

The Fukazawa deposit consists of about ten massive sulfide lenses in an area of 1.5 by 0.8 km, with the long axis of the cluster trending northwest-southeast (Tanimura et al., 1974). The massive ore is predominantly of the black ore type (sphalerite and galena), but there are massive yellow ore lenses (chalcopyrite and pyrite) both above and below black ore in the largest and most easterly deposit, the 480 × 400 × 8

FIG. 17. The $\delta^{18}O_w$ of solutions circulating and cooling the intrusion of Figure 10 are shown at different times for the three kinetic models calculated. Rate ϕ is the maximum rate of basalt alteration and isotope exchanges suggested by laboratory experiments. Rate $\phi \times 10^{-1}$ assumes 10 percent of the rock reacts with fluids at any time, rate $\phi \times 10^{-2}$ assumes 1 percent, and rate $\phi \times 10^{-4}$ assumes 0.01 percent the rock reacts. In the faster two kinetic cases, inflowing zero per mil seawater becomes lighter in coming into isotopic equilibrium with the rock at 2- to 3-km depth, and then becomes heavier as temperature increases and the fractionation factor between water and rock decreases. The degree to which fluid and rock are in equilibrium is strongly dependent on temperature, as shown in Figure 18.

m Tsunokakezawa orebody (Tanimura et al., 1974; Kouda, 1977). Kouda (1977) has described the Tsunokakezawa orebody in English in the greatest detail. He reports that the boundary between black and yellow massive ore at Tsunokakezawa is sometimes very sharp with a strongly altered tuff layer occasionally separating black and yellow ore. Our group observed this in two localities in the field. Sometimes the transition is gradual with semiblack ore lying between black and yellow ore. Kouda's excellent cross sections show that three separate lenses of gypsum-bearing muddy tuff (with occasional massive gypsum-anhydrite patches) underlie the massive sulfide lenses of the Tsunokakezawa orebody. Both black and yellow siliceous ore feeder pipes are present under the orebody. Kouda suggests that each massive ore lens is composed of many smaller units or pods that accumulated near a local vent and are overlain, underlain, and surrounded by neighboring pods. Late-stage veins cut and alter the black ore lens and the hanging-wall basalt and tuff at Tsunokakezawa.

Putting his observation and chemical studies together, Kouda (1977) suggests that mineralization of the Tsunokakezawa orebody occurred in five steps. The first two steps involved silicification and gypsum (anhydrite) deposition only. The third step precipitated the upper gypsum lens, formed the black and yellow siliceous ore, and perhaps deposited massive pyrite ore. Step four deposited, from base to cap, more black and yellow siliceous ore, massive yellow and black ore, barite ore, and tetsusekiei (quartz-hematite-pyrite). Step five deposited some more siliceous ore and gypsum ore, massive yellow, black, and barite ore, and tetsusekiei. Multiple ore lenses are not uncommon in the Hokuroku district. Two stratigraphically distinct mineralogically zoned (gypsum ore-pyrite ore-yellow ore-black ore) lenses occur at the Doyashiki and Matsumine deposits in the Hanaoka area (Takahashi and Suga, 1974). Solomon and Walsh (1978) and Kajiwara (1971) have suggested anhydrite deposition typically occurs in Kuroko deposits in the early (prograde) stages of mineral deposition.

Judging from figures reported by Tanimura et al. (1974) it can be estimated that the Tsunokakezawa orebody contains roughly 1.2 million tons of combined Cu, Pb, and Zn and the Fukazawa deposit as a whole perhaps 1.5×10^6 metric tons Cu + Pb + Zn.[5] From Kouda's (1977) figures we estimate the Tsunokakezawa deposit contains about as much gypsum-anhydrite as Cu + Pb + Zn.[6]

[5] Figures calculated for 4 g/cc massive ore and average grades and dimension given by Tanimura et al. (1974).

[6] Kouda shows three gypsum lenses with plan dimensions: 550 × 150 m (upper), 500 × 100 m (intermediate), 450 × 70 m (lower). We assume each lens is 2 m thick and 30% gypsum-anhydrite (70% tuff). This gives 1.2×10^6 metric tons gypsum-anhydrite.

The Fukazawa orebody is underlain first by variable thicknesses (up to 160 m) of tuff breccia that contains basement phyllite clasts and fragments of footwall rhyolite (Uwamuki-type tuff breccia). The Uwamuki-type tuff breccia occurs in the Hokuroku basin only where Kuroku deposits are present and is thought by district geologists to have genetic significance (Tanimura et al., 1974, p. 148). The Uwamuki-type breccia is underlain by the Yukisawa formation, a brecciated and altered mass of dacite lava that shows double grading (suggesting deposition by pyroclastic submarine flows), contains flattened pumice fragments, and is intensely sericitized and contains fine-grained pyrite in the vicinity of the massive ore. The Yukisawa formation is in turn underlain by the Menaichizawa formation that consists of altered andesite, tuff, and basement conglomerate. The deepest drill hole (AK1) through the Tsunokakezawa deposit penetrated 803 m below sea level or about 720 m below the Tsunokakezawa massive ore lens. This hole does not reach basement.

The Fukazawa deposit is everywhere overlain by submarine basalt lava flows (total thickness $\lesssim$ 140 m). The top and margins of the flows grade into basic tuff. The source of the flows appears to be a swarm of basic dikes south of the Tsunokakezawa deposit. The basalt flow contains fragments of black ore (Tanimura et al., 1974). We observed underground that black ore also contains fragments of basalt. Basaltic volcanism and ore deposition appear therefore to have occurred simultaneously. The Kagoya Formation overlies the basalt flow in the vicinity of the Fukazawa deposits and the Yukisawa Formation elsewhere. This unit consists of alternating mudstone and tuff (Tanimura et al., 1974).

Both footwall and hanging-wall rocks (i.e., rocks underlying the deposit and rocks overlying it) are hydrothermally altered. Iijima (1974, p. 284) has pointed out that the persistence of alteration into the hanging wall means that the hydrothermal system continued to operate (albeit more weakly) for at least 1 to 2 m.y. after ore deposition—from late Nishikurosawa to middle Onnegawa time. Kouda (1977) believes the fracture system under Tsunokakezawa that produced the Kuroko deposits in the late Nishikurosawa also transmitted fluids for vein mineralization in late Onnegawa time. Utada et al. (1982) suggest that the fractures which transmitted mineralizing solutions are oriented northwest-southeast. Scott (1980) has emphasized that both the distribution of sulfide lenses within an ore cluster and the distribution ore clusters appear to be controlled by a nearly orthogonal grid of conjugate northwest-southeast and northeast-southwest fractures. Basement lines of weaknesses, or lineaments, that are reflected also in the orientation of caldera walls, lineaments on satellite photos, and basement faults appear to have localized discharge of hot mineralizing solutions.

Progressive hydrothermal alteration manifests itself first in the conversion of the diagenetic zeolites mordenate and clinoptilolite to the hydrothermal zeolite analcime, then the breakdown of montmorillonite to mixed layer (montmorillonite and illite) clays, and finally the conversion of the mixed layer clays to sericite and chlorite. Clay alteration shows a regular distribution around the Kuroko deposits with a sericite-chlorite zone lacking plagioclase closely surrounding the siliceous ore feeder pipes of the deposits (Iijima, 1974).

Tono (1974) points out and Date (1979) statistically demonstrates that Na is the most diagnostic alteration element. Tono shows that the Na_2O content of footwall dacite drops abruptly from normal levels of 3 to 4 weight percent to ~0.2 percent as an orebody is approached. Total Zn + Cu + Pb values are inversely correlated with Na_2O and abruptly increase wherever Na_2O decreases (see also Izawa et al., 1978). The sharpness of the Na_2O, Pb + Zn + Cu front is impressive. Date (1979) and Date et al. (1983) show that the Na_2O content of dacite is distinctly bimodal (normal and abnormal) and that the abnormal Na_2O-poor dacite that underlies ore can be usefully outlined by the Na_2O = 0.4 weight percent contour. This contour forms an exploration target about twice the size of the area lying within the outer edges of the ore deposits themselves. For example, at Fukazawa the 0.4 percent Na_2O contour encloses an area 1.5 × 3 km which is twice the size of the 0.8 × 1.5 km area whose perimeter would enclose the massive sulfide lenses. Sodium depletion of the dacites found in the footwall is not observed in the hanging wall (Date et al., 1983, table 2).

Date (1979) and Date et al. (1983) have further shown how the Na_2O zoning relates to alteration mineral assemblages. The Na_2O-depleted zone corresponds closely to zone III rocks that lack hydrothermal zeolite and plagioclase (minor at most) but contain sericite and chlorite. Date and Date et al. distinguish other zones, depending on the presence or absence of zeolite, sericite, chlorite, montmorillonite, and plagioclase. The least altered zone, zone I, contains diagenetic zeolite. The higher numbered zones contain no zeolite, increasing amounts of chlorite and sericite, and less or no montmorillonite and plagioclase.

Green et al. (1983) has shown that the $\delta^{18}O_r$ signatures correlate astonishingly well with Date's alteration zones. Zone III footwall rocks are little altered from their initial ~7.5 per mil value (5–9‰). Zone II rocks have $\delta^{18}O$ of 9 to 15 per mil. Zone I has a $\delta^{18}O$ from 15 to 20 per mil. Urabe et al. (1983) have pointed out that this simple zoning picture is not observed everywhere. Some massive sulfide deposits are surrounded by high $\delta^{18}O$ rock near the ore horizon (Fukazawa, Seneca, Corbet, Amulet), and some do not appear to show such a halo (Uwamuki, South Bay).

Urabe et al. (1983) have analyzed the Fe/Fe + Mg ratio in chlorites in the footwalls of massive sulfide deposits. They show that this ratio decreases as the orebody is approached (chlorites near the orebodies are Mg rich and iron poor). The increase in Mg in chlorites and in the bulk rock corresponds to the drop in $\delta^{18}O$ to 5 to 6 per mil in many cases and thus presumably corresponds also in Date's zone III alteration.

Pisutha-Arnond and Ohmoto (1983) analyzed $\delta^{18}O$ from solid quartz in the siliceous ore pipes beneath several of the Kuroko deposits of the Hokuroku basin. Their work and that of others which they summarize shows that the $\delta^{18}O$ of the fluid responsible for mineralization was negative (~ −6‰) in the earliest stages of ore deposition, became heavy (up to ~4‰) and then dropped to ~0 per mil in the main stages of ore deposition, and finally, was very light (~ −10‰) during late tetsusekiei deposition (Tsutsumi and Ohmoto, 1983). The data are provided by oxygen isotope measurements on quartz associated with mineralization in siliceous feeder pipes and are confirmed by direct measurements of $\delta^{18}O_f$ in inclusions trapped in the sulfide minerals.

Pisutha-Arnond and Ohmoto (1983) report the salinity of the fluid trapped in inclusions is typically 3.5 to 5.5 equivalent weight percent NaCl with values as high as 7 percent. The salinities are substantially greater than seawater (3.5 equiv. wt % NaCl). Examining fluid inclusion filling temperatures as a function of sulfide deposition stage in the feeder pipes of several deposits, Pisutha-Arnond and Ohmoto find an increase and then decrease in temperature. At Fukazawa, for example, early primitive sphalerite was precipitated at 260° to 290°C, chalcopyrite was deposited at 300° to 340°C, and sphalerite overgrowths were deposited at 220° to 240°C. Fukazawa appears to have been deposited under somewhat hotter conditions than other deposits in the Hokuroku basin.

Fehn et al. (1983) have analyzed lead isotopes in black and yellow massive ore from several deposits in the Hokuroku basin. There are small but distinguishable differences between the ores of different deposits. In each deposit yellow ore is less radiogenic than black ore. Both black and yellow ore are more radiogenic than the volcanic rocks in the basin but less radiogenic than the phyllitic basement rocks and the Sasahata Formation (which is similar to basement). Fehn et al. conclude that the lead in the ores was extracted from both the volcanic rocks in the basin and from basement (and the basal conglomerate—the Sasahata Formation). They conclude that deposition of yellow ore and black ore must have been separated in time to allow the lead isotope character of the fluid to evolve slightly. Yellow ore has less of a basement contribution to its lead content.

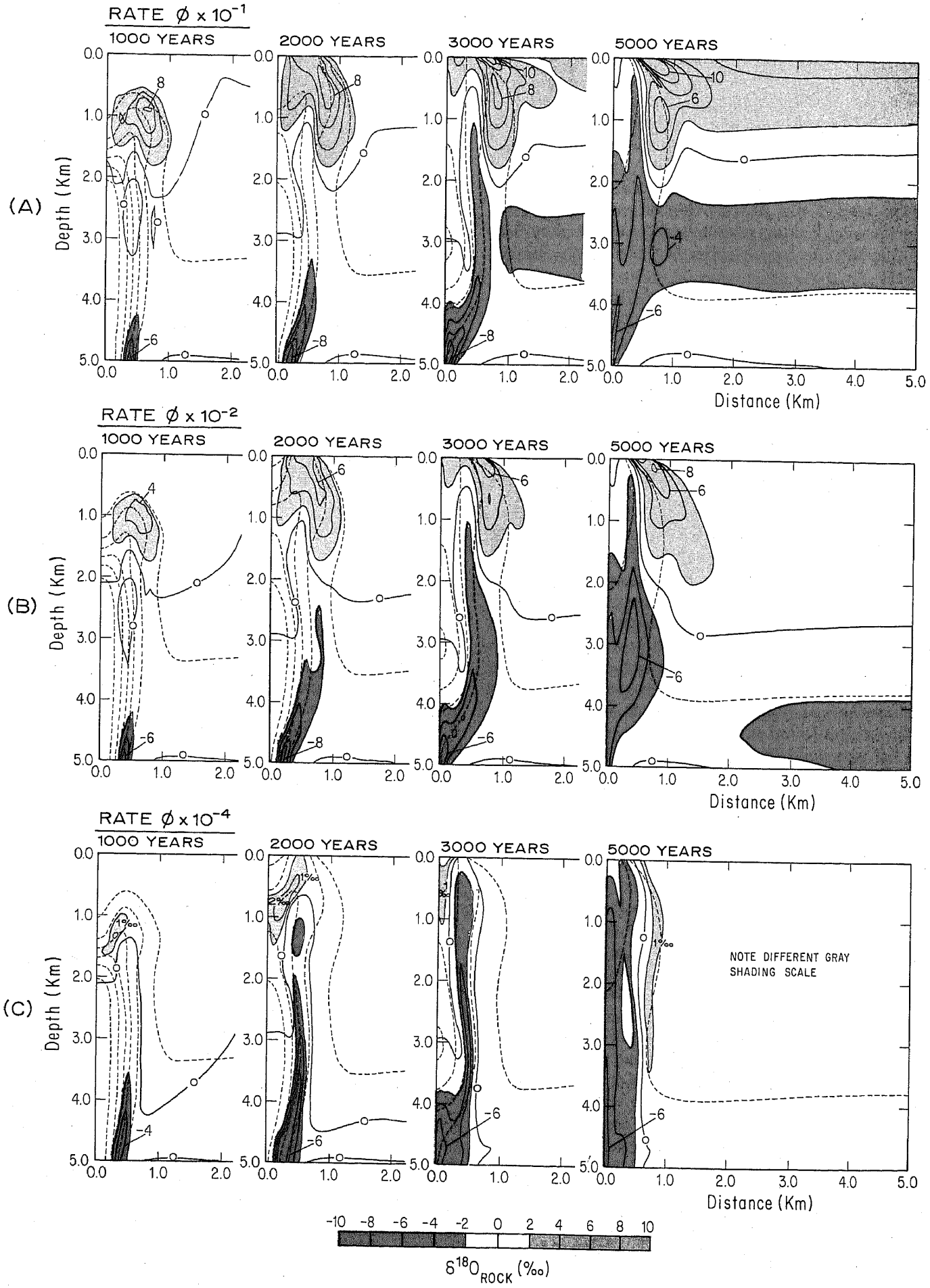
RATE Ø x 10⁻¹
1000 YEARS
2000 YEARS
3000 YEARS
5000 YEARS
(A)
Depth (Km)
Distance (Km)
RATE Ø x 10⁻²
(B)
RATE Ø x 10⁻⁴
(C)
NOTE DIFFERENT GRAY SHADING SCALE
δ18O ROCK (‰)

Farrell et al. (1978) have shown that the $^{87}Sr/^{86}Sr$ ratio of anhydrite (0.70827 to 0.70854) and barite (0.70677 to 0.70820) are slightly less than the $^{87}Sr/^{86}Sr$ of Miocene seawater (0.7088 ± 4), much less than the $^{87}Sr/^{86}Sr$ of the basement rocks which lie only 400 m below some of the Hokuroku deposits (0.713 to 0.750 with an average of 0.723 ± 0.020 for five samples) but heavier than the $^{87}Sr/^{86}Sr$ of the Miocene volcanics (0.703–0.705). They conclude that hydrothermal fluids that passed through the basement could have been involved in the precipitation of anhydrite and barite in only a very minor way. The sulfates thus contrast sharply with the ore minerals, where Fehn shows basement fluids (i.e., fluids which passed through basement) must have been significantly involved. Farrel et al. (1978, p. 289) conclude that the $^{87}Sr/^{86}Sr$ data are best explained if sulfates precipitated from "normal Miocene seawater which reacted to a greater or lesser degree with Miocene volcanics."

Shikazono and Holland (1983) reinforce Farrell et al.'s (1978) conclusion by pointing out that anhydrite from the Kuroko deposits contains too little Sr to have been precipitated solely due to the heating of seawater above 150°C (Bischoff and Seyfried, 1978). They show mixing of seawater (10–20% at 8 ppm Sr) with a hydrothermal solution that contains less and lighter Sr (1 ppm, $^{87}Sr/^{86}Sr$ = 0.705 to 0.707, comprising 80 to 90 percent of the total mixed solution) can explain both the $^{87}Sr/^{86}Sr$ ratios and the amount of Sr observed in Kuroko anhydrites.

Discussion of calculated models from the Hokuroku district: The field evidence and conclusions reached by other workers, and the suggestions of the calculations presented in this paper, are generally compatible and suggest the same overall genetic model for Kuroko mineralization. This section critically relates our calculations to field observations. The calculated models of Figures 10 to 21 are referred to in this section as calculations; the conceptual model of Kuroko genesis indicated by these calculations and interpreted field evidence will be referred to as a model of Kuroko genesis.

The calculations of the last section were designed so that the maximum temperature of vented solutions was less than 350°C. This was done because geothermal systems hotter than ~370°C have never been observed and because field inclusion evidence in Kuroko and other massive sulfide deposits has been interpreted to indicate that the fluids that deposited ore were cooler than ~370°C (Pisutha-Arnond and Ohmoto, 1983). Some further comments on the maximum temperature attained by ore-depositing fluid in Kuroko deposits is warranted.

Fluid inclusions in sphalerite indicate temperatures of ~300°C (Marutani and Takenouchi, 1978), but sphalerite undoubtedly precipitated at lower temperature than chalcopyrite. The assemblage bornite-chalcopyrite-pyrite suggests T < 350°C, but bornite could be a retrograde mineral. The fluid inclusions in Kuroko deposits show no evidence of boiling, yet commonly have salinities up to 5.5 to 6 equivalent weight percent NaCl (Pisutha-Arnond and Ohmoto, 1983). At pressures of 340 bars (Guber and Merrill, 1983) fluid of 5 weight percent NaCl will boil at ~422°C; higher salinity fluids would boil at slightly higher temperatures. At pressures of 390 bars (the top end of Guber and Merrill's depth estimate), fluids with more than 6 weight percent NaCl will boil at about 440°C. At pressures greater than 390 bars 6 equivalent weight percent NaCl fluids are in the supercritical region. Below ~4.3 percent salinity the fluid is supercritical at 340 bars. The lack of boiling thus indicates the temperatures of venting solutions were less than about 440°C.

In the absence of boiling, silica will precipitate when solutions are cooled by mixing with cold, low silica solutions or cooled by conduction without mixing, provided the silica content of the resulting cooled solution is above saturation. Mixing lines are drawn in Figure 14 that illustrate the importance of the shape of the silica saturation curve in determining whether silica will be precipitated when silica-rich solutions are cooled by mixing. The figure shows that the fact that most fluid inclusions were trapped at 300° to 350°C may be in part an artifact of the shape of the silica solubility curve and not, therefore, an accurate reflection of the temperature of the venting solutions. Thus, although we feel the maximum temperatures of our calculated venting solutions are in the correct range, based on

FIG. 19. The $\delta^{18}O_r$ alteration is shown at various times for the kinetic models discussed and shown in Figure 17. Inward-circulating seawater makes the near-surface rock isotopically heavy as the water becomes light and approaches equilibrium with the rock. Where the fluid is in equilibrium with the rock (Fig. 18), the rate of rock alteration is controlled by the rate of fluid circulation along a temperature gradient. Where fluid circulates up temperature, the rock-water fractionation factor decreases, the water becomes heavier and the rock light. This produces a negative isotopic anomaly beneath the positive anomaly in areas of seawater inflow, and a negative anomaly where fluid circulates into the intrusion. Note this negative anomaly does not suggest meteoric water but rather is due to fluid circulation up a temperature gradient at temperatures high enough for the fluid and rock to be in isotopic equilibrium. Where fluid in equilibrium with rock circulates down a temperature gradient, a positive rock isotopic anomaly is produced. A heavy anomaly rides upward with the thermal front above the intrusion as fluid circulation cools the intrusion. The positive anomaly impinges on the surface and is punched through by normal (tending to negative) isotopic values as circulation continues. The magnitudes of positive and negative isotopic anomalies can be estimated, as discussed in the text, since we know a water/rock ratio of ~0.2 is required to move a thermal anomaly through one gram of rock.

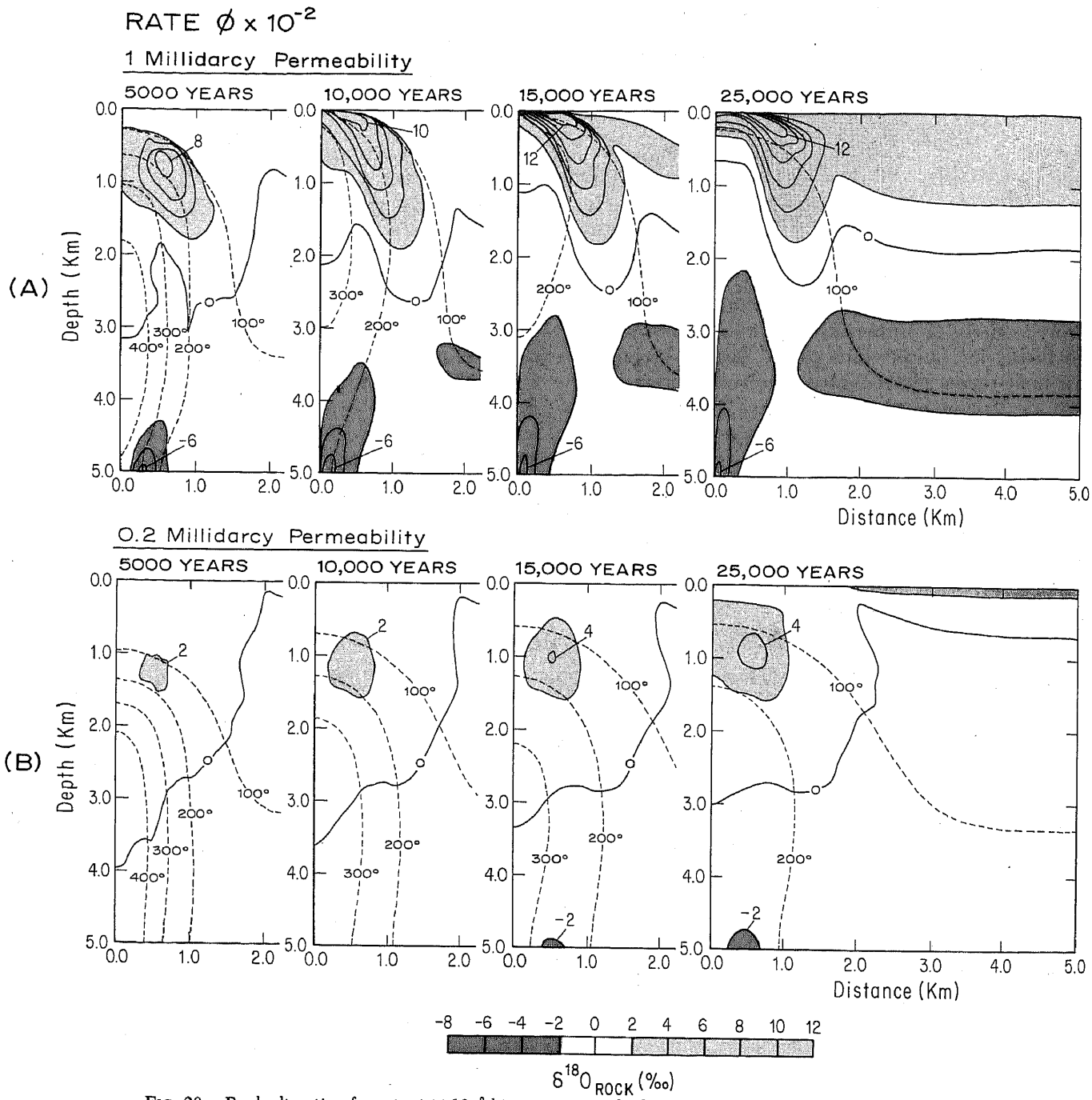

FIG. 20. Rock alteration for rate $\phi \times 10^{-2}$ kinetics (1% rock altering at any time) for 1-mD and 0.2-mD regional permeabilities. The temperature dependence of permeability at temperatures > 300°C is the same as in Figure 10 and the previous isotopic calculations. The decreased rate of fluid flow can be seen to affect the extent of alteration strongly in areas where fluid and rock are in isotopic equilibrium. The rate of alteration in kinetically controlled areas is not affected by the rate of fluid circulation. This is best seen in Figure 21.

observations of the general behavior of geothermal systems, it must be admitted that we lack a tight field estimate of the temperature at which the Kuroko ore-forming fluids actually vented.

The amount of hydrothermal fluid vented at T > 300°C by the 1-km-wide dikelike intrusion in our calculations is nearly sufficient to deposit the metal resources of the Hokuroku basin if the solutions carry and precipitate on the venting 100 ppm Zn + Pb + Cu. Metal resources of Fukazawa estimated in the previous section could be deposited if the flow was drawn to the deposit area from a 10-km-long segment of the dike.

The actual intrusive pulses of the Hokuroku basin could have been bigger or smaller than those calculated. There is evidence that there were several discrete pulses

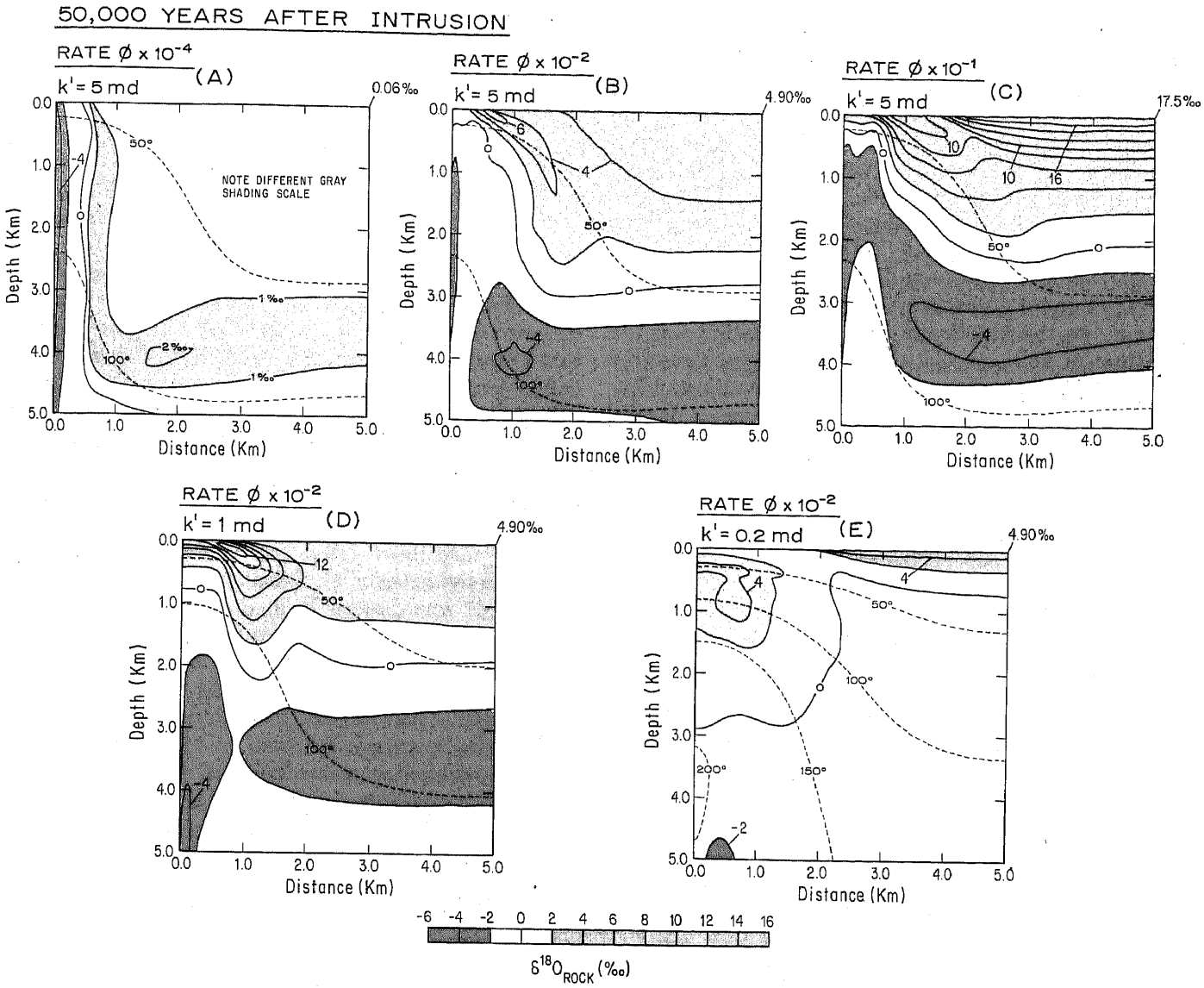

FIG. 21. Rock alteration after 50,000 years for the three 5-mD regional permeability cases shown in Figure 19 and for the 1-mD and 0.2-mD cases shown in Figure 20. The joint control of fluid flow (in isotopic equilibrium areas) and kinetics (in cool disequilibrium areas) on the extent of rock isotopic alteration can be seen. The surface alteration (kinetic control) in the inflow areas of the figures, for example, is the same for the same kinetic models, regardless of the permeability (rate of fluid flow). The rate of fluid flow strongly affects the magnitude of the interior (equilibrium) alteration.

of hydrothermal activity. These pulses could account for Kouda's (1977) five stages of mineralization and for the multiple, stacked massive ore lenses at Doyashiki and Matsumine. The size of intrusive pulse we choose can account for the mineralization in the largest sulfide lenses. It may be about the right size. Cooling of a significantly larger intrusive pulse would take sufficiently longer (compare figs. 9 and 10) that it might be difficult to form numerous sulfate and sulfide lenses. Also, if intrusive pulses were bigger than a few kilometers, venting through common surface fractures to form stacked lenses at the same location would be unlikely.

The $\delta^{18}O$ of our venting solutions are generally in good agreement with those observed (compare Fig. 11 to fig. 8 in Pisutha-Arnond and Ohmoto, 1983). Higher $\delta^{18}O_f$ values are calculated when the 300°C thermal front first arrives at the surface. This is due to the simultaneous arrival of the heavy $\delta^{18}O_r$ anomaly which is swept along with the thermal front. Lighter $\delta^{18}O_f$ values are calculated for the retrograde (cooling) stages. Caution may be indicated for field interpretations—the initial heavy $\delta^{18}O$ could be mistaken for magmatic fluid and the later light $\delta^{18}O$ could be mistaken for meteoric water. Fluid in the calculations is entirely seawater. The rate $\phi \times 10^{-2}$ curve in Figure 11 is in fact nearly identical to the $\delta^{18}O_f$ curve measured by Pisutha-Arnond and Ohmoto (1983, fig. 8). When the venting fluids cool to ~100°C, the calculated $\delta^{18}O_f$ is ~ −10 percent, in excellent agreement with inter-

ferences from $\delta^{18}O$ in tetsusekiei (Tsutsumi and Ohmoto, 1983).

Heavy near-surface $\delta^{18}O_r$ anomalies surrounding a near-normal, ~7.5 per mil, vent area are predicted by the calculations in accord with observations at Fukazawa (compare Fig. 21 to Green et al., 1983). The near-surface heavy values of $\delta^{18}O_r$ result from two causes: (1) solution traveling down the temperature gradient near the vent, and (2) the influx of isotopically heavy (but cold) seawater. The calculations show that development of a near-surface $\delta^{18}O_r$ anomaly depends strongly on the kinetics of isotopic alteration and the duration of fluid circulation. Slow kinetics is roughly equivalent to initially rapid but early cessation of hydrothermal circulation. The near-normal ~7.5 per mil isotopic values in the vent area are the result of the near breakthrough of the deep negative $\delta^{18}O_r$ anomalies (Fig. 19). The $\delta^{18}O_r$ pattern observed is thus a bit precarious. If the duration of hydrothermal activity is short, there may not be sufficient time to form a substantial heavy near-surface $\delta^{18}O$ anomaly. Once formed, anomalies could be altered or erased by later hydrothermal circulation, particularly once the ore horizon is buried. It is perhaps not remarkable, therefore, that oxygen isotope anomalies near massive sulfide deposits should be varied (Urabe et al., 1983).

The extensive silicification of the feeder zones and the amount of anhydrite precipitated requires substantial near-surface satellite convection. The calculations (Fig. 15 and discussion) show that very little silica or anhydrite will be precipitated per unit volume of rock due to the upward migrations of the thermal anomaly. Great quantities of silica are transported upward, but because the discharge velocity is rapid, a mechanism other than conduction is needed to maintain a substantial temperature drop at some location within the rock mass, if more than a few tenths of a weight percent silica is to be precipitated at any one spot. Near-surface seawater convection is an appropriate and expected mechanism. The near surface, especially along a fracture trace, should be more permeable than the rock under greater lithostatic pressures at depth. Shallow (~500 m) circulation of seawater will cool the hot (~350°C) upward-venting solution and cause the silica they carry to be precipitated. At the same time, heating of the shallow circulating water by the deep solution will cause precipitation of anhydrite. Precipitation of anhydrite and silica will tend to seal off and isolate the deep from the shallow circulation systems. Once the deep solutions are sufficiently protected so that they are able to vent without significant near-surface mixing and cooling, precipitation of massive sulfide lenses from black smoker plumes such as are seen along the East Pacific Rise at 21° N can begin. The Falconbridge geologists' concept (Gibson et al., 1981) of early silicification preparing the way for focused venting and massive sulfide deposition is reinforced by the calculations presented here in the sense that the calculations show that the extensive feeder zone silicification and anhydrite precipitation observed in Japan could not have occurred without the operation of a shallow convection system. Silicification was perhaps more widespread at Noranda than in the Hokuroku basin where it appears primarily restricted to feeder zones under the deposits. Anhydrite was not precipitated at Noranda because Archean seawater lacked SO_4^{-2} (e.g., see Large, 1977).

The timing of silicification and anhydrite deposition relative to sulfide deposition predicted by the above scenario agrees well with Kouda's field observations that gypsum beds with associated episodes of silicification precede (underlie) deposition of the massive sulfide lenses at Fukazawa. Since the siliceous ore zones form at different times from the massive sulfide lenses, care must be exercised in interpreting fluid inclusions from quartz or other minerals in the siliceous ore zone in terms of the conditions of massive sulfide deposition. Not only are there restrictions placed on silica precipitation by the silica solubility curve, but the siliceous ore feeder zones were formed before the overlying massive sulfide lenses, not simultaneously with them.

Both the $^{87}Sr/^{86}Sr$ ratio and the Sr concentration of the shallow circulating fluids would be expected to be close to that of seawater but a bit reduced by interaction with the near-surface volcanic rock. The shallow circulating modified seawater fluid will dominate the $^{87}Sr/^{86}Sr$ ratio in any anhydrite deposited so long as it contains substantially more Sr than the deep-circulating solutions which provide the heat for deposition. The deep solution in our calculation interacted with both basement ($^{87}Sr/^{86}Sr \sim 0.723$) and, at high temperatures, with the intrusive heat source ($^{87}Sr/^{86}Sr \sim 0.704$). Because of the high-temperature interaction with volcanics, the isotopic signature of the deep fluids should be significantly less than 0.723. Shikazono and Holland's (1983) calculations suggest, by analogy, that mixing equal amounts of 350°C deep solution carrying 1 ppm Sr with $^{87}Sr/^{86}Sr = 0.710$ and 20° to 100°C modified seawater that contains 4 ppm Sr with $^{87}Sr/^{86}Sr = 0.706$ could account for both the observed Sr concentration and $^{87}Sr/^{86}Sr$ in Kuroko anhydrite.

One could envision a model where fluid interaction is initially mainly with intrusive rock as desired by Shikazono and Holland. This could occur, for example, as the result of downward migration of a cracking front into the intrusion as suggested by Lister (1974, 1977, 1980; see later discussion). After the intrusion was cracked and cooled, a more general circulation that contacts basement could move through the intrusion. Black and yellow ore, with their radiogenic (basement) lead isotopes, could be deposited at this stage.

I feel that such a model is unlikely in the Kuroko case for two reasons. (1) It suggests that the massive ore deposition stage occurs after much of the intrusion is cracked and cooled. Other evidence suggests that the massive sulfide deposition stage is the hottest stage

of mineral deposition. Our calculations show the temperature drops off rapidly once the heat anomaly is everywhere reduced to temperatures below 300°C (i.e., all cracked). (2) A small intrusion (as a large one) should be cracked from the side by fluids that would encounter basement rocks, as well as from the top. Unlike a large intrusion, however, a small intrusion would not have an overhanging magma edifice to shield the solutions attacking the base of the chamber from those attacking the top. It is thus hard to see how deep solutions which contact the basement could be shielded from the areas of anhydrite deposition if we are dealing with a relatively small magma body. The magma bodies must be small if multiple ore (sulfate and sulfide) pulses are to be attributed to multiple intrusive pulses.

Quantitatively, there is no difficulty accounting for the amount of anhydrite precipitated. We have shown that if 100 ppm Zn + Pb + Cu is precipitated from the deep venting solutions when they are quenched upon entering the sea, the metal reserves of, say Fukazawa, could be accounted for. Seawater effectively contains ~3,600 ppm anhydrite (Fig. 14). Thus if anhydrite is stripped from a mass of seawater representing even as little as 10 percent of the mass of deep circulating solution, as Shikazono and Holland (1983) suggest, a tonnage of anhydrite greater than the metal tonnage of the deposit would be precipitated.

Shallow mixing of cold seawater and the discharging hydrothermal solutions is required in the initial stages of the developing hydrothermal system to account for the observed deposition of silica and probably anhydrite (note the reservations of Urabe et al., 1983, regarding the lack of silica in the anhydrite). It is at this stage that Mg is added to the rock by Mg-rich seawater as discussed by Urabe et al. (1983). Soon, however, mineral precipitation isolates the discharging hydrothermal solutions from the downward-mixing seawater. Protracted discharge of the deep hydrothermal solutions now occurs through the isolated vent area. At Fukazawa this discharge zone is about 1.5 km wide—similar to the total width over which hot, deeply circulating solutions vent in the calculations shown in Figure 10. The deep solutions would be expected to be metal rich and Mg, and perhaps Na, depleted. They would thus tend to deposit base metals and remove Na from the rock. They will carry up the lead isotope signature of the basement rocks, modified by the volcanic imprint of the intrusion that drives the hydrothermal circulation and other intervening volcanics, as found by Fehn et al. (1983).

At the fringes of the discharge zone, isolated at a fairly sharp boundary by silica and anhydrite deposition, shallow circulation of seawater should continue, driven by the heat of the adjacent discharge zone. At some additional distance, the fluid that ultimately vents in the discharge zone must circulate into the rock formation. In these intake areas seawater rich in ^{18}O and Mg will continue to enrich the rock in ^{18}O and Mg, and produce high Mg chlorites. Green et al. (1983) have suggested that our intake area is actually a discharge area—that hydrothermal solutions vent most vigorously at the sites of ore deposition but also weakly over a much broader area. This is possible, but I am persuaded by: (1) the sharpness of the Na_2O drop and trace metal jump at the border of the discharge zone, and (2) the agreement between the size and disposition of the observed recharge zone and that expected for reasonable depths of water circulation that the recharge interpretation is the more appropriate. The fluid flow situation I envision at the time of deposition of the massive sulfide ore is generally as shown in the calculation of Figure 10, except there may have been more near-surface solution inflow than shown due to higher near-surface permeability, and surface discharge is focused by major fractures by a factor of ~20.

Figure 12, when compared to Figure 11, suggests that some connate water will be involved in the early stages of ore deposition. Some unshaded fluid is venting at 2,000 to 2,500 years when fluids > 300°C begin to vent the surface. The connate water is undoubtedly seawater, but seawater that has been comparatively stagnant in rock pores prior to magma intrusion and the start of much more active circulation. The coincidence of the surface arrival of the thermal front and the arrival of a seawater tracer in the calculation depends most strongly on the depth of the intrusion beneath the surface, the porosity of the rock formation (which we take to be 2%), and on the permeability distribution. It does not depend on the magnitude of the permeability, which controls how fast circulation everywhere will occur and how fast the thermal anomaly will reach the surface. If near-surface porosity were increased slightly to 4 percent, much more connate water (initially from near-surface rock strata) would be involved in the early stages of high-temperature venting. The early stages of high-temperature venting is the time silicification of the feeder zone occurred.

If fresh layers of volcanics have been deposited since the last intrusive pulse, the salinity of pore solutions in these volcanics could be substantially increased by the formation of hydrated alteration minerals. If the bound water content of the rock in the upper kilometer of the calculation domain is increased 4 weight percent by clay alteration, the salinity of pore solution occupying 4 vol percent of the rock would be increased 2.7-fold (from 3.5–9.45%), the salinity of pore solutions occupying 10 percent of the rock would be doubled. Venting of these abnormal salinity fluids during the early stages of high-temperature venting and stockwork formation could account for the high salinity (relative to seawater) of the siliceous ore fluid inclusions observed by Pisutha-Arnond and Ohmoto (1983) and others.

Urabe (1978) has shown that quartz and barite precipitated in parallel, or sympathetically with one another, in the upper parts of the lower black orebody of the Uwamuki 4 deposit. He suggests this is due to

the mixing of upward-venting solutions with seawater. Seawater supplied SO_4^{-2}, the hydrothermal solution SiO_2, and Ba^{+2}. Mixing caused cooling and brought SO_4^{-2} and Ba^{+2} together and hence caused the coprecipitation of barite and silica. There are other reasons to believe mixing of hydrothermal solutions with seawater is important in the late stages of the Kuroko mineralization event. Tetsusekiei (oxidized ferruginous chert) layers commonly cap the Kuroko massive sulfide deposits. Most workers have interpreted this as the result of a late incursion of oxygenated seawater into the upper parts of the mineralized system (Large, 1977; Sato, 1973; Kajiwara, 1971, 1973; Urabe, 1974, 1978; Urabe and Sato, 1978). Thus, in the late retrograde stages of mineralization, seawater again mixes with deep circulating solutions in the ore zone.

Throughout, hydrothermal discharge is focused by major fractures. Such focusing is required by inferred near-surface paleotemperature gradients (see heuristic calculation section), if the general regional permeability is ~5 mD. There is abundant field evidence for major fracture or lineament control of hydrothermal discharge.

The sequence of events as discussed above that we envision as leading to the formation of Kuroko massive sulfide deposits is summarized in Figure 22.

Evidence from ophiolite suites: The fluid flow pattern we have deduced for the Hokuroku basin of Japan at the time of Kuroko mineralization (general inflow with isolated, fracture-controlled loci of discharge) is similar to the pattern most authors have deduced for fluid circulation in ophiolites. Spooner and Fyfe (1973) concluded from an analysis of metamorphic minerals at eastern Liguria, Italy, and from the fact that massive sulfides in Cyprus overlie a stockwork of intensely altered pillow lavas containing disseminated sulfides, that the circulation in ophiolites is generally downward with fracture-controlled discharge under mineralized

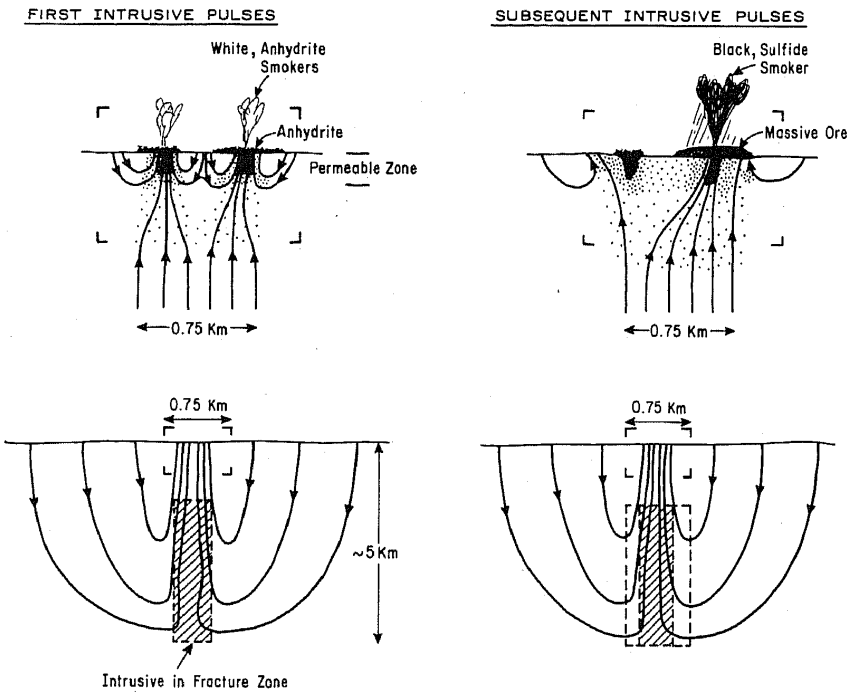

FIG. 22. Summary of the sequence of events that we envision leads to formation of a massive sulfide ore lense. Generally, there are several intrusive pulses and associated episodes of hydrothermal circulation. The lower diagrams show streamlines in our calculation at 3,000 years (Fig. 10), and also show the outlines of two 1-km-wide intrusive pulses. The upper diagrams expand the 0.75-km-wide boxed areas at the top of the model and depict what we visualize happens in the near-surface area where discharge is focused by fractures and ore deposition takes place. Our models are too crude (physically and chemically) to show this directly. The first pulses (shown on the left) do not precipitate massive ore lenses although anhydrite (shown by cross pattern) may be precipitated on the surface. Base metals (shown by dots), silica, and anhydrite are precipitated at depth by this early circulation. Mineral precipitation seals the surface and shields later venting solutions from cool near-surface seawater circulation, so that they can vent into the sea without significant temperature drop. This is shown in the right-hand diagrams. One of the two near-surface fractures that focused outflow in the first intrusive pulse has been sealed off. The full discharge now occurs through the second. Near-surface circulation is sufficiently reduced to allow venting of very hot solutions and a black smoker plume forms. The discharge is vigorous enough to dominate the local oxidizing conditions, and black smoke particles accumulate in a sulfide blanket.

and highly altered parts of the system. The metamorphic assemblage, especially the presence of prehnite in metagabbros, indicated to Spooner and Fyfe that the temperature of the circulating solution was <400°C. Spooner et al. (1977a, b) later confirmed that flow was downward in most areas of ophiolite suites in eastern Liguria and the Troodos Massif, Cyprus, by showing that the degree of rock oxidation decreases downward. Seawater (oxygenated and containing SO_4^{-2}) was the cause of oxidation.

Initial $^{87}Sr/^{86}Sr$ ratios in Cyprus range from those of unaltered rock (0.7034 to 0.7037) to that of Campanian-Maestrichtian seawater (0.7076), suggesting seawater was the cause of the isotopic shift. No significant variation in strontium isotopes with depth is found in the Cyprus ophiolite (Spooner et al., 1977b). A distinct downward decrease in $^{87}Sr/^{86}Sr$ over ~3 km from seawater to unaltered rock values is found in the Semail Ophiolite, Oman (Fig. 23). This prompted McCulloch et al. (1981) to suggest a downward decrease in seawater/rock ratio—i.e., a downward circulation of seawater.

Spooner et al. (1977a) have shown that the basalts in eastern Liguria were hydrated from 0.30 weight percent H_2O (unaltered) to 2.2 to 8.0 weight percent, with an average of 3.8 weight percent. This is similar to, and in part motivated, our suggestion that loss of H_2O to mineral hydration in newly deposited surface volcanics could account for the higher than seawater salinity of the Kuroko ore-forming fluids.

The whole-rock $\delta^{18}O$ profiles measured in ophiolites are both very similar to one another and to our calculated profiles shown in Figure 21. In both eastern Liguria (280-m section, Spooner et al., 1977a) and Cyprus (2-km section, Spooner et al., 1977b), $\delta^{18}O_r$ shows a near-surface enrichment of ~6 per mil ($\delta^{18}O_r$ ~ 12‰). The $\delta^{18}O_r$ was found to decrease with depth at Cyprus, showing a depletion of up to 2.5 per mil at 1.5- to 2-km depth. The Cyprus profile is almost identical to the upper 2 km of the profile obtained recently by Gregory and Taylor (1981) for a composite section through the Semail Ophiolite in Oman (Fig. 23).

In turn, the pattern of $\delta^{18}O_r$ shown in Figure 23 is strikingly similar to our calculated patterns of $\delta^{18}O_r$ alteration (see Fig. 21B, C, D). In both cases there is a near-surface enrichment of 5 to 6 per mil (can be greater for the fast kinetic model), underlain at about a 3-km depth by a zone of ~2 per mil oxygen depletion. The profiles are similar both in magnitude (the amount of oxygen enrichment or depletion) and in scale (the depths at which the anomalies occur).

As discussed previously, the positive anomaly in our models results from inflow of seawater that is isotopically heavy relative to the value it would have if it were in equilibrium with the rock. In the near-surface

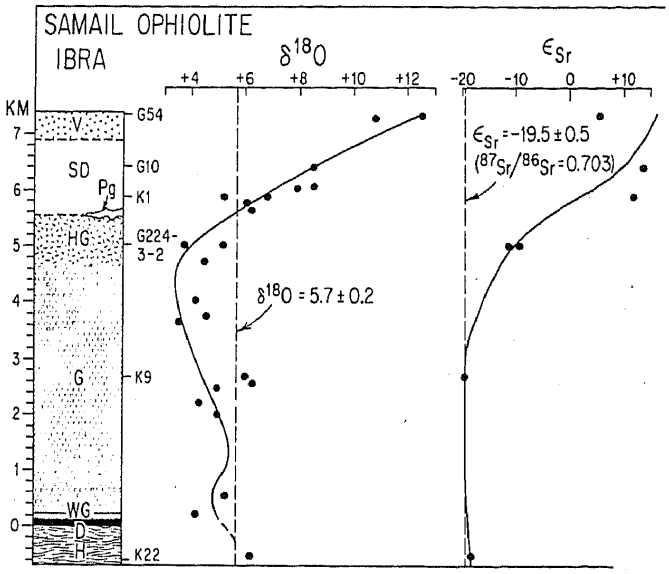

FIG. 23. Measured oxygen and strontium isotope profile through a composite section of the Samail ophiolite, Oman (after McCulloch et al., 1981; Gregory and Taylor, 1981). The strontium isotope profile (ϵ_{Sr} is the enrichment of ^{87}Sr over ^{86}Sr relative to a standard in parts per 10^4) suggests the downward flow of seawater. The oxygen isotope profile is totally compatible with downward flow, being nearly identical to the calculated patterns produced by downward seawater circulation in Figure 21.

zone, the water becomes lighter and the rock heavier at rates allowed by alteration kinetics. Below this 1- to 2-km near-surface zone temperatures are great and alteration kinetics fast enough relative to the rate of fluid flow, that water is very nearly in isotopic equilibrium with the rock. The negative anomaly that lies at 3- to 4-km depth is produced by the downward, up-temperature circulation under very close to equilibrium conditions. Spooner et al. (1977a) were the first to point out that such a transient anomaly could be produced by fluid flow up a temperature gradient, although they felt such transient effects were unlikely to occur because they doubted an alteration reaction could occur quickly enough to allow close fluid-rock equilibrium. With the kinetics assumed our calculations show, however, that the alteration reactions are fast enough to produce such an anomaly even at quite low temperatures (70°C). The anomaly is transient in the sense that if fluid circulation continued for long enough, the heavy near-surface anomaly would migrate downward and eradicate the light anomaly. The light anomaly thus places constraints on the total amount of circulation that can have occurred below 2.5-km depth. Implicit in our comparison of the isotope anomalies computed in Figure 21A, B, and C to those observed in Figure 23 is the conviction that rock alteration and surface sedimentation will progressively inhibit fluid circulation and that uninhibited circulation for 50,000 years roughly mimics the effects of progressively slowed circulation operating over a much longer time period.

The similarity between calculated (Fig. 21) and observed (Fig. 23) $\delta^{18}O$ alteration patterns indicates that the oxygen isotope alteration of the Semail ophiolite could have been produced by low-temperature (~100°–300°C) alteration as a result of fluid circulation. It should be noted that the low-temperature (~150°C) base of the calculated system is controlled by the 1.5-HFU basal heat flow assumed in the calculation. Basal heat flows of 10 to 20 HFU are more reasonable in the near-ridge environment. The basal temperatures would be much hotter and better in accord with metamorphic assemblages observed in the lower parts of the gabbro layer in the ophiolite if higher basal heat flow had been specified in the calculations. The negative anomaly would be produced by downward (up-temperature) flow of solutions regardless of the base level of the temperature. The main effect of a higher basal heat flow would be to diminish the depth extent of the near-surface positive anomaly.

Gregory and Taylor (1981) propose a very different model for the $\delta^{18}O_r$ alteration they observed at Oman. They are convinced by the metamorphic mineral assemblage that the rocks below ~5.5 km in Figure 23 never interacted with significant amounts of fluid at temperatures below 400°C. They thus advocate a high-temperature (T > 400°C) interaction between rock and water and believe that the rock became impermeable and interaction was shut off at T < 400°C. The maximum fluid flux occurred at T ~ 600°C. Their flow pattern is also very different from ours. Instead of a general downward circulation being responsible for both positive and negative $\delta^{18}O$ anomalies, they separate fluid circulation into two isolated regimes: a lower circulation in the gabbro that depletes the gabbro layer in $\delta^{18}O$, and an upper circulation in the pillow and sheeted dike complex that involves seawater more directly and enriches these rocks in $\delta^{18}O$. The two systems interact only at the distal edges of a steady-state magma chamber.

There is essentially no overlap between the temperature regimes for the circulation proposed by Gregory and Taylor (1981) and that proposed in this paper. Either a satisfactory explanation must be found for the "fact" that presently active hydrothermal systems have not been observed to operate at T > 400°C despite the "fact" that metamorphic and isotopic assemblages indicate substantial in fluid-rock interaction occurs at T > 400°C or it must be explained how fluid-rock interaction at <400°C could fail to produce an obvious greenschist facies metamorphic assemblage.

It may be that the problem is only apparent. Gregory and Taylor (1981) ignore minor minerals (<2 wt % of the rock). A vein mineral content of 2 weight percent, however, really represents quite a substantial degree of rock alteration. Ten of 18 samples of the cumulate gabbro which show dominantly an amphibolite grade metamorphic assemblage contain minor calcite, epidote, prehnite, or epidote (Gregory and Taylor, 1981, table 1). Amphibolite facies alteration in cumulate gabbros is itself a vein halo alteration. The amphibolite alteration is presumably produced in the thermal cracking front that separates magma from circulating hydrothermal fluids. Amphibolite facies minerals are not far out of equilibrium with water at 300° to 400°C; alteration from amphibolite to greenschist facies minerals could therefore be slow (M. J. Mottl, pers. commun.). For these two reasons it is not clear that the mineral assemblage observed in the gabbro layer of the Semail ophiolite precludes fluid circulation at T $\lesssim$ 400°C as Gregory and Taylor (1981) presume. The observed abundance of greenschist facies minerals may be sufficient to allow the needed amount of <400°C circulation.

The uniformity of $\delta^{18}O$ profiles from one part of the Semail ophiolite to another (remarked on by Gregory and Taylor) and between ophiolite sequences (Cyprus vs. Oman) may be significant. A general downwelling might tend to produce a more uniform $\delta^{18}O_r$ alteration pattern than a complicated two cell convection pattern.

Evidence from warm and hot springs at mid-ocean ridges: Many of the conclusions we and others have arrived at regarding the hydrothermal system responsible for massive sulfide mineralization have been also reached, quite independently, by those considering how 350°C fluid could vent from the sea floor. Some of the sea-floor circulation work has influenced the modeling we have done of convection in the Hokuroku basin. Future studies of ocean-ridge hydrothermal systems will contribute to our understanding of the genesis of massive sulfide deposits.

Our model of temperature-dependent permeability is really just a way of mathematically incorporating Lister's (1974, 1977, 1980) cracking front model into numerical calculations, although our view of the physical causes of the temperature dependence of permeability differs from Lister's in some (chemical) regards. Lister has long argued that porous media convection above an axial magma chamber will establish large thermal gradients near the chamber. The thermal gradient will be sufficient to crack the rock (by thermal contraction) and open a network of fractures that will have very high permeability. The high permeability leads to the conclusion that the downward migration of the cracking front is rapid and the temperature of the circulating hydrothermal fluid low (100°–300°C). Fluid circulation is episodic—closely tied to periodic pulses of magma injection by sea-floor spreading. According to Lister, downward migration of fluids is stopped only by the compositional transition from gabbro to peridotite. Hydrated peridotite (serpentine) is plastic enough that open (permeable) cracks cannot be maintained. The recent seismic observation of the

progressive growth with time over ~10 m.y. of a low velocity layer at the base of the crust of the Cocos plate, and the interpretation that this represents a 20 to 30 percent serpentization of peridotite (Lewis and Snydsman, 1979), may be an interesting confirmation of the kind of deep seawater circulation proposed by Lister.

Lister's gabbro cracking front advances downward at 5 to 171 m/yr; ours at 0.2 to 1 m/yr. The rate of advance is controlled by permeability. If the country-rock permeability in our calculations were greater, the rate of migration of our thermal front would be faster.

Our calculations imply thermal cracking into the magma chamber from the side is as important or more important than downward cracking. In part this is because we choose to consider a small magma chamber. However, the funnel shape of large magma chambers (see Hopson et al., 1981) in ophiolite suites suggest thermal cracking may be more effective at the sides of the chambers and at depth than near the surface. Our calculations show that this is the zone where ore solutions circulate most strongly against the intrusive boundary.

There is considerable evidence from ridge crest geomorphological studies (Ballard and van Andel, 1977; van Andel and Ballard, 1979) and drilling (Hall and Robinson, 1979) to suggest sea-floor spreading is an episodic process. One hundred years of spreading is perhaps typically followed by 5,000 years of quiescence (Hall and Robinson, 1979). For venting to be sufficiently vigorous to produce black smokers, the regional permeability must be large and hydrothermal activity must be closely tied in time to the spreading pulses. We have suggested that the multiple lenses of mineralization in several deposit clusters in Japan resulted from multiple pulses of rifting and intrusion. Pulses of spreading may also account for the observed temperature variation and periodic mineral deposition in the Red Sea brine fields (Pottorf and Barnes, 1983).

The pillow lava section of the oceanic plate is thought to be very permeable. Anderson and Zoback (1982) report a permeability of ~40 mD in the upper 172-m layer 2A pillow basalt of 6.2-m.y.-old crust of the south flank of the Costa Rica rift. Younger pillow sections of crust could be even more permeable. Ballard et al. (1981) and Mottl (1983) have commented on the need to isolate upflow zones from the near-surface high permeability environment by mineral precipitation, if venting of hot solution is to occur directly into the sea. Their concept is similar to that proposed by Noranda geologists who view silica precipitation and surface sealing as a necessary preparation for high-temperature venting and massive sulfide deposition, and to the suggestion of other massive sulfide geologists that gypsum, silica, and siliceous ore deposition preceded massive sulfide deposition. Mottl feels that the most likely candidate for isolating precipitation are Fe, Cu, and Zn sulfides and anhydrite.

Mottl (1983) has combined laboratory experimental results and observation of the ocean-ridge environment to produce an internally consistent picture of hydrothermal circulation. He identifies areas of upwelling with sulfide-bearing breccia zones that contain Fe- as opposed to Mg-rich chlorites, as we do. Most circulation in Mottl's model is downward. Downwelling solutions produce (at high water-rock ratios) an assemblage of mainly quartz and Mg-rich chlorite. The main difference between Mottl's model and ours is that he considers convection above a wide magma chamber that penetrates progressively into the chamber, whereas our magma chamber is narrow and our fluids penetrate into the chamber mainly from the sides.

Mottl estimates the lifetime of venting activity at ridges in a variety of ways. The estimates range from a few 10s to a few thousands of years, which is the same range we estimate for the Kuroko deposits of Japan.

The concentration of dissolved silica, Ba, Li, and Mg from different samples of the warm (7°–17°C) vents of the Galapagos area are found to depend linearly on temperatures and on each other (Corlis et al., 1979; Edmond et al., 1979a, b). Extrapolating mixing lines for hot Mg-free solutions and seawater back to zero seawater dilution gives the temperature of 350°C. Silica extrapolates to 1,296 ppm at zero Mg concentration, the silica concentration of 365°C fluid in equilibrium with quartz at 700 to 750 bars (Mottl, 1982). Mottl suggests this may indicate the very rapid rise of solutions (velocities of m/sec) from a depth of 4.5 to 5 km below the sea floor. Preservation of 1,296 ppm of silica certainly indicates a very rapid rise of solution from the depth of mixing and cooling with seawater. We question whether the mixing occurs at depths as great as 4.5 to 5 km, however, and prefer a much shallower depth of mixing.

Solomon and Walsh (1979) have pointed out that a large increase in velocity to the meter per second range is possible and even expected where hot solutions enter and mix with seawater. The plume model they adopt applies above the sea floor but might apply approximately below the sea floor, provided the formation is very permeable (in a newly formed pillow basalt layer). In Solomon and Walsh's model, deep hydrothermal solutions do not forcibly penetrate seawater in a fire hose fashion but rather just introduce buoyancy that induces vigorous seawater circulation. Fire hose and passive plumes have similar form. In the passive plume example given by Solomon and Walsh, hydrothermal solutions vent with a true (fracture) subsurface fluid velocity of ~5 cm/sec and accelerate to ~250 cm/sec within the plume above the sea floor. A 250-cm/sec velocity is similar to the 100- to 500-cm/sec velocity

of black smoke eddies in plumes at 21° N (Macdonald et al., 1980). In Solomon and Walsh's model, seawater entrainment causes a rapid thermal quenching of the venting solution, but there is only a gradual drop in plume velocity with distance above the vent. Solomon and Walsh suggest that seawater mixing and thermal quenching in the plume is a way to precipitate zinc and copper sulfide minerals separately and to form a mineralogically layered sulfide lens. Solomon and Walsh's plume also provides a credible way to move quenched fluids rapidly enough to the surface that appreciable precipitating of silica can be avoided—provided the plume can operate below the sea floor.

How deep below the sea floor is it reasonable to apply Solomon and Walsh's plume model? Vertical upflow rates in the m/sec range require formation permeabilities of at least 600 darcies![7] This permeability is reasonable for a very open and fresh near-surface pillow basalt layer. Permeabilities this high are perhaps possible at greater depths if open channelways connect the surface to a very permeable cracking front zone of the type proposed by Lister (1974).

Six hundred darcies is at the very top end of the range of permeabilities observed by field tests in basaltic igneous rocks (Brace, 1980), however, and four orders of magnitude greater than the 40 mD measured for a 6.2-m.y.-old pillow basalt layer by Anderson and Zoback (1982). A 600-D permeability would preclude magma chamber formation at ocean ridges for reasonable episodic spreading rates. The spreading rate would have to be ~600 m/yr to form a magma chamber in a 700-D environment. All things considered, it seems more reasonable to me to attribute the high silica content of the Galapagos fluids to dissolution below the zone of mixing of previously deposited amorphous silica. The required fluid velocity of a few meters per second can presumably be obtained in the very permeable and open pillow basalt layer or in major fractures. A 1,300-ppm SiO_2 content can be obtained by dissolution of amorphous silica at 250 bars (2,500-m water depth) and 370°C. There is no need to dissolve quartz at a 4.5- to 5-km depth and maintain what seems like unreasonably large formation permeabilities of ~600 D to these depths.

Macdonald et al. (1980) take their measured plume velocity of 1 to 5 m/sec to reflect the rate of discharge through the 30-cm-diameter vent of the plume (i.e., assume a forced plume model). They show that if this is done then heat is extracted much more rapidly than it can be replenished by the average rate of sea-floor spreading in the area. Thus they conclude that both the hydrothermal activity reflected in the black smoker plumes and sea-floor spreading must be strongly episodic. It may be worth pointing out that if the plumes at 21° N are passive momentum plumes of the type discussed by Solomon and Walsh (1979), the rate of heat removal is much less (~50 times less) than estimated by Macdonald et al., and episodic hydrothermal and magmatic activity is no longer strongly indicated. To settle the issue, the heat flux should be measured by making temperature and fluid velocity measurements across a plume, but this has not yet been done.

There is reason to believe that the venting that formed the Miocene massive sulfide deposits in Japan was considerably more vigorous than that observed at 21° N. The 21° N area contains abundant fauna—clams, tube worms, crabs, etc. The clams are densely packed in vents and areas of warm discharge. They contain hemoglobin to protect them from periodic anoxic conditions.

It seems certain such abundant life could not have accompanied the venting that produced most massive sulfide deposits. If it had, fossils would certainly have been found in abundance and folk lore would teach that clams created the ore. The most reasonable explanation for the lack of fauna is that venting was rapid and voluminous enough to cause the local environment to become anoxic, thus preventing development of fauna such as clams, tube worms, and crabs that require oxygen.

Summary and Conclusions

The objective of this paper has been to define the characteristics of the hydrothermal system responsible for massive sulfide mineralization in the Hokuroku basin in Japan. The methodology used has been to compare the result of various kinds of calculations to critical field observations. Geologic data from systems thought to be analogous to the Hokuroku basin such as hydrothermal systems at ocean ridges and massive sulfide deposits in the Noranda camp, Canada, have been considered in order to gain a broader perspective and data base. A geologically reasonable model is obtained and shown by detailed calculations to be capable of causing the massive sulfide deposition observed in the Hokuroku basin and elsewhere, and to be consistent with simple geochemical constraints. It is important to recognize that, although it has been shown that a preferred model will work, it has not been demonstrated that it is the only model that will work. Variations around the basic theme will certainly occur in different settings; the existence of an equally valid but quite different model is possible.

Simple heuristic calculations indicate:

[7] This is estimated from equation A5 in Cathles (1981). We assume a flow fracture porosity of 10^{-3} so a 1-m/sec true velocity requires a mass flux of ~0.1 g/cm²/sec. If the zone is an open one and the flow porosity greater than 10^{-3}, proportionately larger mass fluxes and permeabilities would be required.

1. An intrusive heat source with mass at least 1.5 $\times 10^{11}$ metric tons is required to drive the hydrothermal system that produced the known Kuroko mineralization in the Hokuroku basin of Japan. This heat source would be a more than adequate metal source. A substantially larger intrusive mass ($\sim 10^{13}$ metric tons) is required to account for the observed silicification of the ore horizon at Noranda.

2. Fluid inclusion, surface silicification, and mineralogical observations in sulfide blankets provide estimates of the near-surface temperature profile at the time of mineralization. The indicated profiles require vertical fluid flow rates of ~300°C fluid of ~100 g/cm^2/yr for silicification and ~2,000 g/cm^2/yr in areas of massive sulfide deposition.

3. Assuming a 20-fold concentration in surface discharge of ore depositing solutions by major widely spaced (~5 km) fractures, these vertical flow rates require a general, regional permeability of 2.5 to 5 mD.

4. Sulfide blanket permeability at the time of mineralization must have been greater than ~3 mD. Otherwise, flow rates of 2,000 g/cm^2/yr would have caused slumping of the blanket.

5. Intrasulfide blanket convection will occur despite a vertical hydrothermal discharge of 2,000 g/cm^2/yr if the blanket permeability is >250 to 600 mD. If the black ore-yellow ore boundary is an isotherm, its flat, stratiform topography indicates sulfide blanket convection did not occur. The permeability of the sulfide blanket must then be <250 to 600 mD and the general formation permeability is even less.

6. Assuming plumes 50 m high, bottom current velocities less than ~0.5 cm/sec are required to allow the formation of a sulfide blanket with dimensions ~500 m. Unusually stagnant bottom conditions such as might exist in a narrow, protected back-arc basin may be required for massive ore accumulation.

Computer calculations indicate:

7. It is likely that massive sulfide deposits result from the convective cooling of a magma chamber. Magma chambers form at ocean ridges and their existence places limits on the permeability of the ocean crust. For example, the ocean crust must have a permeability of less than ~350 mD if the half opening rate during a spreading pulse is <20 cm/yr (see Fig. 7). The permeability of island-arc crustal rocks is expected to be less than basalt. Consequently, the probable existence of magma chambers at the slowest spreading ridges suggests magma chambers will form in an island-arc rift environment.

8. The general 2.5-mD permeability minimally required for massive sulfide deposition must decrease sharply as rock temperatures exceed ~300°C if solutions hotter than 400°C are not to be vented during cooling of a small intrusion (Fig. 9). Presently active geothermal systems hotter than ~370°C have not been observed. We conclude significant fluid circulation does not occur in rock hotter than ~400°C, and specify a strong decrease of rock permeability at temperatures > 300°C in our calculations (factor of 5 reduction for each 100° above 300°C).

At this point our model departs sharply from that proposed by Norton and Taylor (1979) and Gregory and Taylor (1981). These authors propose that 75 percent of all deep flow takes place at T > 400°C with maximum fluid circulation at T ~ 600°C.

9. The cooling of a small (3.25 km high, 1 km wide) intrusive dike in a 5 mD environment (Fig. 10) adopted as a base model vents 8,160 metric tons of hydrothermal solution > 300°C per cm of dike length. If the 300°C solution vented by this single intrusive pulse deposits 100 ppm Zn + Pb + Cu upon being thermally quenched above the sea-rock interface, a 40-km dike, the length of the Hokuroku basin, could precipitate 75 percent of the known resources of the Hokuroku basin. The system takes about 5,000 years to cool to <300°C everywhere.

10. Silica, anhydrite, and oxygen isotope redistribution are calculated for the base physical model (Figs. 16, 17, 19, and 21). Reasonable alteration kinetics (Appendix II) are incorporated for silica and $\delta^{18}O_r$. Anhydrite precipitation is assumed to be rapid enough so that equilibrium precipitation or dissolution occurs at T > 150°C. Subsurface redistribution of silica and anhydrite are minor (± a few tenths of a weight percent), although surface venting of silica is substantial. The $\delta^{18}O$ anomalies of similar magnitude to those observed near massive sulfide deposits are produced (Fig. 19).

11. Except for the slowest kinetic case calculated, most of the silica and $\delta^{18}O_r$ alteration occurs with the fluid very close to being in equilibrium with the rock (Fig. 18). Alteration occurs as the result of equilibrium fluid circulation up or down a temperature gradient—a kind of alteration first suggested by Spooner et al. (1977a). The rate of alteration is controlled by the rate of fluid flow and the rate of migration of the temperature anomaly, not by chemical kinetics, except in cool zones near the surface. Simple estimates are made that confirm the calculated anomaly magnitudes. Since the fluid is essentially in equilibrium with the rock, it has no oxygen isotope memory of its source (seawater, meteoric, or connate water). Production of the deep negative $\delta^{18}O$ anomaly at the edge of the intrusion does not require light (meteoric) water. It is produced by the circulation of fluids in isotopic equilibrium with the local rock into the intrusion and up the temperature gradient. Given enough time a very characteristic isotope anomaly pattern develops (Fig. 21) as a result of

seawater circulation. A 5 per mil or larger positive near-surface $\delta^{18}O_r$ anomaly extending to ~2-km depth is underlain by a −2 to −4 per mil anomaly at a 3- to 5-km depth. Near-surface zones where hot solutions vent are, ultimately, nearly unchanged in $\delta^{18}O_r$, although their $\delta^{18}O_r$ goes through a substantial maximum at the time of arrival of the thermal front (Fig. 19).

12. The amount of silica deposited in the feeder zones of massive sulfide deposits requires that shallow circulation of seawater maintain the temperature of these zones below 300°C for substantial periods of time. Stockwork formation and anhydrite deposition thus occur before massive sulfide deposition and, in fact, represent a necessary preparatory step that isolates deep solutions from shallow circulating seawater and allows the deep solution to vent uncooled. The suggestion that siliceous ore and anhydrite are deposited predominantly before massive ore deposition, and the control exerted by the shape of the silica solubility curve on silica deposition above ~300° to 350°C (Fig. 14), indicates that caution must be exercised in inferring conditions of massive ore deposition from observations made on quartz or other minerals in siliceous ore feeder pipes.

13. The pattern of oxygen isotope alteration calculated is very similar to that observed near the Fukazawa deposit in Japan. Near-surface positive $\delta^{18}O_r$ anomalies could be produced by the weak venting of hot solutions or by the inflow of cool, isotopically heavy seawater. We identify zones of fluid outflow with nearly unaltered $\delta^{18}O_r$ (~7.5‰) and metal sulfide enrichment, and conclude that the heavy near-surface $\delta^{18}O_r$ anomalies at Fukazawa are mostly the result of fluid inflow, as shown in the calculations (Figs. 10, 19, 21). The near-surface circulation required for the early deposition of silica and anhydrite supports this conclusion. The shallow circulation may become isolated from the deep, but there is no reason for it to turn off. Our preferred model is summarized in Figure 22.

14. Multiple sulfate and sulfide ore lenses observed at the Fukazawa and the Hanaoka deposit clusters are interpreted to represent multiple intrusive pulses. The pulses are believed to be small (as modeled) because several pulses utilize the same surface fractures for discharge and because large (20 km) intrusions would cool slowly enough that formation of separate lenses is less likely. The calculated intrusive pulse is big enough to form the largest ore lenses observed.

15. Because 5 mD is considered a low estimate of the general formation permeability, the small intrusive pulse responsible for deposition of an individual sulfide lens probably cooled in less than 5,000 years. Formation of an individual lens in 500 years or less ($\lesssim$50 mD formation permeability) is quite possible.

16. The model we present is compatible with and supported by observations that have been made on ophiolite suites and at hot and warm springs at mid-ocean-ridge crests. The correspondence between our calculated $\delta^{18}O_r$ profile and that recently measured through a complete ophiolite section (Figs. 21B, C, D and 23) is particularly striking and suggests that the $\delta^{18}O$ alteration observed in ophiolite suites could have been produced by downward low-temperature (T < 300°C) fluid circulation.

The above calculations, discussion, and conclusions have some implications for exploration.

1. Near-surface silicification, particularly if areally extensive, must be considered a very positive exploration sign, as suggested by Gibson et al. (1981).

2. Ore deposits will lie above silicified zones and sulfate lenses. If a region shows gypsum but not much sulfide deposition, the area may not have evolved sufficiently to focus the discharge and deposit massive ore. Attention should be shifted to other areas.

3. Near-surface $\delta^{18}O_r$ anomalies are likely to be complicated; deep variations in $\delta^{18}O_r$ may be more useful in mapping fluid circulation patterns and locating areas of surface discharge where massive sulfide deposits might be formed.

Perhaps the most critical test of the model that could be performed in the Hokuroku district would be to drill a deep (>3 km) hole in an area of fluid inflow away from any massive sulfide deposit. Confirmation of a light $\delta^{18}O_r$ anomaly beneath the near-surface heavy anomaly (Fig. 21) would be strong confirmation of the fluid flow model suggested by the calculations reported in this paper.

Acknowledgments

First of all I would like to thank the Japanese for allowing a foreign group to have access to their deposits and for the cooperation and hospitality they extended to all of us throughout this project. It was a great honor to have been involved in a study of the classic Hokuroku ore deposits and an unforgettable experience to visit and become acquainted with the Japanese people and culture. I would like particularly to thank Jiro Date, Toshi Takahashi, Yoshi Kajiwara, Masa Mizukami, Asahiko Sugaki, Hirotomo Ueno, and Kenichiro Hiashi for their hospitality. From all, I learned a great deal and owe many unforgettable experiences. I am deeply indebted to the organizers of the project, Hiroshi Ohmoto, Ei Horokoshi, and Steve Scott. They bore the administrative burdens that made the work reported here possible and deserve full credit for the results. Steve Scott introduced me to ore deposits in Quebec and Ontario, and to many of the Canadian geologists who contributed much to the work reported here. I would particularly like to thank Steve Scott, Dave Watkins, Hal Gibson, and Leopold Gelinas for many

useful and exciting discussions of the superbly exposed geology and massive sulfide deposits in the Noranda area. The paper owes much to my immediate colleagues at The Pennsylvania State University. I would particularly like to thank Hiroshi Ohmoto, Al Guber, Jeff Green, Frank Dudas, Stu Eldridge, and Visut Pisutha-Arnond for their geological and geochemical help, council, and suggestions. Useful suggestions were made by Dave Converse regarding the effect of bottom currents on massive sulfide deposition. Mike Mottl kindly gave me a preprint of his paper on the structure of hydrothermal systems at mid-ocean ridges. I am indebted to him for this and for several very useful and stimulating discussions on hydrothermal systems of common interest and on the nature of hydrothermal rock alteration. Last, but by no means least, the kinetics discussion in the appendix owes a great deal to discussions with Tony Lasaga, and I would like to thank Tony for his council—both direct and indirect (through lectures and students).

March 16, 1982

REFERENCES

Anderson, R. N., and Zoback, M. D., 1982, Permeability, underpressures and convection in the ocean crust near the Costa Rica rift, eastern equational Pacific: Jour. Geophys. Research, v. 87, p. 2860–2868.

Archer, P. L., 1978, An experimental investigation of seawater/basalt interaction: The role of water/rock ratios and temperature gradients: Unpub. M.S. thesis, Texas A and M Univ., 79 p.

Ballard, R. D., and van Andel, T. H., 1977, Morphology of tectonics of the inner rift valley at lat. 36°50′ N on the Mid-Atlantic Ridge: Geol. Soc. America Bull., v. 88, p. 507–530.

Ballard, R. D., Francheteau, J., Juteau, T., Rangan, C., and Normark, W., 1981, East Pacific Rise at 21° N: The volcanic, tectonic, and hydrothermal processes of the central axis: Earth Planet. Sci. Letters, v. 55, p. 1–10.

Bischoff, J. L. and Seyfried, W. E., 1978, Hydrothermal chemistry of sea water from 25°C to 350°C: Am. Jour. Sci., v. 278, p. 838–860.

Brace, W. F., 1980, Permeability of crystalline and argillaceous rocks: Internat. Jour. Rock Mechanics, Mineral Sci., Geomechan. Abs., v. 17, p. 241–251.

Bredehoeft, J. D., and Papadopulos, I. S., 1965, Rates of vertical ground water movement estimated from the earth's thermal profile: Water Resources Research, v. 1, p. 325–328.

Burnham, C. W., 1979, Hydrothermal fluids at the magmatic stage, *in* Barnes, H. L., ed., Geochemistry of hydrothermal ore deposits: New York, John Wiley and Sons, p. 71–136.

Cathles, L. M., 1977, An analysis of the cooling of intrusives by ground-water convection which includes boiling: ECON. GEOL., v. 72, p. 804–826.

—— 1978, Hydrodynamic constraints on the formation of Kuroko deposits: Mining Geology, v. 28, p. 257–266.

—— 1981, Fluid flow and genesis of hydrothermal ore deposits: ECON. GEOL., 75th ANNIV. VOL., p. 424–457.

Cathles, L. M., and Apps, J. A., 1975, A model of the dump leaching process that incorporates oxygen balance, heat balance, and air convection: Metall. Trans., v. 6B, p. 617–624.

Cathles, L. M., Guber, A., Lenagh, T. C., and Dudás, F. Ö., 1983, Kuroko-type massive sulfide deposits of Japan: Products of an aborted island-arc rift?: ECON. GEOL. MON. 5, p. 96–114.

Clark, S. P., 1966, Handbook of physical constraints: Geol. Soc. America Mem. 97, 587 p.

Clayton, R. N., O'Neil, J. R., and Mayeda, J. K., 1972, Oxygen isotope exchange between quartz and water: Jour. Geophys. Research, v. 77, p. 3057–3067.

Cole, D. R., 1980. Mechanism and rates of stable isotope exchange in hydrothermal rock-water systems: Unpub. Ph.D. dissert., The Pennsylvania State Univ., 303 p.

Corliss, J. B., Dymond, J., Gordon, L. I., Edmond, J. M., von Herzen, R. P., Ballard, R. D., Green, K., Williams, D., Bainbridge, A., Crane, K., and van Andel, T. H., 1979, Submarine thermal springs on the Galapagos rift: Science, v. 203, p. 1073–1084.

Crerar, D. A., and Barnes, H., 1976, Ore solution chemistry V. Solubilities of chalcopyrite and chalcocite assemblages in hydrothermal solution at 200° to 350°: ECON. GEOL., v. 71, p. 772–794.

Date, J., 1979, A consideration on the alteration of dacite below the Fukazawa ore deposits, Fukazawa mine, Akita Prefecture: Mining Geology, v. 29, p. 187–196.

Date, J., Watanabe, Y., and Saeki, Y., 1983, Zonal alteration around the Fukazawa Kuroko deposits, Akita Prefecture, northern Japan: ECON. GEOL. MON. 5, p. 365–386.

Edmund, J. R., Measures, C., McDuff, R. E., Chan, L. H., Collier, R., Grant, G., Gordon, L. I., and Corliss, J. B., 1979a, Ridge Crest hydrothermal activity and the balances of major and minor elements in the ocean: The Galapagos data: Earth Planet. Sci. Letters, v. 46, p. 1–18.

Edmund, J. R., Measures, C., Magnum, B., Grant, B., Sclater, F. R., Collier, R., Hudson, A., Gordon, L. I., and Corliss, J. B., 1979b, On the formation of metal-rich deposits at ridge crusts: Earth Planet. Sci. Letters, v. 46, p. 19–30

Elder, J. W., 1966, Heat and mass transfer in the earth: Hydrothermal systems: New Zealand Dept. Sci. Indus. Research Bull., v. 169, p. 1–115.

Eldridge, C. S., Barton, P. B., Jr., and Ohmoto, H., 1983, Mineral textures and their bearing on formation of the Kuroko orebodies: ECON. GEOL. MON. 5, p. 241–281.

Farrell, C. W., Holland, H. D., and Peterson, U., 1978, The isotopic composition of strontium in barites and anhydrites from Kuroko deposits: Mining Geology, v. 28, p. 281–292.

Fehn, U., and Cathles, L. M., 1979, Hydrothermal convection at slow-spreading mid-ocean ridges: Tectonophysics, v. 55, p. 239–260.

Fehn, U., Doe, B. R., and Delevaux, M. H., 1983, The distribution of lead isotopes and the origin of Kuroko ore deposits in the Hokuroku district, Japan: ECON. GEOL. MON. 5, p. 488–506.

Fitts, D. D., 1962, Nonequilibrium thermodynamics: New York, McGraw Hill Book Co., 173 p.

Fournier, R. O., and Rowe, J. J., 1977, The solubility of amorphous silica in water at high temperatures and pressures: Am. Mineralogist, v. 62, p. 1052–1056.

Friedman, I., and O'Neil, J. R., 1977, Compilation of stable isotope fractionation factors of geochemical interest: U. S. Geol. Survey Prof. Paper 440-KX, 12 p.

Green, G. R., Ohmoto, H., Date, J., and Takahashi, T., 1983, Whole-rock oxygen isotope distribution in the Fukazawa-Kosaka area, Hokuroku district, Japan, and its potential application to mineral exploration: ECON. GEOL. MON. 5, p. 395–411.

Gibson, H. L., Watkinson, D. H., and Comba, C. D. A., 1981, Silicification, hydrothermal alteration in an Archean geothermal system within the Amulet Rhyolite Formation, Noranda, Quebec: Geol. Assoc. Canada/Mineralog. Assoc. Canada/Canada Geol. Union, Joint Ann. Mtg., Calgary 1981, Abstracts, p. 4–21.

Gregory, R. T. and Taylor, H. P., Jr., 1981, An oxygen isotope profile in a section of Cretaceous oceanic crust, Samail Ophiolite, Oman: Evidence for $\delta^{18}O$ buffering of the oceans by deep (>5 km) seawater-hydrothermal circulation at mid-ocean ridges: Jour. Geophys. Research, v. 86, p. 2737–2755.

Guber, A. L., and Merrill, S., III, 1983, Paleobathymetric significance

of the foraminifera from the Hokuroku district, Japan: ECON. GEOL. MON. 5, p. 55–70.

Hall, J. M., and Robinson, P. T., 1979, Deep drilling in the North Atlantic Ocean: Science, v. 204, p. 573–586.

Homsy, G. M., and Sherwood, A. E., 1976, Convective instabilities in porous media with through flow: AICHE Jour., v. 22, p. 168–174.

Hopson, C. A., Coleman, R. G., Gregory, R. T., Pallister, J. S., and Bailey, E. H., 1981, Geologic section through the Samail Ophiolite and associated rocks along the Muscat-Ibra transect, southeastern Oman Mountains: Jour. Geophys. Research, v. 86, p. 2527–2544.

Iijima, A., 1974, Clay and zeolite alteration zones surrounding Kuroko deposits in the Hokuroku district, northern Akita, as submarine hydrothermal-diagenetic alteration products: Soc. Mining Geologists Japan, Spec. Issue 6, p. 267–289.

Ishihara S., 1974, Magmatism of the Green Tuff, tectonic belt, northeast Japan: Soc. Mining Geologists Japan, Spec. Issue 6, p. 235–249.

Izawa, E., Yoshida, T., and Saito, R., 1978, Geochemical characteristics of hydrothermal alteration around the Fukazawa Kuroko deposit, Akita, Japan: Mining Geology, v. 28, p. 325–336.

Kajiwara, Y., 1971, Sulfur isotope study of Kuroko ores of the Shakanai No. 1 deposits, Akita Prefecture, Japan: Geochem. Jour. (Japan), v. 4, p. 157–181.

Kajiwara, Y. 1973, A simulation of the Kuroko type mineralization in Japan: Geochem. Jour. (Japan), v. 6, p. 193–209.

Kouda, R. 1977, Time and spatial relations among sulfide-sulfate mineralization of Fukazawa Kuroko deposits with special references to the mineralogical geochemistry: Unpub. M.S. thesis, Univ. Tokyo, 148 p.

Lambert, I. B., and Sato, T., 1974, The Kuroko and associated ore deposits of Japan: A review of their features and metallogenesis: ECON. GEOL., v. 61, p. 1215–1236.

Large, R. R., 1977, Chemical evolution and zonation of massive sulfide deposits in volcanic terrains: ECON. GEOL., v. 72, p. 549–572.

Lewis, B. T. R., and Snydsman, W. E., 1979, Fine structure of the lower oceanic crust on the Cocos plate: Tectonophysics, v. 55, p. 87–105.

Lister, C. R. B., 1974, On the penetration of water into hot rock: Geophys. Jour. Royal Astron. Soc., v. 39, p. 456–509.

—— 1977, Qualitative models of spreading center processes, including hydrothermal penetration: Tectonophysics, v. 37, p. 203–218.

—— 1980, Heat flow and hydrothermal circulation: Ann. Rev. Earth Planet. Sci., v. 8, p. 95–117.

Macdonald, K. C., Becker, K., Spiess, F. N., and Ballard, K. D., 1980, Hydrothermal heat flux of the "black smoker" vents on the East Pacific Rise: Earth Planet. Sci. Letters, v. 48, p. 1–7.

McCulloch, M. T., Gregory, R. T., Wasserberg, G. J., and Taylor, H. P., 1981, Sm-Nd, Rb-Sr, and $^{18}O/^{16}O$ isotopic systematics in an ocean crustal section: Evidence from the Samail Ophiolite: Jour. Geophys. Research, v. 86, p. 2721–2735.

Marutani, M., and Takenouchi, S., 1978, Fluid inclusion study of stockwork silicious orebodies of Kuroko deposits at the Kuroko mine, Akita, Japan: Mining Geology, v. 28, p. 349–360.

McNitt, J. R., 1970, The geologic environment of geothermal fields as a guide to exploration: Geothermics, Spec. Issue 2, p. 24–30.

Mercer, J. S., Pinder, G. F., and Donaldson, J. G., 1975, A Gelerkin-finite element analysis of the hydrothermal system at Wairakei, New Zealand: Jour. Geophys. Research, v. 80, p. 2608–2621.

Morrow, C., Lockner, D., Moore, D., and Byerlee, J., 1981, Permeability of granite in a temperature gradient: Jour. Geophys. Research, v. 86, p. 3002–3008.

Mottl, M. J., 1982, Metabasalts, axial hot springs, and the structure of hydrothermal systems at mid-ocean ridges: Geol. Soc. America Bull., v. 94, p. 161–180.

Mottl, M. J., and Holland, H. D., 1978, Chemical exchange curing hydrothermal alteration of basalt by seawater—I. Experimental results for major and minor components of seawater: Geochim. et Cosmochim. Acta, v. 42, p. 1103–1115.

Norton, D., and Knapp, R., 1977, Transport phenomena in hydrothermal systems: The nature of porosity: Am. Jour. Sci., v. 277, p. 913–916.

Norton, D., and Taylor, H. P. 1979. Quantitative simulation of the hydrothermal systems of crystallizing magmas on the basis of transport and oxygen isotope data: An analysis of the Skaergaard intrusion: Jour. Petrology, v. 20, p. 421–486.

Ohmoto, H., 1978, Submarine calderas: A key to the formation of volcanogenic massive sulfide deposits: Mining Geology, v. 28, p. 219–232.

Oldenberg, D. W., 1975, A physical model for the creation of the lithosphere: Geophys. Jour. Royal Astron. Soc., v. 43, p. 425–451.

O'Neil, J. R., and Taylor, H. P., 1969, Oxygen isotope equilibrium between muscovite and water: Jour. Geophys. Research, v. 74, p. 6012–6022.

Parmentier, E. M., 1981, Numerical experiments on ^{18}O depletion in igneous intrusions cooling by ground water convection: Jour. Geophys. Research, v. 86, p. 7131–7144.

Parmentier, E. M., and Spooner, E. T. C., 1978, A theoretical study of hydrothermal convection and the origin of the ophiolite sulfide ore deposits of Cyprus: Earth Planet. Sci. Letters, v. 40, p. 33–44.

Peaceman, D. W., 1977, Fundamentals of numerical reservoir simulation: New York, Elsevier, 175 p.

Pisutha-Arnond, V., and Ohmoto, H., 1983, Thermal history, and chemical and isotopic compositions of the ore-forming fluids responsible for the Kuroko massive sulfide deposits in the Hokuroku district of Japan: ECON. GEOL. MON. 5, p. 523–558.

Rimstidt, J. D. and Barnes, H. L., 1980, The kinetics of silica-water reactions: Geochim. et Cosmochim. Acta, v. 44, p. 1683–1699.

RISE, 1980, East Pacific Rise: Hot springs and geophysical experiments: Science, v. 207, p. 1421–1433.

Sato, T., 1973, A chloride complex model for Kuroko mineralization: Geochem. Jour. (Japan), v. 7, p. 245–270.

Scott, S. D., 1980. Geology and structural control of Kuroko-type massive sulfide deposits: Geol. Assoc. Canada, Spec. Paper 20, p. 705–721.

Shikazono, N., Holland, H. D., and Quirk, R. F., 1983, Anhydrite in Kuroko deposits: Mode of occurrence and depositional mechanisms: ECON. GEOL. MON. 5, p. 329–344.

Sleep, N. H., and Rosendahl, B. R., 1979, Topography and tectonics of mid-ocean ridge: Jour. Geophys. Research, v. 84, p. 6831–6839.

Solomon, M., and Walshe, J. L., 1979, The formation of massive sulfide deposits on the sea floor: ECON. GEOL., v. 74, p. 797–813.

Spooner, E. T. C., 1977, Hydrodynamic model for the origin of the ophiolitic cupriferous pyrite ore deposits of Cyprus: Geol. Soc. London, Spec. Pub. 9, p. 58–71.

Spooner, E. T. C., and Fyfe, W. F., 1973, Subsea floor metamorphism, heat and mass transfer: Contr. Mineralogy Petrology, v. 42, p. 287–304.

Spooner, E. T. C., Beckinsale, R. D., Fyfe, W. S., and Smewing, J. D., 1974, ^{18}O enriched ophiolite metabasic rocks from E. Liguria (Italy), Pindos (Greece), and Troodos (Cyprus): Contr. Mineralogy Petrology, v. 47, p. 41–62.

Spooner, E. T. C., Beckinsale, R. D., England, P. C., and Senior, A., 1977a, Hydration, ^{18}O enrichment and oxidation during ocean floor hydrothermal metamorphism of ophiolitic metabasic rocks from E. Liguria, Italy: Geochim. et Cosmochim. Acta, v. 41, p. 857–871.

Spooner, E. T. C., Chapman, H. J., and Smewing J. D., 1977b, Strontium isotopic contamination and oxidation during ocean floor hydrothermal metamorphism of the ophiolitic rocks of the Troodos Massif, Cyprus: Geochim. et Cosmochim. Acta, v. 41, p. 873–890.

Sutton, F. M, 1970, Onset of convection in a porous channel with net through flow: Physics Fluids, v. 13, p. 1931–1934.

Takahashi, T., and Suga, K., 1974, Geology and ore deposits of the Hanaoka Kuroko belt, Akita Prefecture: Soc. Mining Geologists Japan, Spec. Issue 6, p. 101–113.

Tanimura, S., Shimoda T., and Sawaguchi, T., 1974, On the Fukazawa ore bodies, Akita Prefecture: Soc. Mining Geologists Japan, Spec. Issue 6, p. 147–155.

Taylor, H. P., 1974, The application of oxygen and hydrogen isotope

studies to problems of hydrothermal alteration and ore deposition: ECON. GEOL., v. 69, p. 843–883.

Tono, N., 1974, Minor element distribution around Kuroko deposits of northern Akita, Japan: Soc. Mining Geologists Japan, Spec. Issue 6, p. 399–420.

Tsutsumi, M., and Ohmoto, H., 1983, A preliminary oxygen isotope study of tetsusekiei ores associated with Kuroko deposits in the Hokuroku district, Japan: ECON. GEOL. MON. 5, p. 433–438.

Urabe, T., 1974, Iron content in sphalerite coexisting with pyrite from some Kuroko deposits: Soc. Mining Geologists Japan, Spec. Issue 6, p. 377–384.

Urabe, T., and Sato, T., 1978, Kuroko deposits of the Kosaka mine, northeast Honshu, Japan—products of submarine hot springs on Miocene sea floor: ECON GEOL., v. 73, p. 161–179.

Urabe, T., Scott, S. D., and Hattori, K., 1983, A comparison of footwall rock alteration and geothermal systems beneath some Japanese and Canadian volcanogenic massive sulfide deposits: ECON. GEOL. MON. 5, p. 345–364.

Utada, M., Tokoyo, T., and Aoki, H. 1981, The distribution of alteration zones in the central area of the Hokuroku district, northeast Japan: Mining Geology, v. 31, p. 13–25 (in Japanese with English abs.).

van Andel, T. H., and Ballard, R. D., 1979, The Galapagos rift at 86° W: 2. Volcanism, structure and evolution of the rift valley: Jour. Geophys. Research, v. 84, p. 5390–5406.

White, D. E., 1970, Geochemistry applied to the discovery, evaluation and exploitation of geothermal energy resources: Geothermics, Spec. Issue 2, p. 58–80.

Wooding, R. A., 1960, Rayleigh instability of a thermal boundary layer in flow through a porous medium: Jour. Fluid Mech., v. 9, p. 183–192.

Glossary of Appendix Notation

*	Standard or base value
A	Rate of production chemical species in solution ($g/cm^3/sec$)
A_0	That part of A that does not depend on C
A_1	That part of A that does depend on C
a	Surface areas per cm^3 fluid-filled pore space (cm^{-1})
C	Mass fraction of chemical species in water or steam (g/g)
c_m	Heat capacity of water-saturated rock formation (cal/g/°C)
c_f	Heat capacity of fluid phase in cal/g/°C
D	Distance between flow fractures (cm)
D_E	Effective diffusional porosity of impermeable "matrix" rock
d	Grain size of minerals in rock (cm)
F	Fraction of the maximum possible reaction rate at which reaction actually took place
g	Acceleration of gravity in cm/sec^2
H	Depth extent of calculation domain
$\mathscr{H}$	Enthalpy of water or steam in cal/g/°C
$\mathscr{H}^*$	Particular value of enthalpy of water, = 1 cal/g/°C
k	Rate constant characterizing kinetics of a chemical reaction, see equation (IIA 11)
k′	Bulk permeability of the porous media or fractured rock formation in cm^2($10^{-11}cm^2$ = 1 mD)
$\bar{k}'$	Bulk permeability of the porous media in millidarcies, = k/k^*, where $k^* = 10^{-11}$ cm^2
K_m	Thermal conductivity of the rock formation in cal/cm/sec/°C
L	Heat of crystallization of a magma (cal/g)
p	Fluid pressure in dynes/cm^2
$\underline{q}$	Mass flux of steam or water (assumes two phases are not mixed), = $\underline{\nabla} \times \underline{\Psi}$
$\bar{\underline{q}}$	Normalized mass flux, $\bar{\underline{q}} = \frac{H\mathscr{H}^*}{K_m T^*}\underline{q}$
R	Heat of reaction that augments the heat capacity of an intrusion, = 0.66 cal/g/°C (see Cathles, 1977)
$\mathscr{R}$	Rayleigh number, = $c_f g k' \rho_0 \alpha T_0 H/\nu K_m$, H = thickness of convecting layer, T = temperature at base
s	Distance along a streamline (cm)
T	Temperature of fluid and rock in °C
T_m	Temperature of intrusion
$\bar{T}$	Normalized temperature, = T/T^*, T^* = 1°C
t	Time in seconds
v	True fluid velocity along streamline (=$\underline{q}/\phi\rho$)
$\bar{v}_r$	Normalized half-spreading rate at ridge, = $v_r \rho_m c_m H/K_m$, v_r = half-spreading rate in cm/sec
y	Horizontal distance (cm)
z	Depth, positive upward (cm)
α	Coefficient of thermal expansion of water or steam ($°C^{-1}$) or the equilibrium fractionation factor between rock and water as defined in equation IIA 3
δ	Skin depth; the depth at which the alteration reaction penetrates matrix blocks; see equation (IIA 28)
ν	Dynamic viscosity of water in stokes
$\bar{\nu}$	Dynamic viscosity of water in millistokes, $\bar{\nu} = \nu/\nu^*$, $\nu^* = 10^{-3}$ stokes
ϕ	Fluid-filled porosity of rock
ϕ_f	Porosity associated with fractures in which flow takes place
Ψ	Steam function (g/cm/sec)
$\bar{\psi}$	Dimensionless steam function = $\psi\mathscr{H}^*/K_m T^*$
$\bar{\rho}$	Density of water in g/cm^3
ρ_0	A particular base density of water, = 1 g/cm^3
ρ_m	Density of water-saturated rock formation (g/cm^3)

Abbreviations

amph	amphibole
bdy	boundary
equil, e	equilibrium
f	fluid
hydro	hydrothermal
obsv	observed
ox	oxygen isotopes
r	rock
sat	saturated
w	water

APPENDIX I

Modeling Techniques

Physical model

The physical model conserves fluid mass, fluid momentum, and energy and is similar to that described in Cathles (1977). We assume fluid flow has achieved steady state and that there are no sources or sinks of fluid. This leads to

$$\bar{\nabla}\cdot\bar{q} = 0 \text{ and} \qquad \text{(IA 1)}$$

$$\bar{\nabla}\cdot\frac{\bar{\nu}}{\bar{k}'(T)}(p, T)\bar{\nabla}\bar{\Psi} - \frac{\mathcal{R}}{\rho^{\circ}\alpha T_0}\frac{\partial\rho}{\partial\bar{y}}(p, T) = 0 \qquad \text{(IA 2)}$$

which are the equations expressing conservation of fluid mass and momentum. Abbreviations and symbols are defined in the glossary; a superscript bar indicates that the quantity or operator has been normalized to a convenient set of units. As indicated, and as discussed in Cathles (1977), viscosity ($\bar{\nu}(p, t)$) and fluid density ($\rho(p, t)$) are considered to be functions of pressure and temperature. Values appropriate for pure water are looked up in a table for each point on the finite difference grid; realistic values are therefore used in the calculations. Permeability can have a temperature dependence (see discussion in text) and can also vary as a function of spatial position. The energy balance equation is:

$$\left(1 + \frac{R}{c_m}\right)\frac{\partial T}{\partial t} = \bar{\nabla}^2 T = \bar{\underline{\nabla}}\cdot\bar{\underline{q}}T + \bar{v}_r\frac{\partial T}{\partial\bar{y}} = 0. \qquad \text{(IA 3)}$$

The heat capacity of the fluid is assumed to be constant at 1 cal/g/°C; $\bar{v}_r$ is the normalized half-spreading rate produced by steady dike injection.

When the cooling of an intrusion is calculated, $\bar{v}_r = 0$ and an area of the computation domain corresponding to the intrusion is set initially at high (700°C) temperature. In the dike injection models, the computation domain initially has a normal temperature increase with depth; heat is introduced at the left boundary as a consequence of dike injection and crustal spreading.

Boundary conditions for the case of a cooling intrusion are no flow out of the sides or base, free flow out of the top surface, insulating sides, constant 20°C top surface temperature wherever there is fluid inflow or weak fluid outflow, and normal heat flow (1.5 HFU) into the base except where heat from an intrusion causes the basal temperature to be elevated above normal, in which case the basal heat flux is set equal to zero.

Boundary conditions for the dike injection model are the same as the intrusion model for fluid flow but differ for heat flux. Heat flux through the left side (the side away from the dike axis) is still zero. Heat flux in the right side is:

$$K_m\frac{\partial T}{\partial y}\bigg|_{bdy} = -\rho_m v_r(L + [T_m - T]c_m). \qquad \text{(IA 4)}$$

Equation (IA 4) is the boundary condition suggested by Oldenberg (1975) and used in previous calculations by the author (Fehn and Cathles, 1979). The equation states that the heat flux into the side of the computation domain equals the total heat contained in the dike magma in cooling from its intrusion temperature, T_m, to whatever the quasi-steady state temperature, T, at a point on the boundary happens to be at a particular time. T is computed implicitly, i.e., solved for at the end of the time step. The total heat includes the latent heat of crystallization, L, as well as the heat released by cooling of the dike, $(T_m - T)c_m$.

Heat flow in the base is normal (1.5×10^{-6} cal/cm^2/sec) except where a new plate has been created by dike injection. In these areas the basal heat flux is

$$K_m\frac{\partial T}{\partial z} = -11.5 \times 10^{-6}/\sqrt{t}, \qquad \text{(IA 5)}$$

where t is the age of the new plate in millions of years. To avoid unreasonably large heat flow, t is always considered to be greater than some cutoff value, t_c.

If the fluid flow out the top surface is fast enough that it would transport 25 percent more of the heat than would be transported across the surface by conduction with the surface held at 20°C, then the top surface boundary condition is considered insulating. This avoids some numerical instability and corresponds physically to conditions under which hot hydrothermal solutions are vented directly through the surface without a significant drop in temperature.

Equations (IA 2) and IA 3) are related by the auxiliary relation

$$\bar{\underline{q}} = \bar{\underline{\nabla}} \times \bar{\underline{\Psi}} \qquad \text{(IA 6)}$$

and are solved cyclically to obtain the history of fluid flow and cooling. First, the temperature at Δt_1 is calculated using equation (IA 3) and assuming $\bar{q} = 0$. Then steady state fluid flow is calculated for this temperature distribution, using equation (IA 2). Finally, fluid mass flux is calculated using equation (IA 6), and a new temperature distribution is calculated at $\Delta t_1 + \Delta t_2$, etc. The equations are solved for a grid with variable x and y spacing using an iterative alternating direction implicit technique that has particularly good stability and convergence characteristics. Generally, the grid had 29 points in the vertical direction and 39 points in the horizontal direction. The closest grid spacings are at the top surface and at the edge of the intrusion where the horizontal temperature gradients are greatest. The equations describing conservation of

fluid mass and momentum and total energy and the techniques to solve the physical problem are not new. The interested reader is referred to the discussion and references in Cathles (1977).

Chemical model

The chemical model is simply a statement of conservation of atomic mass. The total quantity of any chemical species must be conserved. In the cases we consider, diffusion of chemical species through the water-filled pores of the rock is very slow and very local (at most a few centimeters to a few meters from the fractures through which fluid flows). Thus, the products and reactants of chemical reactions are treated as fluxes into and out of the circulating hydrothermal fluid—as sources or sinks of chemical species. Diffusion is omitted from the global mass balance equations, which are consequently hyperbolic in character. We use a simple point-tracking method of solution.

Mathematically, if there is no diffusion or dispersion, conservation of mass of a chemical species with weight fraction C in the hydrothermal fluid can be expressed:

$$\frac{\partial \rho\phi C}{\partial t} + \underline{\nabla}\cdot \underline{q}C = A \qquad \text{(IA 7)}$$

(e.g., Fitts, 1962, p. 10). The temporal and spatial derivatives may be expanded and, assuming there are no sources or sinks of fluid in the domain considered, this equation reduces to

$$\frac{DC}{Dt} = \frac{A}{\rho\phi}. \qquad \text{(IA 8)}$$

D/Dt is the material derivative and refers to the rate of change of mass fraction C in a specified parcel of fluid; the observer travels with the fluid as it circulates through the rock formation.

Time in equation (IA 8) relates to the distance traveled along a streamline, s. Using the chain rule,

$$\frac{DC}{Dt} = \frac{DC}{Ds}\frac{Ds}{Dt} = \frac{DC}{Ds}v, \qquad \text{(IA 9)}$$

where v is the true fluid velocity along the streamline. The source term, A, will generally consist of a concentration dependent and a concentration independent part (see Appendix II):

$$A = A_0 + A_1C. \qquad \text{(IA 10)}$$

Thus equation (IA 8) becomes

$$\frac{DC}{Ds} = \frac{A_0}{q} + \frac{A_1C}{q}, \qquad \text{(IA 11)}$$

where we have used the identity $\underline{q} = \phi\rho\underline{v}$. Over a small increment ΔS, where q can be considered constant, equation (IA 11) can be integrated:

$$C(s + \Delta s) = \frac{A_0}{A_1}(e^{A_1\Delta s/q} - 1) + C(s)e^{A_1\Delta s/q}. \qquad \text{(IA 12)}$$

If $A_1 = 0$, the proper equation can be found by expanding the first exponential on the right in a power series so that

$$C(s + \Delta s) = C(s) + \frac{A_0\Delta s}{q}. \qquad \text{(IA 13)}$$

Equations (IA 12) and (IA 13) form the basis for our point-tracking method. At each point in the computation domain, the fluid is chased backward, toward its source, with an initial guess, C(s), at what the concentration should be at that point. The fluid is chased backward along the streamline until: (1) the fluid has looped back to the starting point twice, (2) the interval of time over which the change in fluid and rock chemistry is requested has elapsed, (3) the fluid has crossed the top surface of the computation domain into the sea above, or (4) the fluid has entered a region where the kinetics are fast enough that it is very close to being in chemical equilibrium with the surrounding rock. Time (for condition 2) is defined as the distance chased divided by the true velocity of the fluid. After a chase of n increments of Δs_i each, for example,

$$t_n = \sum_{i=1}^{n}\Delta s_i\rho_i\phi/q_i. \qquad \text{(IA 14)}$$

The fluid is in equilibrium with the rock if at any point $A_{1i}\Delta s_i/q_i$ is very large. In this case equation (IA 12) reduces to $C(s) = -\frac{A_0}{A_1}$, which is the equilibrium concentration of C. Note that A_1 is always negative, and we chase the flow backward so q has the opposite sign from Δs. Thus $A_{1i}\,\Delta s_i/q_i$ will always be positive. In our computations local equilibrium is assumed if:

$$A_{1i}\Delta s_i q_i > 10. \qquad \text{(IA 15)}$$

Generally when any of the above four conditions for the end of the chase are fulfilled, the initial guess at the concentration at the starting point is corrected:

$$C = C(s) + (C_{obsv} - C(s)/\exp(\sum_{1}^{n} A_{1i}\Delta s_i q_i). \qquad \text{(IA 16)}$$

If the chase terminated by the fluid parcel leaving the computation domain, the boundary conditions specify C_{obsv} (the fluid composition entering the domain). If the chase terminated by time running out, C_{obsv} equals the fluid composition at the point in the domain where the chase ended. If the fluid circulates back to its starting position twice, $C_{obsv} = C_{initial}$. If condition (IA 15) is met, the fluid concentration at that point in the backward chase is set equal to its equilibrium value $-A_0/A_1$, where A_0 and A_1 have values appropriate to

the temperature at that spot. In all of these cases, the rate of rock alteration is calculated from the kinetic expression that defines A. In practice, a maximum change in rock alteration over any single time step is specified (e.g., ±1‰ for oxygen isotopes and ±0.1 wt % for silica alteration) and the time step is adjusted so this maximum is not exceeded.

There will generally be at least one point in the computation domain where the fluid simply rotates with no translation and the stream function has a local maximum or minimum. In this circumstance the fluid is considered to be in equilibrium with its rock environment and the rate of alteration of the rock is zero.

At high temperature the kinetics of alteration are very fast and the rock and water very close to equilibrium. High precision would be required to compute rock alteration from the kinetic expressions for A. Consequently, when the kinetics are fast enough that equation (IA 15) is satisfied at the beginning of a chase, the fluid composition is set at its equilibrium value and the rate of rock alteration computed from equation (IA 7).

$$A = \nabla \cdot qC_{equil}. \qquad \text{(IA 17)}$$

Equation (IA 17) follows directly from (IA 7) if the fluid is in quasi-steady state with the rock, and hence $\frac{\partial \rho \phi C}{\partial t} = 0$ and $C = C_{equil}$. When fluid and rock are everywhere in equilibrium equation (IB 11) produces a particularly simple way to compute rock alteration. We use this method to compute anhydrite deposition.

The point-tracking method of solving the equations describing the chemical interaction between circulating hydrothermal solutions and rock has the following advantages:

1. Numerical dispersion depends only on the point spacing and is roughly equal to that spacing (e.g., see Peaceman, 1977).

2. The method of solution is direct. The criteria for ending the chase provides useful insight. For example, if the fluid is in equilibrium initially or if it obtained equilibrium along the flow path with respect to a particular chemical species, that chemical species has no memory and contains no information of fluid-rock interaction farther upstream than the point at which equilibrium was obtained.

3. Results depend importantly only on A and q. It is true that initial transients depend on ρ and ϕ which govern the distance traveled by a fluid packet if Δt and q are specified (e.g., IA 13). However, the initial transients are only important at early times when cool seawater first circulates into the computation domain. The lack of dependence of ϕ is convenient since q is a better known parameter than ϕ; q depends only on the permeability of the rock formation, not on the details of the mode of flow through the formation (i.e., density of fractures, etc.). All the uncertainty in the chemical calculations, including uncertainty in ϕ, is therefore clearly placed in the chemical source term, A, where it belongs.

The point-tracking method follows streamlines. The locations of streamlines change with time, so in some cases the path actually followed by a packet of solution can be substantially different from that defined by the instantaneous streamline pattern. This problem is circumvented in our calculations by calculating rock alteration over short time intervals. Provided the streamline pattern does not change much over each time step (it does not), the calculated alteration will be correct.

APPENDIX II

Kinetics of Silica Solution-Precipitation and Oxygen Isotope Exchange

The kinetics of chemical processes enters the mass balance equations that describe rock alteration in a hydrothermal system through the term A in equations (IA 7) and (IA 8). Two different kinds of chemical reaction will be considered: the net rate of dissolution of silica from (or onto) the silica mineral surfaces exposed to the hydrothermal fluid, and the rate of oxygen isotope exchange between the fluid and rock. Isotopic exchange can occur either by diffusion of oxygen atoms into unaltered mineral grains and exchange of ^{18}O and ^{16}O within the grains or during the hydrothermal alteration of mineral grains. As we will see later, the former process is very much slower than the latter. In this paper we consider only the oxygen isotope exchange that occurs as the result of mineral alteration.

Both silica and alteration-related oxygen isotope exchange kinetics can be usefully described as surface area-controlled (heterogeneous) reactions. Thus, in addition to the kinetic expressions that describe the reaction rates for a unit surface area of exposed reactive mineral, we need estimates of the reactive mineral surface area exposed to the circulating hydrothermal pore fluid per unit volume of rock. The first section of this Appendix summarizes the kinetic data, the second part defines the magnitude of reactive surface area per unit of rock volume.

It is important to emphasize that this Appendix is intended to summarize briefly the kinetic data and show how the kinetic data are reformulated for use in the overall convective cooling model. An in-depth review of kinetic data, which is drawn primarily from two recent Pennsylvania State University theses, is not

attempted. In fact, our calculations show that the fluid is in equilibrium with the rock wherever the temperature exceeds ~100°C. In hot areas the rate of alteration is therefore controlled entirely by the rate of fluid flow along temperature gradients. Chemical kinetics is important only in the lower temperature areas or in areas such as large open fractures where the fluid flow is unusually rapid and focused, and the exposed rock surface area is small (and therefore, where the chemical kinetics will be unusually slow relative to the fluid-flow-controlled kinetics).

Oxygen isotope exchange

Cole (1980) has measured whole-rock $\delta^{18}O$ values and deduced the kinetics of alteration-related oxygen isotope exchange from two separate experiments involving the interaction of seawater and basalt at temperatures ranging from 200° to 500°C, and from eight experiments where granite was reacted with water at various salinities and temperatures between 200° and 300°C. One basalt experiment was carried out at Harvard and is described by Mottl and Holland (1978). The other was carried out at Texas A and M and is described by Archer (1978).

Cole's kinetic analysis is based on a simple formula for the rate of isotopic exchange:

$$\frac{dW_{18}}{dt} = a_T\left(r_1 \frac{R_{18}}{R}\frac{W_{16}}{W} - r_2 \frac{R_{16}}{R}\frac{W_{18}}{W}\right). \quad \text{(IIA 1)}$$

W_{18} is the moles of ^{18}O atoms in the water contained in the experimental system (and similarly for W_{16}), R_{18} is the moles of ^{18}O atoms in the rock contained in the experimental system (similarly for R_{16}), R is the total moles of rock oxygen atoms in the system, W is the total moles of water oxygen atoms, a_T is the total surface area of rock exposed to water, and t is time; r_1 and r_2 are the forward and reverse rate constants (moles oxygen exchanged/cm^2/sec) for the exchange reaction:

$$R_{18} + W_{16} \underset{r_2}{\overset{r_1}{\rightleftarrows}} R_{16} + W_{18}. \quad \text{(IIA 2)}$$

Equation (IIA 1) may be simplified somewhat by noting that an equilibrium $\frac{dW_{18}}{dt} = 0$ and therefore,

$$\frac{r_2}{r_1} = \frac{R^e_{18}}{R^e_{16}}\frac{W^e_{16}}{W^e_{18}} = \alpha, \quad \text{(IIA 3)}$$

where α is the equilibrium fractionation factor between rock and water. Thus

$$\frac{dW_{18}}{dt} = a_T r_1\left(\frac{R_{18}}{R}\frac{W_{16}}{W} - \alpha \frac{R_{16}}{R}\frac{W_{18}}{W}\right). \quad \text{(IIA 4)}$$

Cole (1980) works from IIA 4 to obtain an expression relating the percent fractionation of the rock to W, R, a_T, α, r_1, and t. Since W, R, and a_T are known from experimental conditions, and α can be deduced from long-term experiments, experimental data giving the percent fractionation as a function of time (t) are sufficient to determine r_1 at a particular temperature. In this fashion, Cole deduces the temperature-dependent expressions for r_1 that are given in slightly different form in Figure IIA 1.

To use Cole's results, we recast equation (IIA 4). First we modify it slightly by introducing a multiplicative factor $\frac{\rho}{\rho_0}$ to the left-hand side. This is required for the cases we consider where ρ, the density of the hydrothermal fluid, can be quite small (~0.2 g/cc or less); ρ_0 is the density of water under standard conditions and is taken to be 1 g/cc. The rationale for this modification is that the two terms in parentheses represent, respectively, the probability of exchanging a water ^{16}O for a rock ^{18}O, and the probability of exchanging a water ^{18}O for a rock ^{16}O. These probabilities are proportional to the fraction of ^{16}O and ^{18}O atoms. In the case of water ^{16}O exchanging for rock ^{18}O, the probability is proportional to the product of the fraction of ^{16}O atoms in water and ^{18}O atoms in rock. For exchange of ^{18}O for rock ^{16}O, the probability is proportional to the product of fraction of ^{18}O atoms in water and the fraction of ^{16}O atoms in rock. The probabilities of exchange differ slightly due to the different bonding energies of oxygen in water and rock and to the mass difference between ^{16}O and ^{18}O. This probability difference is reflected in the fact that α differs slightly from unity. The probability of exchange

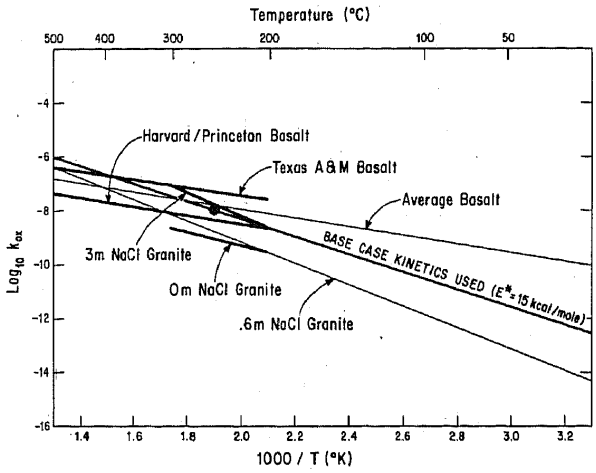

FIG. IIA 1. The kinetic data determined by Cole (1980) from water-rock basalt experiments at Harvard-Princeton and Texas A and M and from his own granite experiments are converted to the notation used in this article and shown by heavy lines. Light extrapolated lines for average basalt and 0.6-m NaCl-granite are also shown. The kinetic model used in this study is chosen to pass through the midrange of Cole's data (the large black dot) and have a thermal activation energy of 15 kcal/mole.

must also depend on the number of oxygen atoms per unit volume in water, however. (This is true also for rock, but the rock density varies little so this is ignored.) In principal, the water and rock atom fraction could remain unchanged as the density of the fluid phase is reduced to zero. But at zero density, the rate of oxygen isotope exchange must be zero. Hence we modify (IIA 4) to (IIA 5):

$$\frac{dW_{18}}{dt} = a_T r_1 \frac{\rho}{\rho_0}\left(\frac{R_{18}}{R}\frac{W_{16}}{W} - \alpha\frac{R_{16}}{R}\frac{W_{18}}{W}\right). \quad \text{(IIA 5)}$$

Next we note $W_{16}/W \approx R_{16}/R \approx 1$. We then divide equation (IIA 5) by a gram of hydrothermal fluid and make use of the fact that W can be taken as 0.055 moles O/g H_2O, whereupon IIA 5 becomes:

$$\frac{dC}{dt} = \frac{\bar{a} r_1 \rho \alpha}{0.055\rho_0}(C_{equil} - C), \quad \text{(IIA 6)}$$

where C is the moles of ^{18}O per gram of hydrothermal fluid, C_{equil} is the isotopic concentration of ^{18}O in water in equilibrium with the rock, and $\bar{a}$ is the surface area of reactive mineral exposed to each gram of hydrothermal fluid. The consumption rate of ^{18}O per cm^3 of rock formation, A′, is now just:

$$A'\left[\frac{\text{moles}^{18}\text{O}}{\text{cm}^3/\text{sec}}\right] = \rho\phi\frac{dC}{dt}$$

$$= \frac{\rho\phi a r_1 \alpha}{0.055\rho_0}(C_{equil} - C), \quad \text{(IIA 7)}$$

where $a(=\rho\bar{a})$ is the surface area per cm^3 of fluid-filled pore space. Equation (IIA 7) is the kinetic expression needed to complete equation (IA 7) or (IA 8). α may be dropped from the above equation since its value is very close to unity.

It is convenient to go one step further and recast the equations in terms of the notation commonly used in oxygen isotope analysis. By definition, the per mil oxygen isotope composition of a sample of water is:

$$\delta^{18}O_w \equiv \left(\frac{(W_{18}/W)_w}{(W_{18}/W)_{SMOW}} - 1\right) \times 1{,}000, \quad \text{(IIA 8)}$$

where SMOW refers to the standard Standard Mean Ocean Water. Seawater has an oxygen isotope composition of 0 per mil. If we let $X_{SMOW} = (W_{18}/W)_{SMOW}$ and remember that $C = 0.055(W_{18}/W)_w$, equation (IIA 8) may be rearranged:

$$C = 0.055\, X_{SMOW}\left(\frac{\delta_w}{1{,}000} + 1\right), \quad \text{(IIA 9)}$$

which is a linear transformation relating $\delta^{18}O_w$ (here simplified to δ_w) and C. Equation (IIA 9) may be substituted into any of the equations in the section on the chemical model in Appendix I with the result that the second term on the right of equation (IIA 9) is cancelled everywhere, either by subtraction or differentiation. The multiplicative expression $\frac{0.055_{SMOW}}{1{,}000}$ can therefore be cancelled throughout all equations, and the result is that δ_w is just exchanged for C. The units of A become somewhat nonphysical, however,

$$A\left[\frac{‰ \cdot g_{H_2O}}{\text{sec}}\right] = \phi a k_{ox}\left(\frac{\rho}{\rho_0}\right)(\delta_{we} - \delta_w). \quad \text{(IIA 10)}$$

$$k_{ox} \equiv \frac{r_1\alpha}{0.055} \simeq \frac{r_1}{0.055}. \quad \text{(IIA 11)}$$

$$\delta_{we} = \delta_r - \Delta_{rwe}. \quad \text{(IIA 12)}$$

Δ_{rwe} is the equilibrium fractionation between rock and water and δ_r is the per mil isotopic composition of the rock.

The rate of rock alteration in per mil per second can be related to A. Let $^{18}\bar{R} \equiv$ moles $^{18}O/cm^3$ rock formation, and $\bar{R}$ = moles O/cm^3 rock; thus, by definition:

$$\delta_r \equiv \left(\frac{^{18}\bar{R}/\bar{R}}{X_{SMOW}} - 1\right) \times 1{,}000 \quad \text{(IIA 13)}$$

and

$$A'\left[\frac{\text{moles } ^{18}\text{O}}{\text{cm}^3/\text{sec}}\right] = \frac{\partial^{18}\bar{R}}{\partial t} = \bar{R}\frac{X_{SMOW}}{1{,}000}\frac{\partial\delta}{\partial t}r. \quad \text{(IIA 14)}$$

Substituting for A from equations (IIA 7), and using (IIA 9) and (IIA 10), we find

$$\frac{\partial\delta_r}{\partial t} = \frac{0.055}{\bar{R}}A = 0.55A, \quad \text{(IIA 15)}$$

where we have used the fact that $\bar{R} \simeq 0.1$ moles O/cm^3 rock.

Cole (1980) determined Δ_{rwe} as a function of temperature for basalt as well as r_1 as a function of temperature. Cole's (1980, fig. II-4, p. 148) expression for Δ_{rwe} is:

$$\Delta_{rwe} = 2.15 \times 10^6/(T + 273)^2 + 0.692. \quad \text{(IIA 16)}$$

The significance of Cole's Δ_{rwe} is that it differs significantly from those generally used (see e.g., Fig. 16) but is in better agreement with field evidence from Kuroko deposits in Japan (see text of this article).

The kinetic model used in this study (see Fig. IIA 1) is:

$$\log_{10} k_{ox} = -3{,}260/(T + 273) - 1.81. \quad \text{(IIA 17)}$$

This kinetic expression implies an alteration activation energy of 15 kcal/mole, in the middle of the activation energy range of 10 to 20 kcal/mole that Lasaga (1981) offers as typical for alteration reactions and passes through the middle of the kinetic data deduced by Cole.

Equations (IIA 10), (12), and (17) represent the kinetic oxygen isotope alteration model used in this study. The surface area per cm^3 fluid pore space effectively accessed by circulating hydrothermal solution is defined in a later section on reactive surface area and is also a required part of the kinetic model.

Kinetics of silica solution and deposition

Rimstidt and Barnes (1980) have recently compiled data on the kinetics of silica solution and deposition. If C in the equations of Appendix I has the units of g_{SiO_2}/g_{H_2O}, then A has the units $g_{SiO_2}/cm^3/rock/sec$. The kinetic rate expressions of Rimstidt and Barnes (1980) adjusted to these units for a fluid close to seawater composition (low ionic strength) and for amorphous silica solution and deposition are:

$$A\left[\frac{g_{SiO_2}}{cm^3/sec}\right] = \phi a k_{SiO_2\ amph} \frac{\rho}{\rho_0} (C_{sat} - C) \qquad \text{(IIA 18)}$$

and

$$\log_{10} k_{SiO_2} = \frac{-2{,}598}{T + 273} - 1.7. \qquad \text{(IIA 19)}$$

Again, we have modified the kinetic expression (IIA 18) by the factor ρ/ρ_0. If C_r represents the silica precipitated or dissolved per cm^3 of rock, then

$$\frac{\partial C_r}{\partial t} = A. \qquad \text{(IIA 20)}$$

The k_{SiO_2} is the same for amorphous silica, cristobalite, and quartz; C_{sat} is quite different for different silica phases.

Rimstidt and Barnes (1980) do not consider pressure as a variable in their investigation and so we cannot correct the expression for $k_{SiO_2\ amph}$ to allow for insertion of the ρ/ρ_0 term as we did for k_{ox}. The error introduced will be small (less than 30%) and of no significance. Silica kinetics are much faster than those of alteration-related oxygen isotope exchange (compare eq. IIA 19 to IIA 17). The rate of silica alteration is therefore controlled almost completely by fluid flow. In this regard, silica concentration as a function of pressure and temperature is for our purposes by far the most important parameter in the kinetic model.

The saturation concentration of amorphous silica as a function of temperature and fluid density can be deduced from Fournier and Rowe (1977). Their figure 4 shows that at least to 400°C, $\log_{10} C_{SiO_2\ sat}$ increases linearly with fluid density at any temperature and the rate of increase with density does not depend on temperature. Their expression for the saturation concentration of amorphous silica as a function of temperature at 1,034 bars can therefore be easily corrected back to $\rho = 1.0$, saturation values refit to a function $\alpha/T + \beta$, and the density correction introduced. When this is done, the following expression for the saturated concentration of amorphous silica in g_{SiO_2}/g_{H_2O} as a function of T and ρ results:

$$\log_{10} C_{SiO_2} = \frac{-1{,}194}{T + 273} - \frac{1 - \rho}{0.64} - 0.19. \qquad \text{(IIA 21)}$$

Equations (IIA 18 to 21) represent our kinetic model for silica dissolution and precipitation.

Reactive surface area per unit volume of rock

The isotopic alteration model (eq. IIA 10) and the silica solution and precipitation model (eq. IIA 18) both contain an as yet undefined product, ϕa, which is the cm^2 of reactive mineral effectively exposed to the circulating hydrothermal fluid per unit volume of rock formation. The proper value of ϕa is perhaps the most uncertain quantity in the alteration model. Consequently, we treat it parametrically and calculate models with a wide range of values of ϕa. In this section, we seek to place a reasonable upper bound on the magnitude of ϕa. Two approaches are taken. The first is most applicable to silica dissolution-precipitation, the second to oxygen isotope alteration.

The ϕa if fluid-rock chemical interaction is restricted to the edges of flow fractures: Consider a square grid of fractures of aperture d and separation D. The fluid mass flux through such a set of fractures can be shown to be:

$$\underline{q} = \frac{d^3}{6D\nu} \nabla p. \qquad \text{(IIA 22)}$$

Hence, by analogy to Darcy's law, the permeability of the fracture system is $k = d^3/6D$. The porosity of the flow fractures is $\phi_f = 3d/D$, and the surface area per unit volume of fluid in the flow fracture is $a = 2/d$. Thus, using ϕ_f to eliminate D in the expression for k, and the new expression for k to eliminate d in the expression for a, we see

$$a = \sqrt{\frac{2\phi_f}{9k'}}. \qquad \text{(IIA 23)}$$

Permeability is thus inversely related to a^2; permeability provides a direct measure of surface area per unit fluid volume. Thus, if ϕ_f were known, the permeability of a given model could be confidently converted to a, a term needed for the chemical kinetic model.

However, ϕ_f is quite uncertain. For flow evenly distributed in an igneous rock, ϕ_f is typically a tenth the total porosity of the rock which is typically ~1 percent (Norton and Knapp, 1977). If ϕ_f is 0.1 percent and $k' = 10$ mD (10^{-10} cm^2), $a = 1{,}490$ cm^2/cm^3 fluid, and $\phi a = 1.49$ cm^2/cm^3 rock. Note ϕ in this case equals ϕ_f, and ϕa decreases as ϕ_f. Thus ϕa could be very small

if flow is dominated by a few widely spaced open fractures. For a fixed formation permeability, ϕ_f determines how far apart the fractures are. As ϕ_f decreases, the aperture of the fractures must increase to keep the permeability constant. Increasing either separation or aperture decreases surface area per unit fluid volume.

A reasonable upper bound on fracture ϕa appears to be $\sim$5 cm^2/cm^3 rock. This would correspond to ϕ_f = 0.1 percent and k′ = 1 mD. Fracture surface area is likely to be of greatest interest in silica dissolution and precipitation where rapid kinetics will restrict these processes to very near the fracture walls (see last subsection of Appendix II). Of course, not all the fracture surface will consist of amorphous silica, so even if ϕ_f were known, the reactive surface area per cm^3 of rock would need to be reduced by the fraction of the fracture surface area that consists of amorphous silica.

The ϕa if fluid-rock interaction occurs uniformly throughout the rock formation: Uniform reaction between the pore fluid and all the rock is the other extreme from reactions limited to fracture surfaces. If we envision mineral grains as little cubes of dimension d spaced 2ϵ from neighbor cubes, it can easily be shown that the total mineral surface area per cm^3 fluid, a, is:

$$a = \frac{6(1-\phi)}{d\phi}, \qquad \text{(IIA 24)}$$

where ϕ is the total porosity of the rock. Thus, the total mineral surface area per cm^3 of rock, ϕa, is:

$$\phi a = \frac{6(1-\phi)}{d}, \qquad \text{(IIA 25)}$$

for d = 100 μm, ϕ = 2 percent, and ϕa = 612 cm^2/cm^3 rock. The surface area per unit volume depends very little on ϕ and almost entirely on d.

The grain size of tuffs and basalts is typically small. Fifty microns might be considered typical. Therefore, ϕa will be about 1,200 cm^2/cm^3 rock. A reasonable upper bound would be $\sim$2,000 cm^2/cm^3.

The surface area per unit volume must be reduced from this maximum. If the isotope exchange reactions are at all rapid, the alteration reactions will not penetrate great distances into the rock from the fractures that allow flow through the rock. Reaction halos will form around fractures that transmit fluid. These halos will grow with time and eventually all the rock may be isotopically altered. But at any one time the fraction of rock interacting chemically with the fluid will be reduced by a factor equal to the ratio of the thickness of the reaction zone to half the average separation between flow fractures. Limits are placed on the thickness of the reaction zone near a fracture in the next section.

The thickness of the reaction zone near a fracture and its effect on the rate of chemical alteration: If there is no flow through the matrix blocks between flow fractures, the diffusive supply of reactant must balance the chemical reactions in the matrix blocks. Considering one dimensional diffusion away from a flow fracture,

$$D_E \frac{\partial^2 \Delta C}{\partial x^2} - \phi a k \frac{\rho}{\rho_0} \Delta C = 0. \qquad \text{(IIA 26)}$$

D_E is the effective diffusional porosity of the matrix blocks, $\Delta C = C_{sat} - C$, and the second term, the sink term, comes from equation (IIA 10) or (IIA 19). The equation has the solution

$$\Delta C = \Delta C_0 \exp\left(-\sqrt{\frac{\phi a k \rho}{\rho_0 D_E}}\, x\right), \qquad \text{(IIA 27)}$$

where ΔC_0 is the departure from saturation in the flow fracture and x is the distance into the matrix block. Thus, the chemical reaction extends a distance into the matrix block that can be conveniently characterized by a skin depth δ defined as the distance into the matrix block where $\Delta C = \Delta C_0/e$:

$$\delta = \sqrt{\frac{\rho_0 D_E}{\phi a k \rho}} \qquad \text{(IIA 28)}$$

We can evaluate δ as follows. ϕa is the factor discussed in the previous section, reduced by the fraction of glass in the rock matrix. If the matrix is initially 25 percent glass, a reasonable estimate for ϕa would be 300 cm^2/cm^3 rock. D_E, the effective diffusional porosity of the matrix, is typically 4 percent of the total porosity of the rock (Norton and Knapp, 1977) times the diffusion constant of the reactant species in water. Taking this diffusion constant as 2×10^{-5} cm^2/sec and the rock porosity at 2 percent, a reasonable estimate of D_E as a function of temperature will be:

$$\log_{10} D_E = \frac{-1{,}090}{T + 273} - 4.19. \qquad \text{(IIA 29)}$$

If we let $\rho/\rho_0 = 1$, and take k from equation (IIA 17) for oxygen isotope exchange and from equation (IIA 19) for silica, we see that

$$\log_{10} \delta_{ox} = \frac{1{,}085}{T + 273} - 2.73 \qquad \text{(IIA 30)}$$

and

$$\log_{10} \delta_{SiO_2} = \frac{755}{T + 273} - 2.79. \qquad \text{(IIA 31)}$$

Thus, at 20°, 100°, and 300°C the oxygen isotope reaction skin depth will be 9.4, 1.5, and 0.15 cm, and the silica reaction skin depth will be 0.61, 0.17, and 0.03 cm, respectively. Silica precipitation and dissolution will initially at least be limited to very near the fracture walls. The sharpness of oxygen isotope alteration halos will depend strongly on temperature, being

quite sharply defined at temperatures > 100°C. If flow fractures are ~1 m apart, only a few percent of the total rock volume will be isotopically exchanging at any time.

A skin depth as small as a centimeter has another implication. After an initial period when the rate of isotopic exchange is equal to $F\phi ak\frac{\rho}{\rho_0}\Delta C$, then $F = 2\delta/D$, where D is the separation between flow fractures and the reaction zone will migrate toward the interior of the matrix blocks and the rate of isotopic exchange will decrease. Reactants must now diffuse through an altered halo with which they are in equilibrium to reach the zone of reaction (see Cathles and Apps, 1975, for another example of shrinking core reaction control). This time-dependent leach rate could be easily modeled by the method recommended and used by Parmentier (1981). We do not account for this time-dependent drop in alteration rate in our calculations. Such a modification would only be important in areas of seawater inflow—the only areas where alteration is kinetically controlled.

In our calculations we use the following kinetic expressions:

$$A_{ox}\left[\frac{‰ \cdot g_{H_2O}}{sec}\right] = \frac{6(1-\phi)}{d} F_{ox}k_{ox}\frac{\rho}{\rho_0}(\delta_{we} - \delta_w) \quad \text{(IIA 32)}$$

and

$$A_{SiO_2}\left[\frac{g_{SiO_2}}{cm^3/sec}\right] = \sqrt{\frac{0.22\phi_f^3}{k'}} F_{SiO_2}k_{SiO_2\ amorph}\frac{\rho}{\rho_0}(C_{sat} - C), \quad \text{(IIA 33)}$$

where $F_{ox} = \frac{\delta}{D}$, and is assumed to be the same for all temperatures, F_{SiO_2} = fraction of amorphous silica along flow fractures, k_{ox} is given by equation (IIA 17), and $k_{SiO_2\ amorph}$ is given by equation (IIA 19). In our calculations $\phi = 0.02$, $\phi_f = 0.002$, d = 200 μm, $F_{SiO_2} = 0.2$, and $F_{ox} = 0.1$, 0.01, or 0.0001.